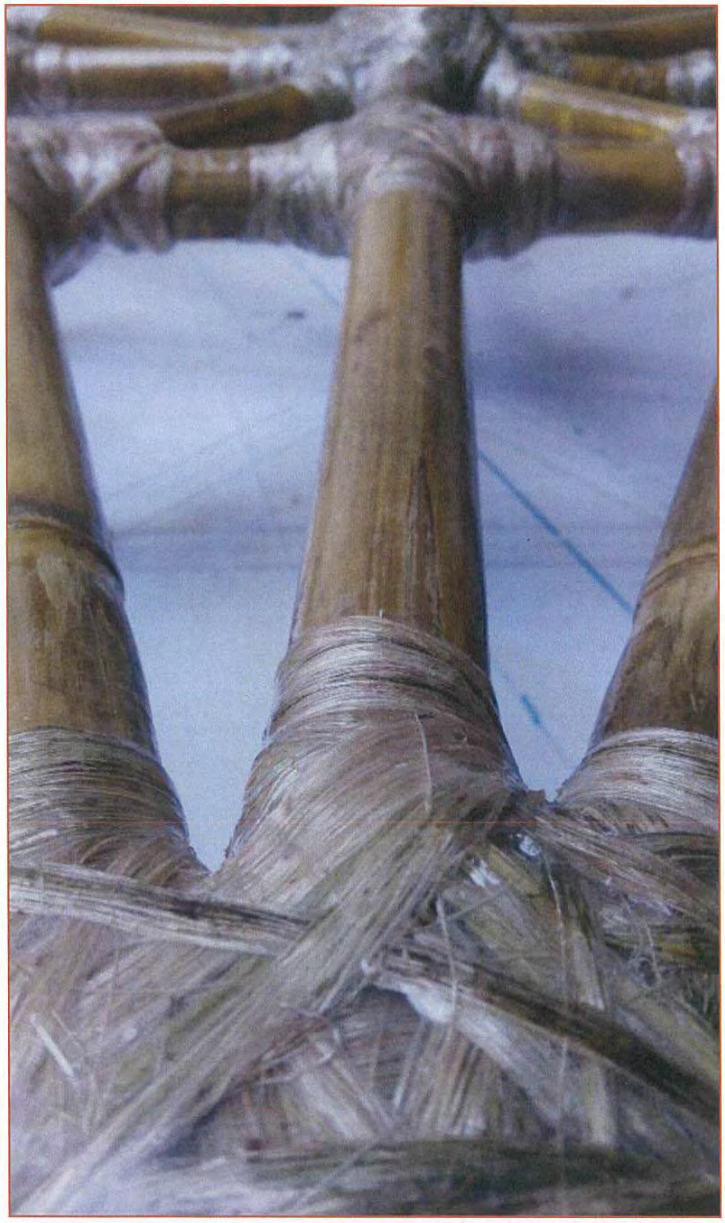

FINAL REPORT

Bamboo Velomobile Development Project

Tod Coxhead

05007247

BEngTech Otago Polytechnic 2014

ASSESSMENT COVER SHEET

OTAGO POLYTECHNIC
Te Kura Matatini ki Otago

> Architecture, Building and Engineering

Course: MG7001 (SMS Code) ENGINEERING DEVELOPMENT PROJECT (Title of course)

Assessment Title: FINAL REPORT

Lecturer's Name: DOUG ROGERS

ID Number: 05007247

Due Date and Time: 1:00PM, 14th NOVEMBER 2014

Declaration:

I hereby certify that the assignment being submitted for assessment is entirely my own work.

STUDENT'S SIGNATURE: _____ **DATE:** 14-11-14

Feedback Comments: _____

_____ **Grade:** _____

LECTURER'S SIGNATURE: _____ **DATE:** _____

Time and Date Received: (Office Use Only)

TIME: _____ **DATE:** _____ **INITIALS:** _____

CONTENTS

LIST OF FIGURES

LIST OF TABLES

EXECUTIVE SUMMARY

This project report presents documentation of the steps that were performed during the acquisition, testing of bamboo specimens, followed by designing and prototyping of a bamboo velomobile spaceframe using those specimens.

Mechanical properties tests yielded insight into the maximum stress tolerances of the *Himalayacalamus hookerianus* specimens which were harvested near Dunedin. Specimens were heat treated prior to testing that was performed in accordance with ISO 22157-1/2 recommendations. Values for properties that were obtained through testing are:

Maximum bending stress $= 42.9MPa$

Maximum parallel fibre shear stress $= 4.4MPa$

Maximum tensile stress $= 63.0MPa$

Maximum compressive stress$= 37.5MPa$

Calculated conditions of the three highest load scenarios that could be expected during velomobile operation which were high speed cornering, impact with a step in the road surface, and deceleration under maximum braking yielded values for direct frame loading scenarios. Material mechanical properties and frame loading values were combined in Solidworks software models to develop a frame design which displayed an appropriate factor of safety under the simulated conditions. The highest stressed section of this frame was located around the front wheel axle mount. This frame section was isolated as a separate model and then prototyped using the earlier tested bamboo specimens and an experimental flax fibre and epoxy resin joint wrapping technique. Testing of the prototype under the same loading orientation and fixture conditions as the highest-load simulated scenario (high speed cornering at $0.65g$ horizontal) failed to damage the prototype and a factor of safety value for this section of the frame was calculated at a minimum of 4.43 without failure being exhibited. Results from this prototyping experiment concluded that the Solidworks models had a tendency to understate the strength of the bamboo frame as a result of a number of input factors.

1 INTRODUCTION

The use of technical materials in human powered vehicle development plays a vital role by facilitating constant improvements in quality and performance of vehicles by allowing them to become faster, and stronger while maintaining their light weight functionality. At the current forefront of these developments is the use of composite fibre reinforced plastics to create moulded components and structures which have optimized shapes and designs to obtain high strength and low weight. Velomobile design is one such area of human powered vehicle development where composite plastics reign as the most popular material. In this design area the main undesirable feature of composite plastics is amplified by the complexity of the mouldings used and the volumes of materials required. The field of velomobile design would benefit greatly from an alternative material that can be used to cheaply produce the structures required to support a rider and tolerate the loads and stresses applied to the frame during use.

Bamboo has been used to fabricate structures for hundreds of years, and is a strong and durable material with a high strength to weight ratio. Bamboo grows in a large range of sizes, with the most common being of similar dimensions to the frame tubes commonly used in bicycle construction. The properties of bamboo when combined with modern jointing techniques developed through composite plastic technology have led to it experiencing a recent resurgence as a material for high performance bicycle frame construction. This has caused this author to wonder whether bamboo could also be adapted for use in velomobile design too. The use of a spaceframe design to create an integrated frame structure that can support the required loads and provide the required rigidity would allow velomobile design and construction companies to utilise a much cheaper material that also has a lower environmental impact.

This project investigates the potential for the construction of a bamboo velomobile spaceframe using bamboo that has been sourced from within the Dunedin region, and presents the process steps required to successfully design a spaceframe using a variable natural material of unknown mechanical properties.

2 BAMBOO AS A MATERIAL FOR VELOMOBILE DESIGN

2.1 PRIOR RESEARCH

The topic for this project is based on researched information obtained from the literature review that can be found in Appendix A of this report. The review investigates existing literature related to the topic of lightweight velomobile construction and design, with the purpose of investigating new possible construction methods for frame and fairing design. Technical topics covered include frame materials, frame design techniques, and aerodynamic fairing structure creation. Literature was sourced from a variety of locations and includes thesis papers, engineering reports, books, magazine and newspaper articles, blog posts and various types of other web-based content. All content discussed and referenced is relevant to the topic and this review demonstrates an accurate portrayal of the knowledge base that is publically available relating to the topic.

While the literature shows that commercial HPV manufacturers are generally focusing on using increasingly technical materials in the development of velomobile designs, other evidence suggests that strong potential exists to develop materials and technology such as bamboo frames and stretched skin fairings to create velomobile designs that perform in a manner comparable to their commercial counterparts, whilst having a more desirable smaller environmental footprint and lower materials cost.

2.2 ENGINEERING FIELD OVERVIEW

Human powered vehicles have been in a constant state of development since the bicycle was first invented in the early 19th century; in the context of urban travel using road infrastructure, the velomobile is arguably the most appropriate design developed to date.

Figure 2-1: High end commercial velomobile models are efficient, attractive and expensive (Velomobile.NL, 2014; Go-One, 2014; Milan Velomobile, 2014)

A velomobile consists of three bicycle wheels supporting a rider who is seated and pedalling in a recumbent position, both the vehicle frame and rider are enclosed inside an aerodynamic fairing. Commonly available in Europe and North America, with Australian manufacturers being the closest available sources to New Zealand, this transport product has yet to take a substantial sector of the New Zealand human powered vehicle market. One significant factor contributing to the slow uptake of velomobiles is the current cost. Prices range from NZ$7,500 to NZ$15,000, depending on brand, model, features, unique materials and size.

2.2.1 STANDARD VELOMOBILE CONSTRUCTION TECHNIQUES

Most commercially available velomobile models are constructed using a composite fibre reinforced plastic monocoque shell to which drive, steering and seating components are mounted. This method of construction creates a lightweight and strong structure and makes mass production of units fast and simple. However this method of construction also contributes significantly to high unit costs and substantial embodied environmental impacts through the use of expensive fibres and resins and complex moulds.

2.2.2 BAMBOO FRAME CONSTRUCTION

Bamboo is a lightweight and strong material that is readily available in New Zealand at low cost; its uses for construction purposes including mechanical properties and jointing techniques have been explored in many other engineering contexts including building construction, fibre reinforced plastic development and bicycle frame construction. A more recent resurgence in high-end bicycle frame construction demonstrates the suitability of this material to the construction of a suitable velomobile frame. Bicycle frame construction examples commonly utilise the bamboo culm in its unmodified cylindrical form, where it acts as a substitute for metal or composite plastic tube shaped frame members. This is the cheapest form of use however it also has the least predictable properties. Variation in key tube dimensions such as diameter, wall thickness and fibre density can fluctuate according to a range of species and environmental factors. Manufacturers such as Hero Bikes have explored modifying the culm section for greater consistency (HeroBike, 2014), however this leads to significant increases in material costs and time in processing, and the resulting products have only spent a short time on the market so far so their durability remains uncertain.

2.3 ADDITIONAL PROJECT REASONING

There are a number of commonly known economic, social and environmental drivers for development of more sustainable and affordable methods of personal transport, these all stem from a shared desire to develop a society that can maintain its current mobility while operating efficiently and in a resilient manner. Human powered vehicles are currently able to meet these specifications in an operational sense, the next step in their development is to

ensure that they can also be designed and produced using materials and techniques that do not undermine the benefits they deliver to the end user.

3 BAMBOO RESEARCH AND DATA COLLECTION

The use of bamboo as the focal point of this project meant that a significant portion of the work required related directly to the research and collation of information about the bamboo being used; this included investigating and applying processes for treatment and a selection of load-testing experiments, followed by calculating the range of maximum allowable stress values for the bamboo. This chapter outlines the various theories applied during this phase of the project, including the experimental procedures performed and the data gathered from these. Data is collated into a set of estimated mechanical properties which are then utilised during the following chapters of this report to perform simulated testing on designs.

Much of the research performed in this section is based on assumptions about the accuracy of measuring and testing equipment, for which error and inconsistency could not be calculated. The processes followed and results gathered include some significant inferences with particular regard to the mechanical properties. Any use of this data by other parties should be done so with care and due regard given to what may appear to be great leaps of judgement – for the most part these have been necessitated by the timeframe and scope of the project, rather than informed but un-recorded knowledge. Data and processes found in this report are not intended to be used as a guide in isolation of the references cited, nor are the values gathered guaranteed to be relevantly accurate by the author, although due care has been taken to try and ensure this wherever possible.

3.1 BAMBOO SELECTION FOR CONSTRUCTION

While this project involves performing testing on specimens before use, an understanding of what gives bamboo its strength and physical properties is helpful to inform during selection of species. This can enable more useful and higher stress tolerance results from the testing and provide insight into the reasons behind test results should they not be obvious.

3.1.1 PHYSIOLOGY

Bamboo is a large grass species which grows shoots from the base of the plant. These shoots develop into long narrow circular sectioned culms which are hollow and divided at regular intervals by nodes. This growth pattern allows for regular harvesting of material without damaging the productivity of the plant. Long fibres in the culms run parallel along the length and are dispersed through the wall of the culm in highest fibre densities (volume ratio) at the outer surface, this volume ratio reduces towards the inside of the culm wall, (Jansen, 2000) affecting the strength properties in the same manner.

Figure 3-1: Bamboo Himalayacalamus hookerianus specimen split in half exposing node boundary and wall cross section (dark colour is due to heat treatment)

3.1.2 DESIRABLE SPECIES

In selecting species that are suitable for construction, both the species type and the physical dimensions make up a portion of the desirability. Species need to be capable of growing to physical dimensions necessary to provide the required strength for construction, and they also need to develop strong fibres and structures within the culm which will help support loads applied during use. There are a number of species in New Zealand which are renowned for their strength and durability, and commonly used overseas for construction, the most popular of these are *Phyllostachys bambusoides* and *P. edulis*. However these species were unavailable in Dunedin as they do not grow in the temperate climate present. The nearest locations were found in the North Island of New Zealand. With regards to physical dimensions, it was determined that these should be in the approximate range of $20 - 50mm$ in diameter and as long as possible. This was based on the observation of other bicycle construction projects which used specimens of this approximate size. It was determined that if bamboo could be temporarily assumed to have consistent strength and flexural characteristics, then the selection of the specimens of the appropriate size would be important to optimise one of the goals of the project was to enable a balance between rigidity, strength and weight to be obtained. If specimens were too large in diameter then designing and constructing a spaceframe that provided rigidity, and light weight characteristics would be difficult, and if specimens were too small then obtaining the desired strengths would be difficult. The assertion at this point was that the $20 - 50mm$ range would provide balance between these properties.

3.1.3 SPECIES USED

Specifying locally sourced bamboo created restrictions on the species that were available. Through contact with the New Zealand Bamboo Society and the staff at the Dunedin Botanical Gardens, a contact was established with a grower located on the Otago Peninsula near Dunedin, who had a collection of various species and was willing to allow the harvest of some specimens for the purposes of the project. On inspection of the available species in the collection, it was decided that the largest growing variety would be most suitable due to its diameter and uniformity of growth; this species was *Himalayacalamus hookerianus*, also known as 'Himalayan blue bamboo'. In Dunedin, this grows to a maximum of $30mm$ diameter (when green) and up to $5m$ long culms which taper gradually from the base. A selection 16 of the largest diameter culms available were picked, these ranged from $20 - 30mm$ in diameter and were cut to $3m$ lengths for transport, keeping the larger diameter sections and discarding the narrow and leafy tops. Specimens were collected on 11/04/2014.

3.2 HEAT TREATMENT

The bamboo stock gathered had not completely dried by the time this project needed to begin meaning heat treatment was necessary to remove additional moisture content. Additionally, given the similarities between timber and bamboo, heat treatment theoretically should increase the stability of the stock (through conversion of the starches in the bamboo to sugar which produces a more stable chemical structure), resulting in the bamboo being tougher, more water resistant and also more resistant to microbial attack and decomposition. (Hill, 2006)

Full details of the technique used to heat treat the bamboo stock including the trial heating, apparatus and final process used are outlined in Appendix B of this report.

The heat treatment process applied was based on research and documentation by Schott (2006) who – after testing of heat treated specimens subjected to a range of variables – outlined parameters in his findings which allowed for moisture removal without loss of structural integrity. Schott suggests in his findings that the easiest way to ensure that this does not occur is to avoid high temperatures ($> 200°C$) and monitor the colour change of the material during heating to ensure that it does not darken substantially.

The method used for this project was validated through a trial procedure where a small selection of samples were heated and colour change over time was monitored by removing and inspecting small sections of the samples at ten minute intervals. Results from the trial run showed steady loss of moisture and during heating, with some moisture being present in the samples after the heating had been completed (Figure 3-2). After 50 minutes of exposure to heat, specimens began visibly browning through the wall cross section and the process was stopped.

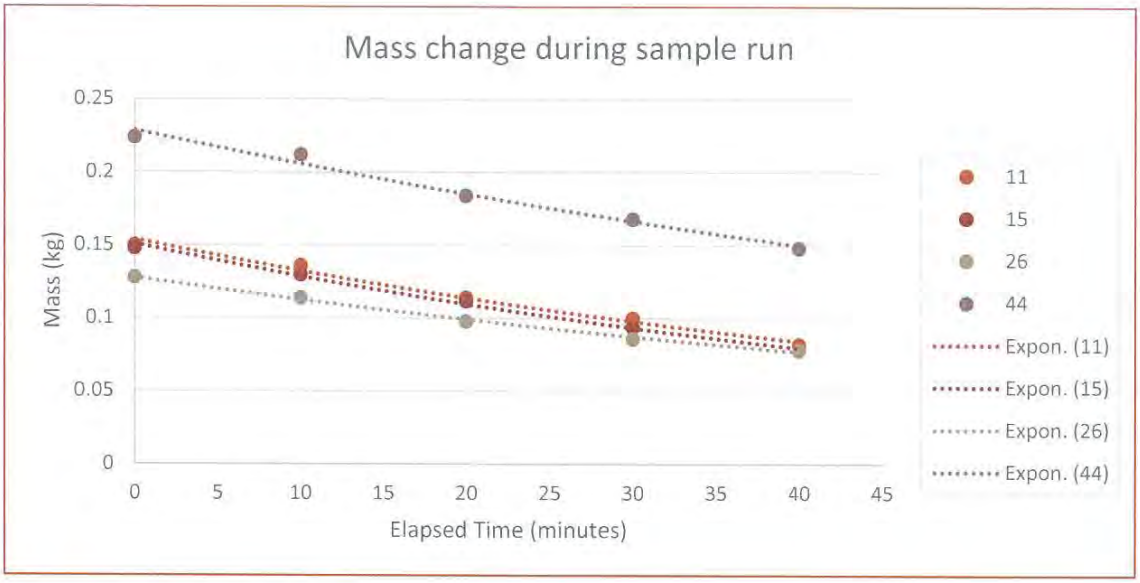

Figure 3-2: Plotted results of mass reduction (moisture loss) during sample specimen heat treatment.

The final heat treatment process exposed the remaining culms to ~180°C temperatures for two concurrent 20 minute periods, with specimens being removed, inverted and returned to the kiln after the first period. This resulted in specimens with a significantly reduced weight and loss of green colouring, but little or no darkening of the internal culm structures. No splitting or structural damage was noted to have occurred to the culms during this process.

3.3 MECHANICAL TESTING

For the purposes of this project it was required to know the mechanical properties of the bamboo stock that would be used for the prototype construction. Because bamboo is a natural product, the effect of varying growth patterns between species, growing climate, and plant/culm age all contribute to variation in mechanical properties. It was difficult to obtain mechanical property data consistent with the stock that has been sourced locally. To obtain this data it was necessary to perform mechanical property tests directly on a representative sample of the stock available, and apply the results to a set of assumptions regarding the entirety of the stock available.

Investigations into standards and procedures for bamboo testing yielded few results, with the only official publication being produced by the International Organisation for Standardisation (ISO) (2008). ISO 22157 '*Bamboo - Determination of physical and mechanical properties*' is made up of two separate parts; part one of the standard describes the theories used to derive the recommended series of appropriate tests for determining mechanical properties of a sample of specimens, part two is an approximate laboratory guide for the implementation of these tests, and an outline of the data processing necessary to yield accurate and representative results.

Numerous other relevant works relating to mechanical properties exist, including a PhD Thesis by Oscar Antonio Arce-Villalobos *Fundamentals of the design of bamboo structures* (1993) which discusses the detailed testing of specimens and the micro-structural responses of the material to loading scenarios. This work looks very closely at mechanical properties of various bamboo species (although not *Himalayacalamus hookerianus*) and the level of detail explored is beyond the scope of this project, however data from the calculations is used later in this report to compare validity of observed results.

A technical report by Jules Janssen *Designing and building with bamboo* (2000) outlines testing parameters and addresses the feasibility of bamboo use particularly in structural design applications, but also includes processed forms such as woven fibre matts and isolated-fibre reinforced plastic composites. Janssen looks at economic feasibility in detail and uses this to construct a convincing case for the use of bamboo in place of steel and timber for many applications. A series of summary literature reviews by Dr. Ing. Evelin Rottke (2001, 2002) that look at existing research and existing values for mechanical properties have also been considered, values listed in these reviews are also used to compare validity of observed results found in this report.

Using ISO 22157, a set of testing protocols were developed which could be used to assess the mechanical properties of the *Himalayacalamus hookerianus* specimens which had been gathered and heat treated as per processes outlined in Appendix B. The following is a summary of the tests performed and an analysis and presentation of the results gathered.

3.3.1 TESTING OBJECTIVES

Prior to designing and testing of the prototype bamboo velomobile frame, data relating to four key mechanical properties of the bamboo was required.

- Full culm ultimate bending stress ($\sigma_{bending}$)
- Parallel fibre ultimate shear stress ($\tau_{parallel\ fibre}$)
- Axial ultimate tensile stress ($\sigma_{tensile}$)
- Axial ultimate compressive stress ($\sigma_{compressive}$)

When combined, these individual properties yield a description of how the bamboo specimens which the prototype is to be comprised of will perform when subjected to probable loading scenarios.

Other mechanical properties required for the simulation process are the Modulus of Elasticity (E), the Shear Modulus (T) and Poisson's ratio (υ). The testing and calculation of these three values for the bamboo specimens was not performed as it required the use of strain gauges and other equipment that was unavailable. A summary of researched values that have been used in place of gathered data is presented in Section 4.4.4 (Table 4-8).

3.3.2 GENERAL ASSUMPTIONS

For the purposes of this project, a limited quantity of *Himalayacalamus hookerianus* specimens were collected and processed. Because of this physical limitation on available resources, the determination of sample sizes for testing purposes was difficult to optimise. ISO 22157 provides guidelines for selecting sample sizes based on statistical accuracy and suggests that an optimum balance between representation and quantity of tests performed can be found at a sample size of $n = 12$ whereupon the sample data can be stated to be accurate to $\pm 10.6\%$. To provide statistical representation of the population size while still maintaining substantial stock numbers for use in prototype construction, it was decided that approximately one quarter of the specimens would be tested, this amounted to approximately $n = 10$ specimens per test.

3.3.3 SAMPLE SPECIMEN SELECTION

Criteria for selection of specimens for mechanical testing attempted to produce the targeted outcome of defining the lowest tolerable stress values for the entire population of specimens while still preserving a substantial portion of the population for later use in the prototyping of a frame. Given the expected variation between specimens within the population, a selection was made based representation of all of the visible variables that could be identified. The most weighted of these variables were physical size and colour after treatment. Additional to this, density estimates were made and also used during selection.

Tests were performed in a designated order to optimise the use of material, bending tests were performed first on the full specimen section followed by cutting the undamaged portions of the same specimens so that compression, tension and shear tests could be performed without consuming any additional specimens. In accordance with ISO 22157-2, bending test specimens needed to have a length of at least $27 \times Mean\ diameter$ to avoid failure due to shear along the neutral axis. This meant that priority was given to the longer specimens, as sections had been cut close to this threshold in order to fit them into the kiln for heat treatment.

3.3.4 TESTING APPARATUS

All of the following four loading experiments were performed using the same Dennison Universal Testing Machine located at the Otago Polytechnic. This apparatus is shown in Figure 3-3. It consists of a vertically aligned set of three crossheads, the upper and lower of which are fixed in place and the central crosshead is moved hydraulically at controlled rates downwards. The central crosshead is equipped with a hemispherical bearing on its underside for uniform load distribution; wedge-tightened vice grips are located on its upper side, these align with inverted wedge-tightened vice grips mounted to the upper fixed crosshead. Tension experiments were performed using the central and upper crossheads, compression, shear and bending applications used the central and lower crossheads. Downward movement

of the central crosshead is controlled via a large wheel mounted on the control panel, upward movement is obtained through the use of a lever actuated pressure release valve.

Gauge outputs provide digital readings of the head movement in mm, and analogue readings of the force being applied by the head. The loading is presented on a large dial, with maximum loading value is also being recorded using this dial, enabling the load at failure to be determined. Further details of the specimen mounting apparatus used in each experiment are provided in the sections relating to each individual experiment. Accuracy of the readings provided by this apparatus is unknown, as it had not been calibrated since 2012, for the purposes of this project any possible data reading error values for this experiment will be regarded as insignificant/incalculable.

Figure 3-3: Dennison Universal testing machine used for mechanical loading of specimens

3.3.5 STATIC BENDING STRESS

Figure 3-4: Loading and failure of specimen under static four-point bending test.

To obtain data which demonstrates the range of static bending stress which any given sample in the population of specimens is capable of bearing, a four point bending test was carried out on a representative selection of specimens. In order to encourage the most amount of bending while reducing the possibility of crush failure to the specimen, specimens were selected which were both long and had nodes located close to or at the ends. This is in accordance with ISO 22157-2 which notes that the nodes have a higher tolerance to radial loading and so are less prone to crush failure than the internode areas. Length of specimens was limited to the longest specimens available, these ranged from $750 - 800mm$ because they had been cut to fit in the kiln during the heat treatment process.

Full details of the technique used to test the maximum static bending stress which the bamboo stock was capable of supporting, including the calculations and a detailed discussion regarding the results gathered during this experiment are outlined in Appendix CA of this report.

During application of load, specimens all exhibited large amounts of deflection before failure, some deflected by up to $1/30^{th}$ of the total span. While the modulus of elasticity for bamboo in this scenario was not calculated, this is a substantially high value.

Calculated results for stress values in this experiment are shown in Table 3-1, they demonstrate a large amount of variation over the specimens which were tested. Use of any maximum bending stress values for design purposes should therefore implement the lowest calculated value of $42.9MPa$.

Table 3-1: Summary of critical values from bending stress experiment

Sample Size (n)	Min	Max	Range	Average	Standard Deviation
10	$42.9Mpa$	$144.4Mpa$	$101.5Mpa$	$82.4MPa$	$28.4Mpa$

3.3.6 SHEAR STRESS

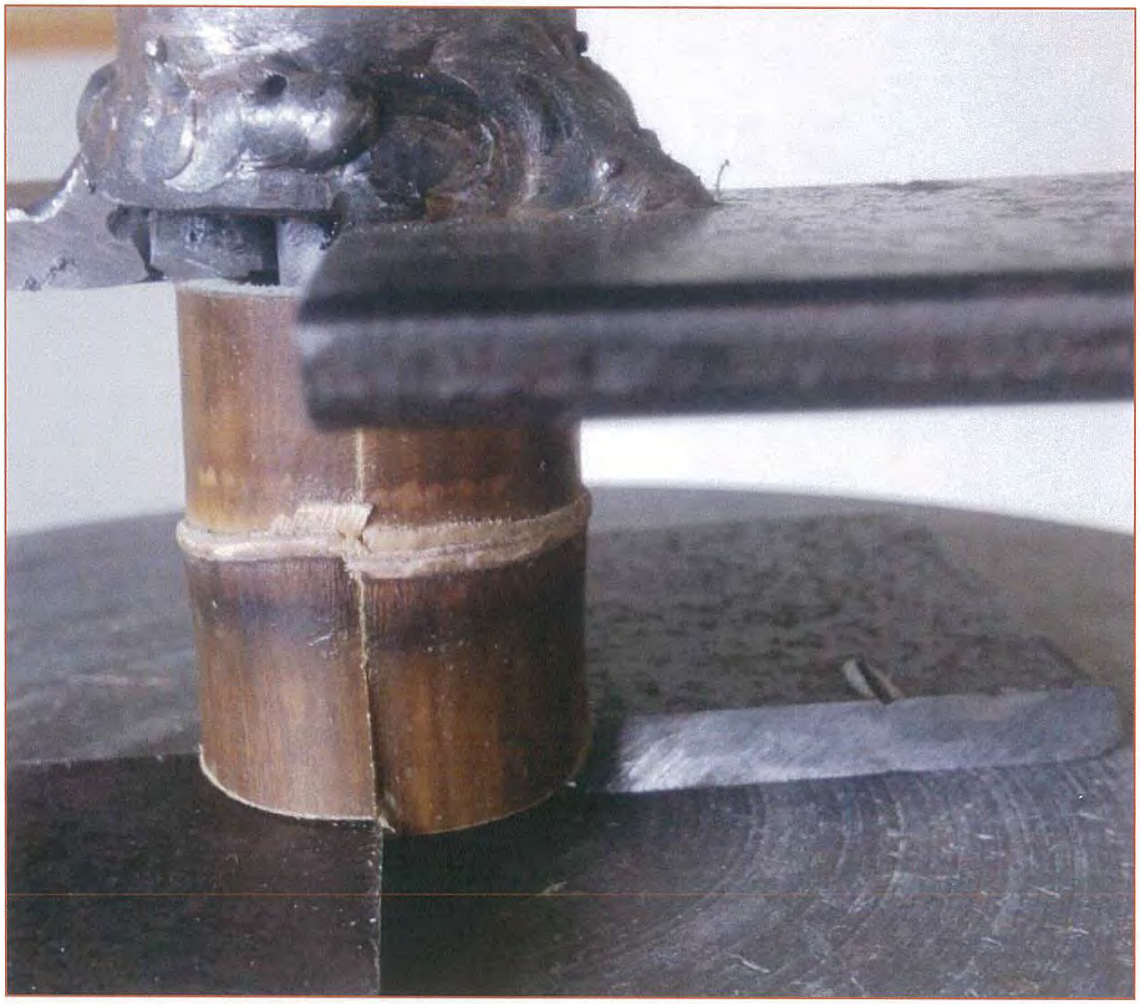

Figure 3-5: Axial shear failure of specimen using testing apparatus

To obtain data which demonstrates the range of shear stress parallel to the specimen fibres which any given sample in the population of specimens is capable of bearing, shear load testing was carried out on a representative selection of specimens. Samples were cut to a length approximately equal to their diameter in accordance with ISO 22157-2, and the experiment included specimens with and without nodes present in the sections being tested.

Full details of the technique used to test the maximum shear stress which the bamboo stock was capable of supporting, including the calculations and a detailed discussion regarding the results gathered during this experiment are outlined in Appendix CB of this report.

Specimens performed poorly under shear loading as was expected due to the parallel-fibre structure of the bamboo culms, Table 3-2 shows the calculated results for stress values in this experiment. A moderate range is present, showing some variation between tested specimens. No significant variation was noted between specimens with a node and specimens

without a node during this experiment. Use of any maximum shear stress values for design purposes should implement the lowest calculated value of $4.4MPa$.

Table 3-2: Summary of critical values from shear stress experiment

Sample Size (n)	Min	Max	Range	Average	Standard Deviation
12	$4.4MPa$	$11.1MPa$	$6.7MPa$	$8.45Mpa$	$1.94Mpa$

3.3.7 TENSILE STRESS

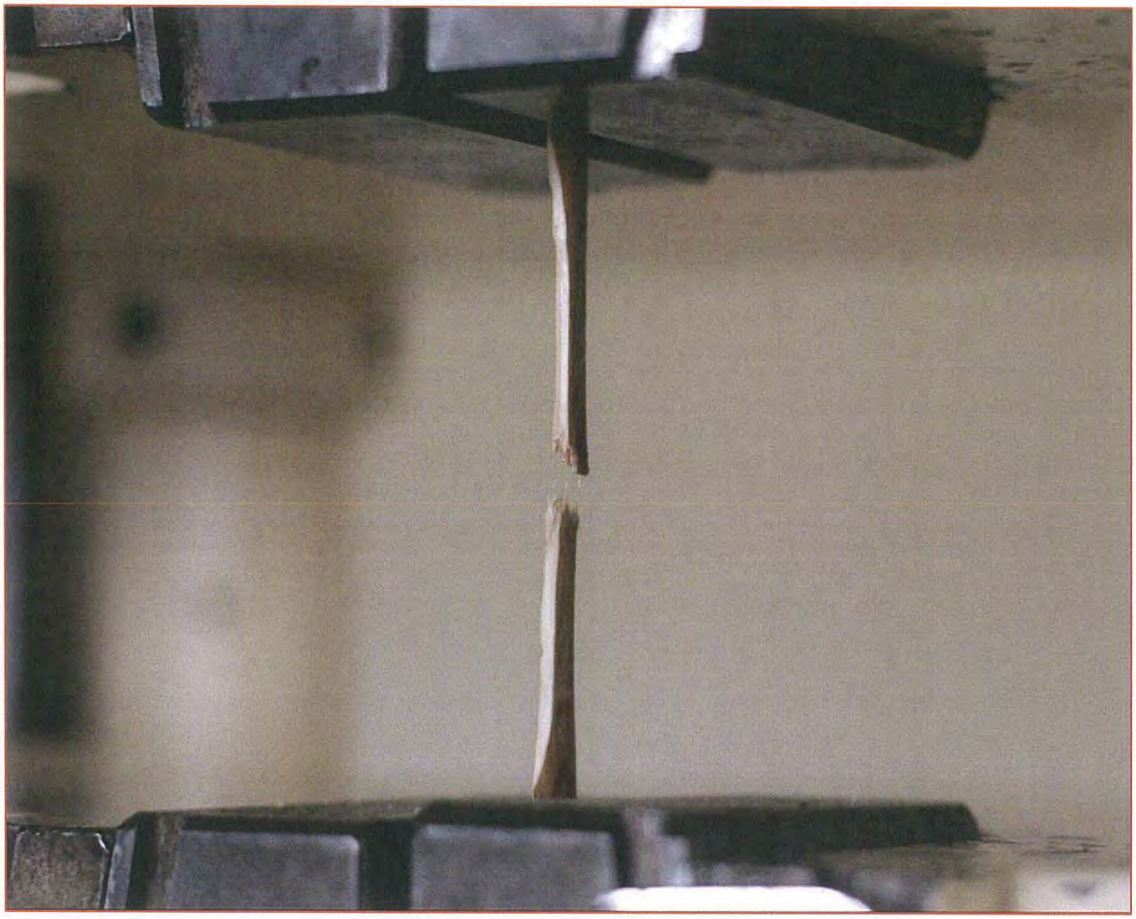

Figure 3-6: Tensile test of specimen showing failure point at node and separation just after fracture

To obtain data which demonstrates the range of tensile stress acting parallel to the specimen fibres which any given sample in the population of specimens is capable of bearing, tensile load testing was carried out on a representative selection of specimens. Samples for testing were cut from long narrow strips of culm wall and shaped in accordance with ISO 22157-2 so that a narrow section in the middle would fail while the ends would be supported by the apparatus. Specimens with and without nodes in the narrow section were tested.

Full details of the technique used to test the maximum tensile stress which the bamboo stock was capable of supporting, including the calculations and a detailed discussion regarding the results gathered during this experiment are outlined in Appendix CC of this report.

Results showed that bamboo fibres can support a large amount of tensile stress, however this value is markedly lower when there is a node present in the area being tested. Table 3-3 shows the results from these two sets of experiments, with a 250% higher average tensile stress in specimens without a node as compared to specimens with a node. Use of any maximum tensile stress values for design purposes should implement the lowest calculated value of $63.0MPa$ regardless of whether there is a node present in the specimen.

Table 3-3: Summary of critical values for tensile test experiment

Node in specimen?	Sample Size (n)	Min	Max	Range	Average	Standard Deviation
No	4	$174.6MPa$	$275.0MPa$	$100.4MPa$	$223.7MPa$	$51.0MPa$
Yes	6	$63.0MPa$	$108.2MPa$	$45.2MPa$	$86.7MPa$	$17.7MPa$

3.3.8 COMPRESSIVE STRESS

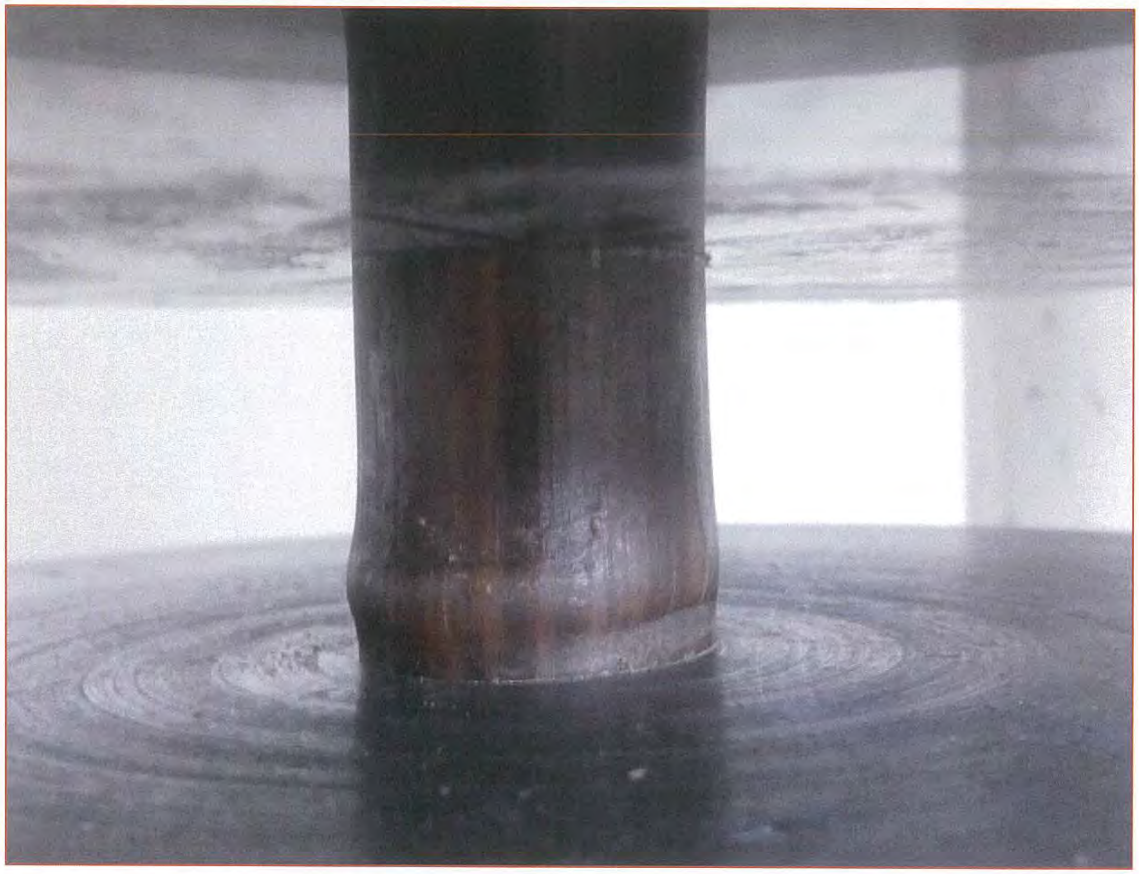

Figure 3-7: Compression failure of specimen under loading

To obtain data which demonstrates the range of compression stress acting parallel to the specimen fibres which any given full culm section in the population of specimens is capable of bearing, compressive load testing was carried out on a representative selection of specimens. Samples were cut to a length approximately equal to their diameter in accordance with ISO 22157-2, and the experiment included specimens with and without nodes present in the sections being tested.

Full details of the technique used to test the maximum compressive stress which the bamboo stock was capable of supporting, including the calculations and a detailed discussion regarding the results gathered during this experiment are outlined in Appendix CD of this report.

Results showed that bamboo can support moderate amounts of direct compressive stress in full culm sections, the range of data gathered was small, showing consistency across the specimens tested. Use of any maximum compressive stress values for design purposes should implement the lowest calculated value of 37.5MPa.

Table 3-4: Summary of critical values for compression test experiment

Sample Size (n)	Min	Max	Range	Average	Standard Deviation
11	37.5MPa	62.8MPa	25.3MPa	50.0Mpa	8.0Mpa

3.3.9 TESTED PROPERTIES CONCLUSIONS

The results of the mechanical property experiments described in the previous chapters provides enough information to gain insight into the use of bamboo for spaceframe design. Table 3-5 outlines the values gathered from this testing, these are values which during the design and simulated testing process will be set as the target maximum values for stress present in spaceframe members. This table also shows this maximum stress values if an overall factor of safety of 2 or 5 is to be implemented in the design.

Table 3-5: Maximum allowable stress in design components under imposed factors of safety (values in MPa)

Stress property	F.O.S = 1	F.O.S = 2	F.O.S = 5
$\sigma_{bending}$	42.9	21.5	8.58
$\tau_{parallel\ fibre}$	4.4	2.2	0.88
$\sigma_{tensile}$	63.0	31.5	12.6
$\sigma_{compressive}$	37.5	18.75	7.5

4 VELOMOBILE FRAME DESIGN

Developing a design for a bamboo velomobile spaceframe which is successful requires an understanding of the material being used for the design, and the establishment of dimensional parameters which the frame could be expected to operate within. Using the *Himalayacalamus hookerianus* bamboo materials data from the previous Section and a series of requirements and specifications which have been determined to include the highest plausible loading scenarios for a vehicle of this type, a three dimensional model has been developed and tested using the Solidworks 2013 software package. The layout of this model was based initially on estimates for frame shape and developed through use of simulated loading scenarios (also in the Solidworks program) to assess the induced stress concentration and deflection levels. This Section outlines the process which was undertaken to complete the design that is described; included are details of the design itself, as well as the information and assumptions that were utilised to create it.

4.1 SPECIFICATIONS

Specification parameters selected to be considered and assessed within the scope of this design include the following (including both the imperative outcomes as used to define success, and the desirable outcomes which were used to enhance the value of the design):

- **Rider clearances** – the frame design **must** provide enough space to accommodate the rider without impeding their ability to operate the pedals and various controls.
- **Physical dimensions** – the frame design **must** allow for appropriate component mounting clearances and mounting points, and other external geometric values such as ride height and turning circle.
- **Loading and performance capabilities** – the frame design **must** be able to tolerate the applied loads associated with riding without failure due to induced stress in the frame members. At the same time, the frame design **should** provide a lightweight structure which is comparable to available velomobile models.

The following details outline the scope of these parameters and any relevant assumptions made to conclude the magnitude of these parameters.

4.1.1 RIDER DIMENSIONS

When using the velomobile the rider will be seated in a recumbent position (feet first and seated with a supported abdomen), to ensure that this is position is able to be maintained for any length of time, and that the various functions of the velomobile (pedals and steering equipment) may be operated in comfort and safety it is necessary to design the frame to meet both ergonomic and space requirements. Also of note is the effect that the increase in space has on the overall size of the velomobile fairing – this should be minimized so as to also keep the bluff-body air drag component of the frame as low as possible.

A number of assumptions have been made regarding the category of rider that this design is to be capable of safely supporting, because this is primarily a research project it was decided that the dimensions and capabilities of this author would be as suitable. Physical dimensions were taken and combined with research into seating and height configurations from existing manufacturers to develop a three dimensional model representative of the space that the rider requires within the velomobile. Figure 4-1 shows the development of this clearance shape and the position of the rider relative to the wheels.

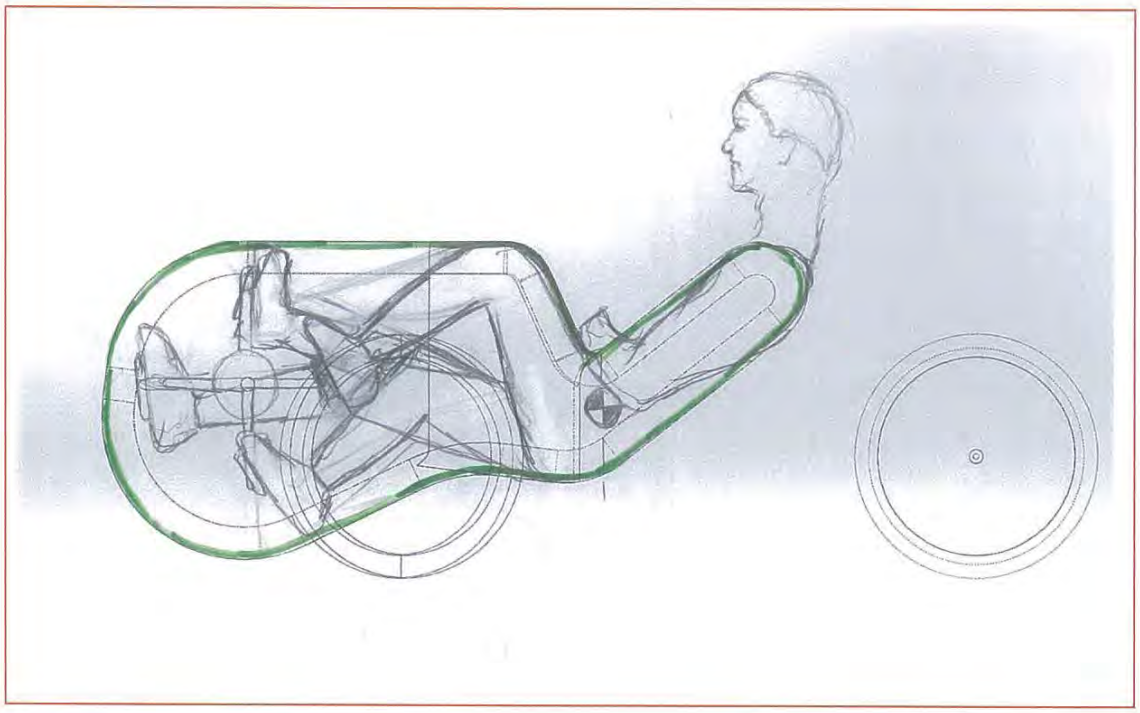

Figure 4-1: Rider geometry for frame design clearances

The other important and relevant measurement is rider mass. A value of $85kg$ will be used for calculations; given that one of the targeted outcomes of this project is for the complete velomobile and frame mass to be $25kg$ or less, the total combined mass of rider and velomobile will then be $110kg$.

4.1.2 FUNCTION AND ADDITIONAL COMPONENT REQUIREMENTS

The frame has been designed to allow direct mounting of the most commonly available velomobile components, and provide a similar condition of ride to commonly available velomobile models. A summary of specifications that this design has been created to emulate can be found in Table 4-1, data for this has been compiled through an informal review of the popular designs that are currently available, and the relevant capabilities and design properties that popular designs exhibit. These details have only been assessed where they are relevant to the design of the frame. Specifically this includes the physical dimensions

required to emulate the performance and handling of popular velomobile models, and considerations relating to the use of popular components which provide this performance.

Table 4-1: Function and component dimensions

Design feature	Specified detail/dimension
Wheel arrangement	Tadpole
Wheelbase (length)	1250mm
Wheelbase (width)	730mm
Wheel + Tyre diameter	465mm
Wheel axle length	120mm
Tyre width	50mm
Turning radius (outer front wheel)	12m
Front wheel angle range (lock-lock)	35 degrees
Lowest point ride height	70mm
Crank arm length	165mm
Pedal spacing	200mm
Centre of gravity location behind front axle	415mm

4.1.3 LOADING AND PERFORMANCE CAPABILITIES

During operation of the velomobile, the frame will be subject to loading of various different magnitudes and in various directions. It is important to ensure that during these loading scenarios the frame is able to maintain its structural integrity. Design of the frame including quantity, orientation and dimensions of the bamboo members will determine how the frame reacts to applied forces and how the stress is distributed across all of the members. This design described in this section was developed using trial and error techniques in combination with Solidworks finite element analysis processes. The goal of the trial and error process was to establish a frame design which would provide an overall Factor of Safety (FOS) of 2 or more, under any of the calculated maximum loading scenarios. The reason that the target FOS has been set at such a low value is because the total mass of the frame is also required to be kept to a minimum to satisfy the performance requirements of a human powered vehicle and maximize the limited power capacity of the rider. The designed frame uses bamboo from the same batch of *Himalayacalamus* specimens as were tested in Chapter 3. The frame is held together with joints that are constructed based on available examples of constructed bamboo bicycles. Details of the joints used are provided in the Section 5.3 on prototype construction. Because of the inherent complexity involved in designing fibre reinforced plastic joints for bamboo, it was decided that the joints used should be over constructed using excess bulk of fibre and resin than is likely required to obtain strengths that are comparable to the bamboo

itself. The performance of the bamboo frame members could then be observed in isolation from the performance of the joints. The optimization of these joints remains a task worthy of another independent research project altogether. Variables including fibre type, strength, layup, orientation and quantity combined with quantity and type of resin in the structure would all make a difference to the performance of the joint (Bamboo Bike Supplies, 2013; Calfee, Building Bamboo Bikes, 2014).

The identification and calculation of the loading scenarios during which maximum forces and induced stresses would be present in the frame is addressed in detail in Section 4.3. Identification of the main situations worthy of consideration, and a described calculation process which isolates the maximum forces on the frame during that scenario has been included, and the information that outlines the scenarios of interest was sourced from existing manufacturers.

4.2 INDUSTRY DESIGN SPECIFICATIONS

In order to establish the commonly recognised high loading scenarios which a velomobile would be subject to during operation, companies who are already in the velomobile construction industry were contacted. Information was requested on the design standards which they used and the main considerations that they made when designing velomobile frames. Of the five leading manufacturing companies contacted (Velomobiel.NL, Sinner Bikes, Bluevelo, Trisled and Mosquito Velomobiles) only three responded, and all stated that they knew of no standards relating to velomobile design. Both Velomobiel.NL and Sinner Bikes said that they had built the majority of their designs using a trial and error approach, basing improvements to designs on observed failures and unwanted performance features such as excessive flex or deflection in elements of the design.

Sinner bikes suggested that it would be very difficult to calculate all of the potential loading scenarios, but hypothesized that the highest loadings would come from impacts such as road surface irregularities (potholes, guttering/kerbing, gravel etc.) and that this would be a good focus for maximum loading design parameters.

Velomobiel.NL outlined two field experiments that they had performed, the first of which involved measuring G-forces experienced during cornering at maximum possible speed. The second experiment was a stoppage test from a speed of $50km/h$ measuring the stopping distance at full braking power. Data provided has been used to calculate the loading scenarios that both experiments apply to the velomobile frame, the results of this will contribute to goals for the prototype designed during this project to meet to satisfy similar requirements to industry standard. For these experiments it is assumed that Velomobiel.NL has used standard velomobile front wheels ($405mm$ diameter (20")) fitted with medium volume tires, giving an overall wheel diameter of $465mm$ (Schwalbe, 2014).

4.3 LOADING SCENARIOS

Designing a bamboo velomobile spaceframe that will be capable of performing under expected conditions involves the assessment of a number of variables and the determination of what the extreme cases of these expected conditions could include.

This section investigates three loading scenarios which have been identified as situations where the frame of a velomobile would be exposed to high load conditions, and which could be reasonably expected to occur during the life of the velomobile. The pretext for these scenarios is based on information provided by companies mentioned in the previous section, who currently manufacture velomobiles – suggestions for performance specifications which their velomobile designs seek to emulate have been considered and used to produce the input values for the three scenarios. The three scenarios are:

1. Impact with road surface irregularity
2. Cornering at maximum velocity
3. Brake-induced deceleration

Each of the three scenarios has been examined in isolation and the maximum loading forces that would be applied to the frame during the scenario have been calculated. Resulting data was used during the design process to ensure that the frame is capable of supporting expected maximum forces from each of the scenarios. The assessment of design success was exhibited in its ability to support these forces without higher-than-tolerable stress levels being inducing in any of the bamboo frame members.

The specifications of the rider make up one whole section relating to the loads which the rider is able to apply to the frame through pedalling, braking and cornering – as a function of their physical dimensions, strength, mass (and its distribution) and riding abilities. The other performance criteria relates to unpredictable circumstances such as accidents and impacts with both stationary and moving objects.

A discussion of additionally considered parameters and assumptions relating to these scenarios made can be found in Appendix D.

4.3.1 IMPACT WITH ROAD SURFACE IRREGULARITY

In calculating the impact loading that would be present during a collision with a road surface irregularity such as a pothole, it is important to note that there are a lot of variables which will affect the outcome. For the purposes of calculating the worst case scenario, these variables have been taken to their reasonable limit to determine the maximum possible loading that could be present under the conditions posed.

Figure 4-2 shows the initial and final stages during impact of a wheel of diameter (d) with a $90°$ angled step-up of height (h) with the resulting forces shown in red acting in a

combination of horizontal (F_x) and vertical (F_y) directions to create a resultant force (and impulse) (F_r) which is applied to the frame through the wheel axle mount at angle (θ). The following input parameters were used along with the assumptions outlined in appendix XX to calculate the magnitude of F_r and orientation θ. The green arrows show the kinetic energy of the wheel (KE) and the gravitational potential energy (PE), present in both the initial and final stages.

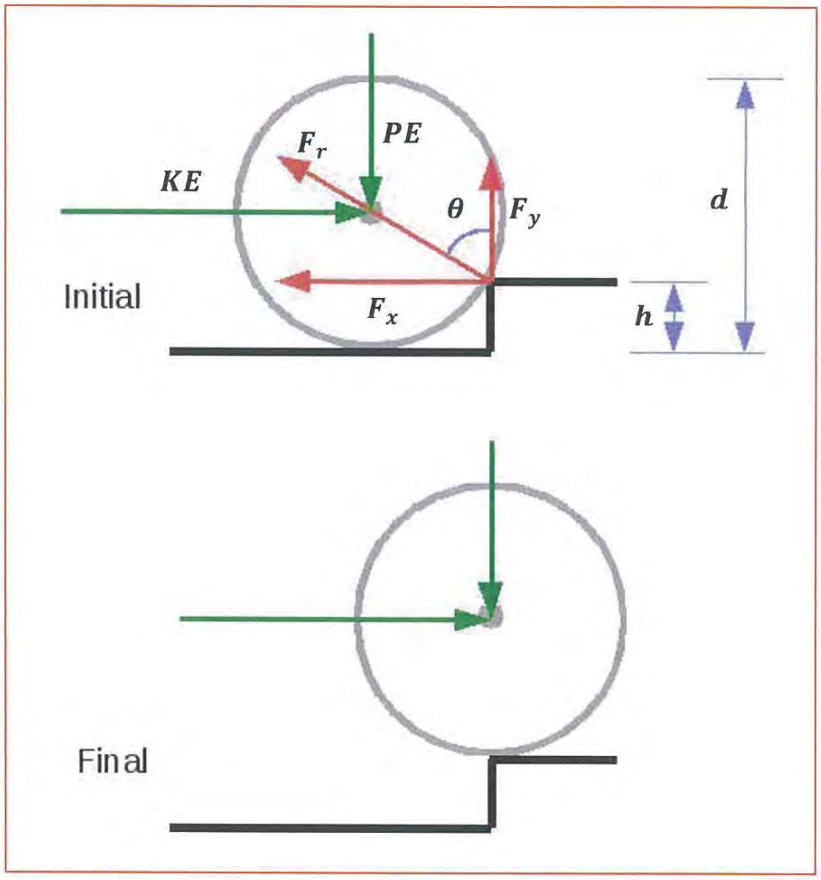

Figure 4-2: Kinematic dissemination of factors present during impact of wheel with step in roadway

Table 4-2: Input parameters for impact scenario

Initial velocity $v_1\ (ms^{-1})$	Step height $h\ (m)$	Vehicle total mass $m\ (kg)$	Gravity $g\ (ms^{-2})$	Wheel diameter $d\ (m)$	Wheel radius $r\ (m)$
13.89	0.05	110	9.81	0.465	0.2325

Because the mass of the vehicle is distributed between the front and rear wheels at a ratio of 2/3 front and 1/3 rear, a distinction needed to be made between the mass due to gravity acting on the front wheel in the vertical direction (m_y) and effective mass due to inertia of

the velomobile and rider moving in the horizontal direction (m_x) as shown in Equation 1 which describes the gravitational potential and kinetic energy balance that is maintained during the scenario. m_y is the total mass of the velomobile and rider, while m_x at the front wheel is only 2/3 of the total mass with the rest being supported by the rear wheel.

Using the input parameters from Table 4-2 and the Equations' 2 and 3, solutions for the F_x and F_y direction forces acting on the wheel during this scenario were found. These forces are caused by the energy input to the system which is in turn equal to the change in gravitational potential energy caused by the step in the road. This produces the energy balance shown by Equation 1 where the energy changes in the vertical direction translate to change in velocity in the horizontal direction via a change in the kinetic energy. Combining functions for linear acceleration and change in velocity during contact yields equation X, which was used to calculate the force F_x that acts in the x direction on the wheel.

$$m_y g \Delta h = \frac{1}{2} m_x \Delta v_1^2 \tag{1}$$

$$F_x = \frac{2 \cdot m_x \cdot v_1 \left(\sqrt{v_1^2 - \frac{2 m_y g h}{m_x}} - v_1 \right)}{r \cdot \cos^{-1}\left(\frac{r-h}{r}\right)} \tag{2}$$

The resultant force F_y that acts on the wheel in the y direction was then calculated using equation 3, which incorporates the angle which the axle of the wheel makes with the vertical plane at the point where the change in acceleration is a maximum – presumed to be half of the angle θ that the wheel makes with the vertical plane at initial contact with the step.

$$F_y = \frac{2 \cdot m_x \cdot v_1 \left(\sqrt{v_1^2 - \frac{2 m_y g h}{m_x}} - v_1 \right)}{\tan\left(\frac{r-h}{2r}\right) \cdot \left(r \cdot \cos^{-1}\left(\frac{r-h}{r}\right)\right)} \tag{3}$$

Because of the deformation in the wheel and frame components during impact, the application of the resultant force actually causes a changing acceleration (called a jerk), this means that the force is also changing over the course of the impact as the frame and wheel absorb force and the induced stresses in these components ramps up. The point at which the change in acceleration reverses is and the induced stresses in the frame start to release has been assumed to be halfway up the step (i.e. halfway through the time period of contact, where the contact angle is $\theta/2$). This infers that the contact patch of the wheel does not actually leave the surface of the road after passing over the step, and constitutes to the

maximum loading example of this scenario. This is shown in Figure 4-3 which plots the average acceleration over the impact period, and shows the anticipated change in acceleration with the peak at $\theta/2$. Peak acceleration is double the average, as utilised for calculations in Equations 2 and 3.

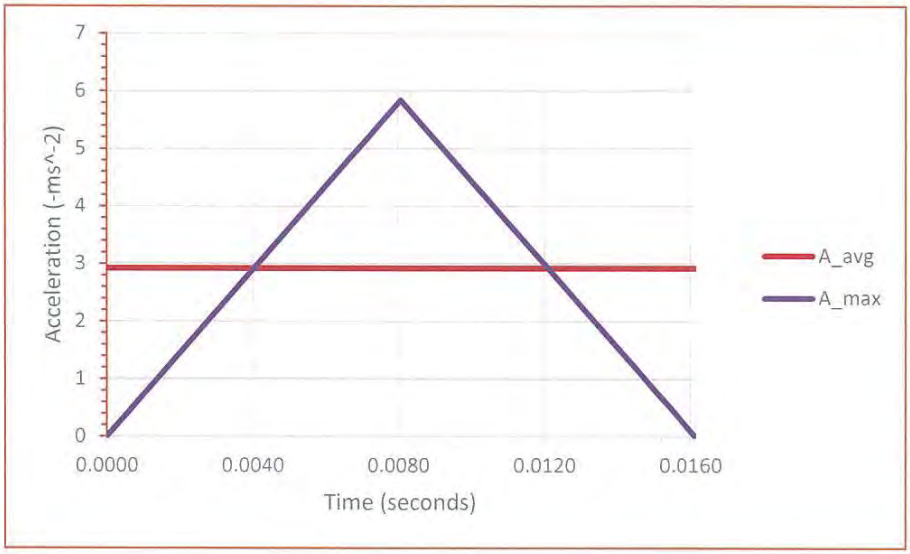

Figure 4-3: Rates of acceleration during impact with step, demonstrating difference between calculated average and peak values.

Table 4-3: Calculated forces acting on front wheel axle mounting point of frame as a result loading of scenario 3.3.1

Horizontal force $F_x\ (N)$	Vertical force $F_y\ (N)$
642.75	1227.99

4.3.2 CORNERING LOADING

Travelling around the radius of a turn at speed produces a complex loading scenario through the combination of horizontal and vertical forces acting on the frame through the wheels. Vehicles which rely on friction from the tyres have an inevitable maximum cornering force that can be reached before the friction forces are overcome and the tyres skid, or the vehicle overbalances and rolls off its wheels. The highest loading scenario during cornering is therefore experienced at the limit of cornering without either overcoming the tyre friction or overturning the vehicle.

Velomobiel.NL described performing cornering tests with their designs to determine the maximum cornering radius and speeds which were possible. In their experiments, maximum cornering speed was the point at which the inside front wheel of the velomobile lifted from the ground, meaning that the majority of the mass was being supported by the outside wheel.

By measuring the 'g-force' at this point using an iPhone accelerometer they were able to determine how much horizontal force was present to initiate this rollover effect. This measurement has been used to calculate the maximum loading that is likely to be present on the outside front and rear wheel axle mounting points during cornering manoeuvres at speed. The values used for assessing this situation are the same as those provided by Velomobiel.NL during their experiments.

Figure 4-4 shows the applied forces in this scenario as they occur at the front wheel. The vehicle of mass (m) moving at maximum velocity (v) turns through a sufficiently tight arc to just overcome the gravitational force and cause the inside front wheel to begin to break contact with the ground. At this point the specific gravity (SG) (horizontal acceleration) is measured. The effect of this inside wheel leaving the ground results in the all of the mass of the vehicle being transmitted through the outside front wheel and rear wheel in the vertical direction. This is combined with the centripetal force due to the friction of the tyre on the road surface to create a resultant reaction force $(F_{resultant})$ that acts through the centre of the wheel axle mounting point at an angle (θ) and a moment $(M_{resultant})$ that acts about the same point as a function of the wheel diameter (d). The reaction force is comprised of a vertical component (F_x) and a horizontal component (F_y).

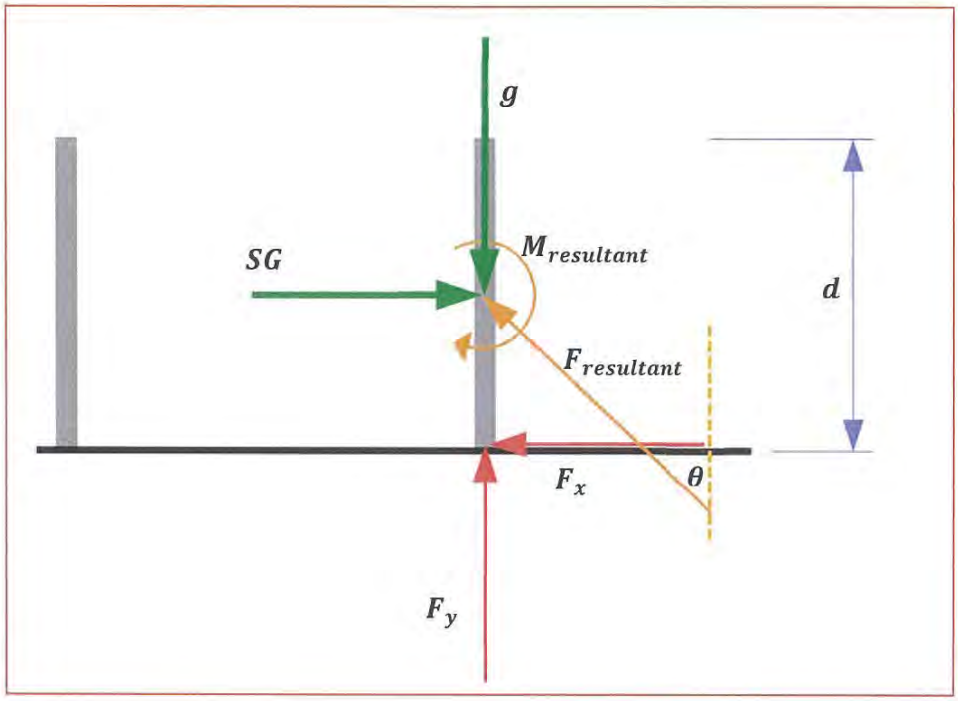

Figure 4-4: Kinematic dissemination of maximum speed cornering loading showing relevant factors present

Table 4-4: Input parameters for cornering scenario

Static total mass $m\ (kg)$	Velocity $v\ (ms^{-1})$	Specific gravity $SG\ (ms^{-2})$	Acceleration due to gravity $g\ (ms^{-2})$	Wheel diameter $d\ (m)$	Wheel radius $r\ (m)$
110	13.89	$0.65g$	9.81	0.465	0.2325

Calculating the vertical and horizontal component of the force in this scenario is possible through the use of the values provided by Velomobiel.NL for the horizontal specific gravity, and the assumption that the centre of gravity of the velomobile is located as described in Table 4-1. Equations 4 and 5 respectively show the calculation of the vertical F_y and horizontal F_x components the loading on the velomobile and rider. These values are multiplied by the distribution ratio which the location of the centre of gravity produces. This is shown by Equations 7a and 7b,

$$F_{y,total} = mg \tag{4}$$

$$F_{x,total} = 0.65mg \tag{5}$$

$$M_{total} = F_{x,total} \cdot r \tag{6}$$

$$Load_{total} = Load_{front} + Load_{rear} \tag{7a}$$

$$Load_{front} = 2 \cdot Load_{rear} \tag{7b}$$

Table 4-5: Applied loads to rear and outside front wheel axle mounting points of velomobile as distributed according to location of centre of gravity.

	Mass $m\ (kg)$	Reaction force due to gravity $F_y\ (N)$	Friction force due to specific gravity $F_x\ (N)$	Moment about axle mount $M\ (Nm)$
Total	110	1079.1	701.4	–
Front wheel	73.33	719.4	467.6	108.7
Rear wheel	36.67	359.7	233.8	54.4

4.3.3 BRAKING-INDUCED DECELERATION TESTS

Velomobiel.NL described performing stoppage tests of their designs to measure the distance that was required to come to a complete stop under maximum possible braking power. The effect of applying full braking power at speed utilizes the friction between the tyres and road surface to apply a deceleration force to the moving vehicle. This force acts on the frame through the wheel axle mounting points for as long as it takes for the vehicle to come to a complete stop. The values used for assessing this situation are the same as those that were provided by Velomobiel.NL during their experiments.

Figure 4-5 shows the applied forces in this scenario, the vehicle of mass (m) decelerates at a constant rate (a) from an initial velocity $(v_{initial})$ to final velocity (v_{final}) as a result of an applied braking force (F_{brake}) over a braking distance (s). The braking force acts on the bamboo frame in the form of a translated direct force (F_{brake}) and a moment about the axle centre (M). Both forces are applied to the front wheel axle mounts only, assuming that the velomobile only uses these brakes to stop with in this scenario.

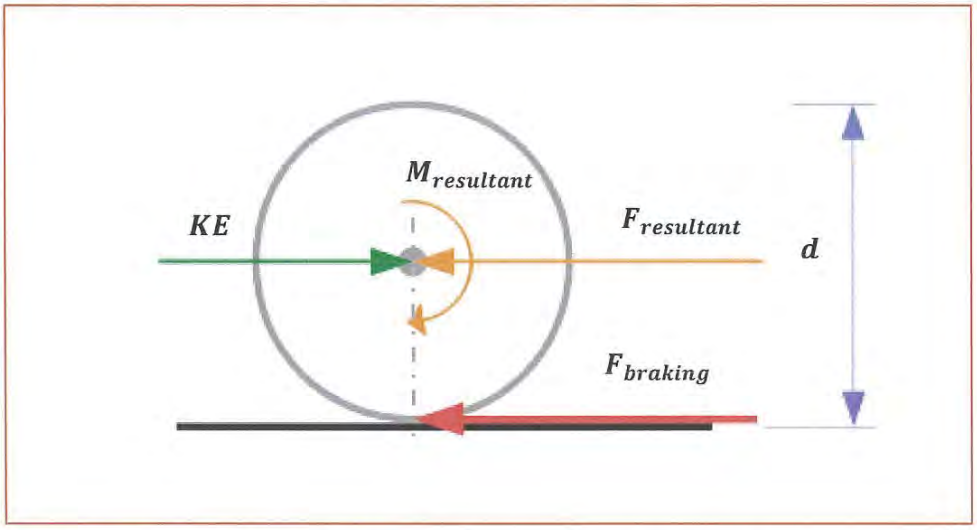

Figure 4-5: Kinematic dissemination of brake-stop loading showing relevant factors present

Values calculated show that the direct force loading due to a full speed brake-stop is relatively small. This loading scenario is important though because its additional direction of application as a moment acting about the wheel axle mounting point is unique, and the moment is large.

Table 4-6: Input parameters for brake stopping distance calculations

Mass $m\ (kg)$	Initial velocity $v_1\ (ms^{-1})$	Final velocity $v_2\ (ms^{-1})$	Stopping distance $s\ (m)$	Wheel diameter $d\ (m)$	Wheel radius $r\ (m)$
110	13.89	0	10	0.465	0.2325

During the brake loading, the full mass of the vehicle is distributed to the front wheels. This would occur as the centre of gravity moves forward under braking. Calculating the force per wheel due to braking is performed using Equation 8 with half of the total load calculated being

applied per wheel. This result can be used to calculate the moment per wheel due to the braking as shown in Equation 9.

$$F_{brake,total} = \frac{m \cdot v_1^2}{2d} \tag{8}$$

$$M_{per\ wheel} = \frac{r \cdot m \cdot v_1^2}{2d} \tag{9}$$

Table 4-7: Calculated load values applied to frame at both front wheels as a result of loading scenario

Acceleration $a\ (ms^{-2})$	Braking force (both wheels) $F_{brake}\ (N)$	Braking force (per wheel) $F_{brake}\ (N)$	Moment due to braking $M\ (Nm)$
−9.64	1061.1	530.6	123.4

4.4 DESIGN PROCESS

The process for developing a spaceframe design which met the specifications outlined in the previous sections of this chapter involved a number of stages of concept development, assessment and improvement. An outline of the process is displayed in flow-chart form in Figure 4-6. Initial concepts were based on the required layout geometry of the rider and component mounting points, as these were the primary input parameters which the frame had to satisfy. These dimensional parameters were modelled using the Solidworks package, and different views of the model were printed in hardcopy for sketching on. Once a hand sketched concept had been selected based primarily on heuristic assessment of the frame member layout, this was modelled into the initial Solidworks part to ensure that required clearances were maintained. Once modelled in this format it became easier to visualize additional placement of frame members in the structure, and these were added and rearranged until a satisfactory looking structure was created. Empirical assessment of this concept was performed using the Solidworks Simulation package, and a translated version of the three maximum loading scenarios (adjusted to provide accurate and representative simulation data) was performed in three separate simulations. Results from these simulations provided insight into the placement of additional frame components in order to create a structure that distributed the applied loads as induced stresses and deflections in a more uniform manner. This refinement and testing process was repeated until the maximum stress limits of the bamboo material were not exceeded under the simulated loading conditions. The final design from this process was then used for the prototyping process that is described in Chapter 5.

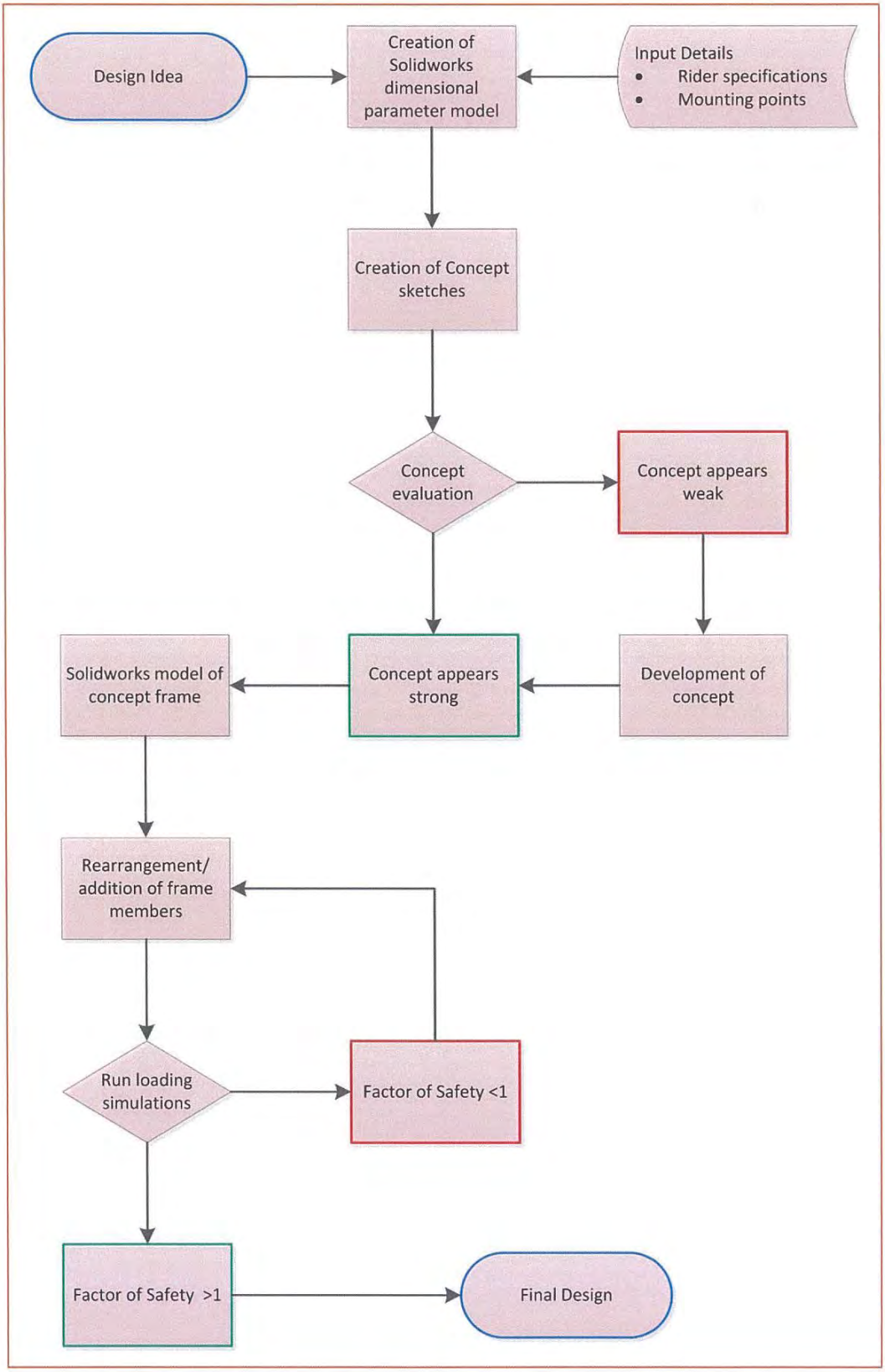

Figure 4-6: Flow chart of spaceframe design development process

4.4.1 MODELLING OF DIMENSIONAL PARAMETERS

Data from Sections 4.1.1 and 4.1.2 was combined to create a Solidworks model of the mounting points which the frame needed to provide support for; and the relevant dimensional clearances for both rider and components which the design needed to meet to allow uninhibited performance. This model is shown in Figure 4-7, with labelled features of clearance geometry and relevant mounting points identified.

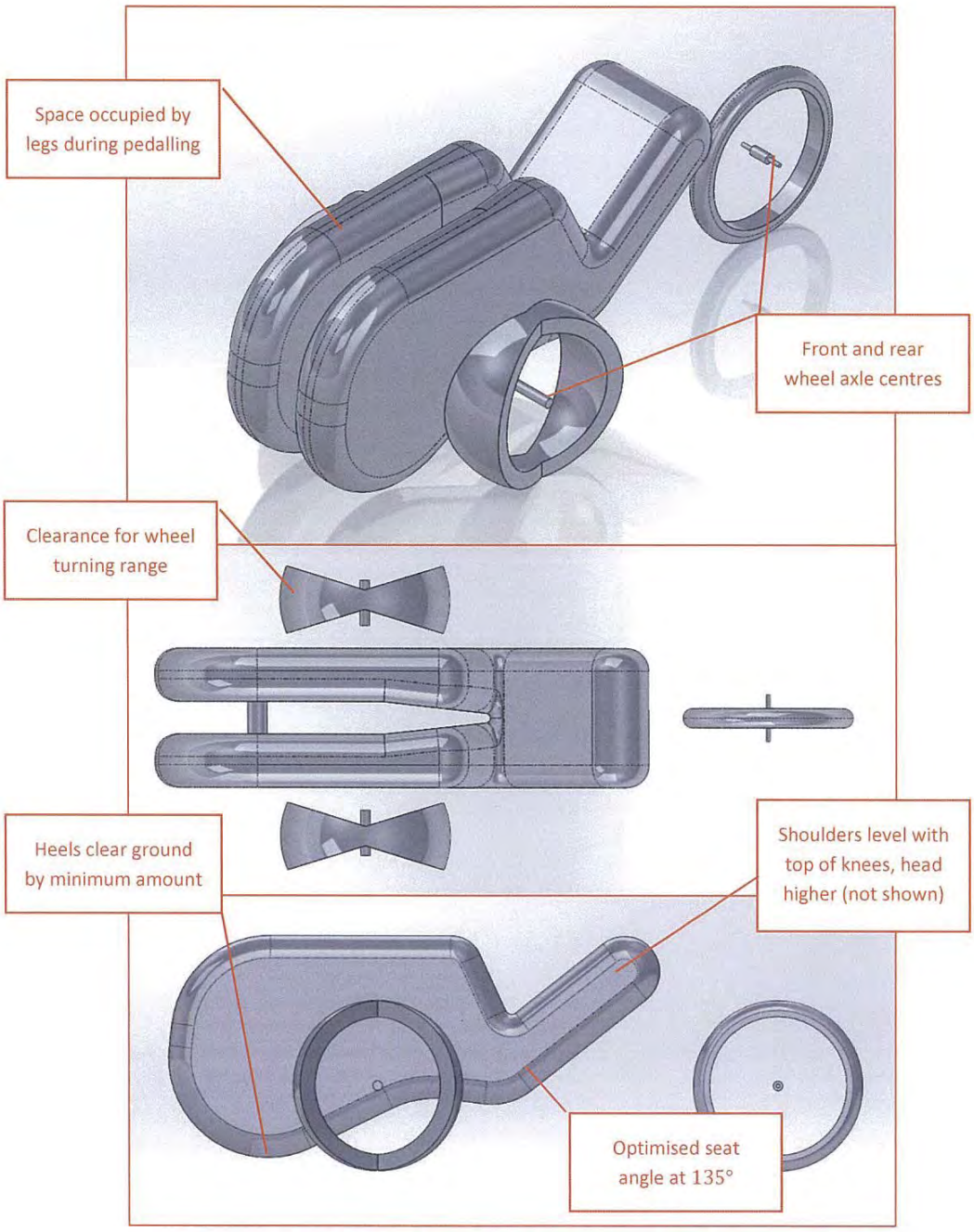

Figure 4-7: Solidworks model of dimensional parameters that frame design must accommodate

4.4.2 CONCEPTS

Creation of concepts which would come close to providing the required stress tolerance capabilities while maintaining the clearances required was initially performed by hand. These concepts were developed based on initial impressions of what the frame should look like, and impressions of how the loads from the various scenarios would be distributed throughout the frame members in each concept. This heuristic process was difficult to perform with any assurance of success as the distribution of force and stress in a three dimensional spaceframe is complicated to assess without extensive calculations. Concepts developed are shown in Figures' 4-8 and 4-9 and 4-10

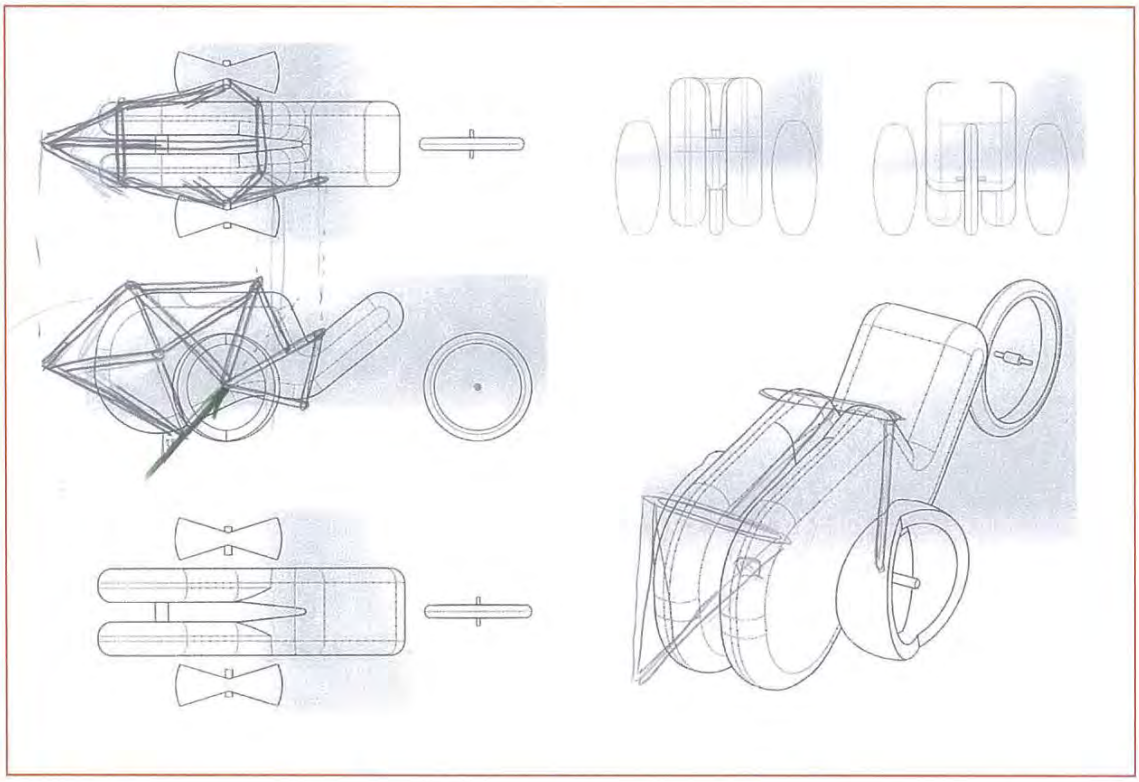

Figure 4-8 Concept development of frame

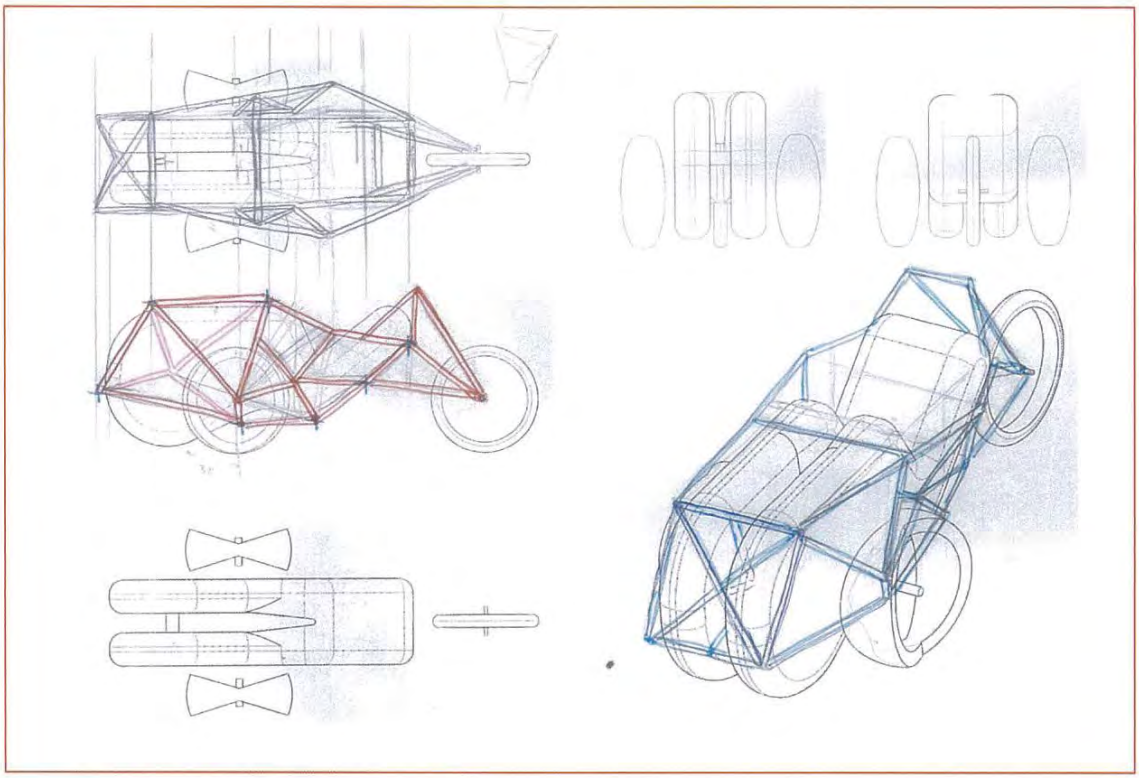

Figure 4-9: Concept development of frame

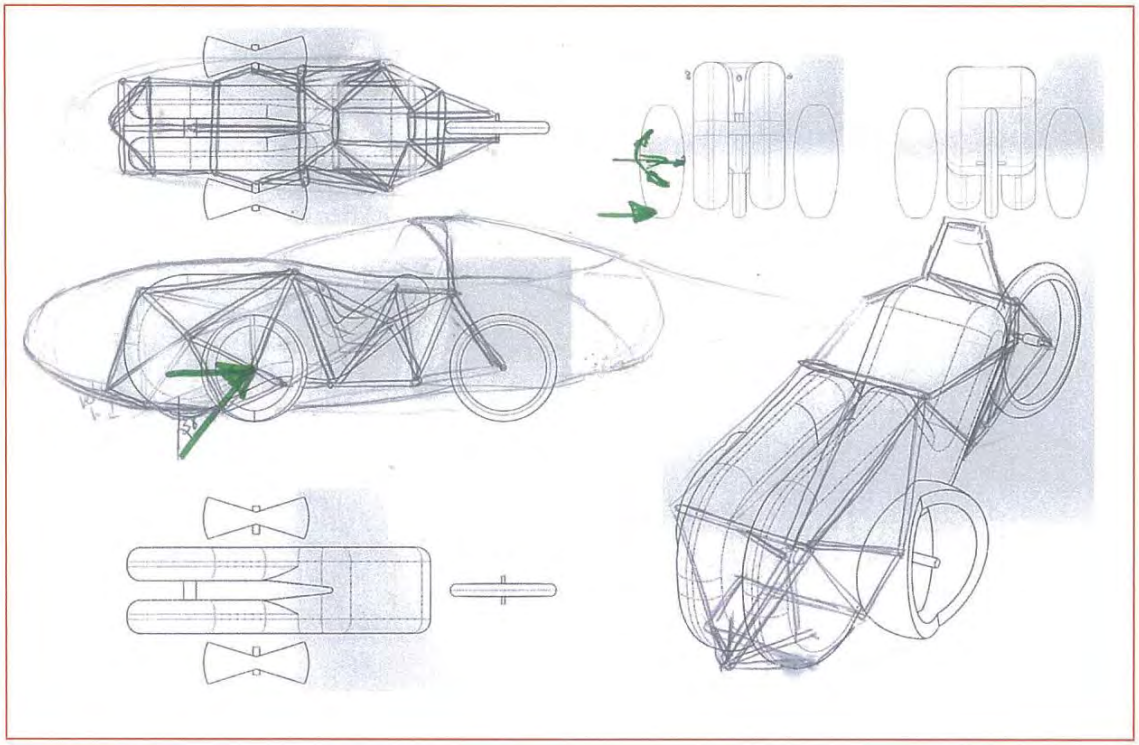

Figure 4-10: Concept development of frame

4.4.3 SOLIDWORKS MODEL DEVELOPMENT

Using the Solidworks model which contained the required dimensional input data, the developed frame concept was built up as sketch entities around the existing bodies in the model. Frame members were located at the appropriate component mounting points, ensuring that their placement did not impinge on the modelled clearances of the rider's body and the front and rear wheels. Sketched locations of frame members were converted to 'weldments' in the Solidworks program, the weldment feature allowed the line sketches to be converted into a spaceframe that is constructed from members of a specified cross section, and allows for detailed mitring of frame member ends at joints. The dimensions of the tube cross sections were specified as the average outside diameter and wall thickness dimensions of the measured *Himalayacalamus* specimens. This cross section is shown in Figure 4-11.

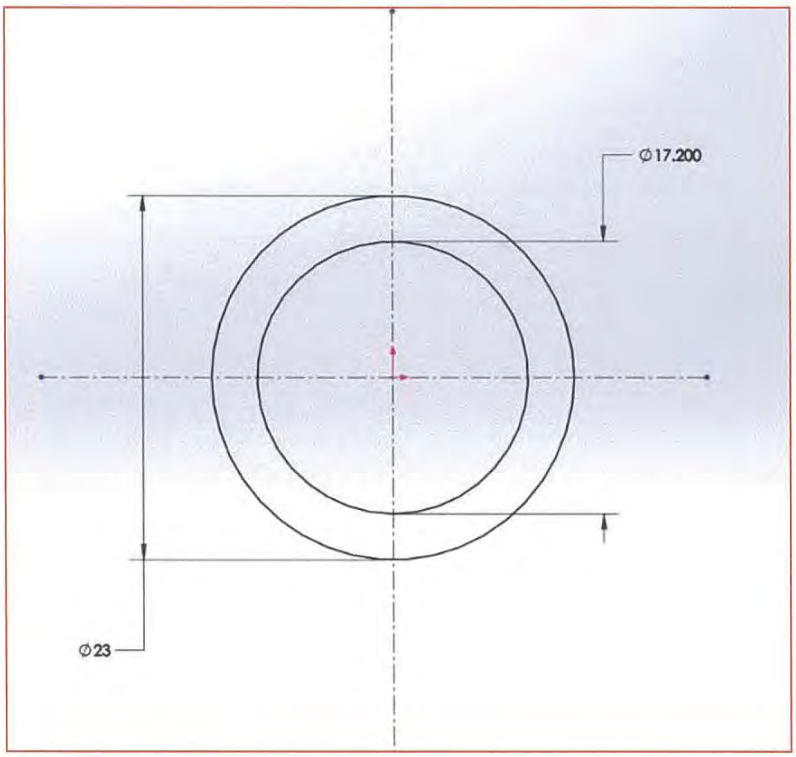

Figure 4-11: Weldment profile of bamboo frame members

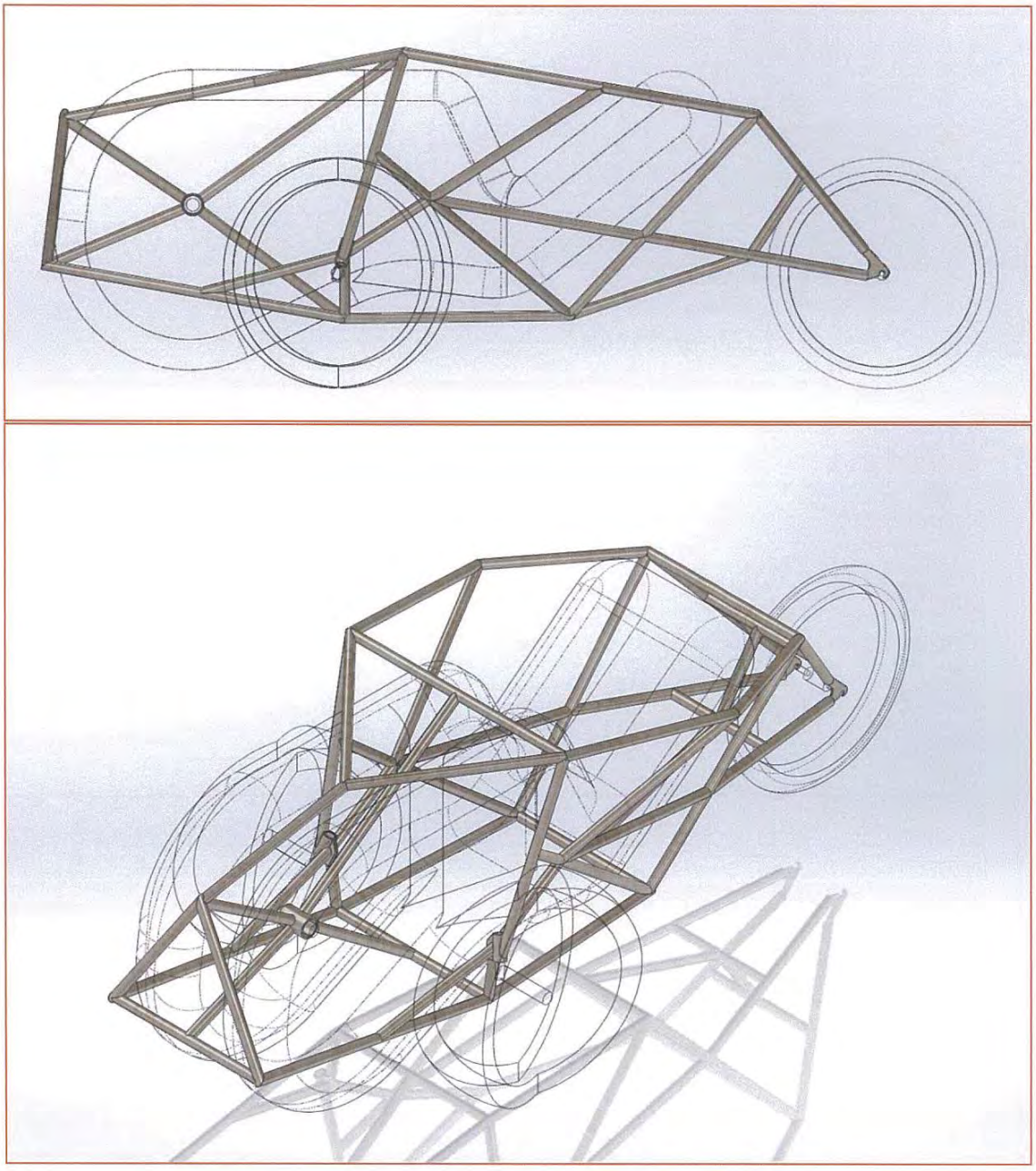

Figure 4-12: Modelled initial frame concept showing overlay onto dimensional parameters and mounting points

During the process of concept conversion from sketches to a three dimensional model which could be viewed from any angle, the requirement of further frame members was realised, and these were added as the model evolved. The final frame concept is shown in Figure 4-12, with all of the frame members in position.

4.4.4 MATERIAL DATA INPUTS

Material properties for the model were based on tested data that is presented in section 2.3.9 of this report, however to complete the material data profile in the Solidworks program, additional values for stress-strain relationships were also required. Table 4-8 shows the full list of material properties that were used for the simulation, and includes the source for each value.

Table 4-8 Material properties of *Himalayacalamus* bamboo as used for Solidworks simulations

Property	Value	Source
Maximum Stresses		
$\sigma_{bending}$	$42.9MPa$	Test results
$\tau_{parallel\ fibre}$	$4.4MPa$	" "
$\sigma_{tensile}$	$63.0MPa$	" "
$\sigma_{compressive}$	$37.5MPa$	" "
Additional Properties		
$E\ (Elasticity_{modulus})$	$4GPa$	(Rottke D. I., 2002)
T $(Shear_{modulus})$	$0.6GPa$	"
$v\ (Poissons\ ratio)$	0.31	"
$\rho\ (Density)$	$600kg/m^3$	"
Model Type	*Linear elastic isotropic*	–

4.4.5 REFINEMENT THROUGH SIMULATION

The application of loading scenario data to the modelled frame was performed using the Solidworks simulation package. By developing the simulation input parameters within the modelled part file it was a relatively straightforward process to run the simulations, evaluate the results, modify the model and then re-run the simulation to assess the change in stress concentrations and deflection in the new frame under the same conditions.

Solidworks simulations were performed as a constant static loading application of the maximum forces (as a combination of F_x and F_y directions and bending moments where appropriate) found to be present in each of the calculated loading scenarios described in section 4.3. Frame members were treated as a combination of rigidly attached joints and beams constructed from hollow round tubes. Reaction forces in the scenarios (such as rider mass and inertia) were applied as fixtures to allow the simulation to remain stationary under loading. Figures' 4-13, 4-14 and 4-15 show each of the three loading scenarios as they were translated into the Solidworks program prior to running the simulations. Green arrows denote fixed or limited motion regions. Purple arrows denote the applied forces and their direction.

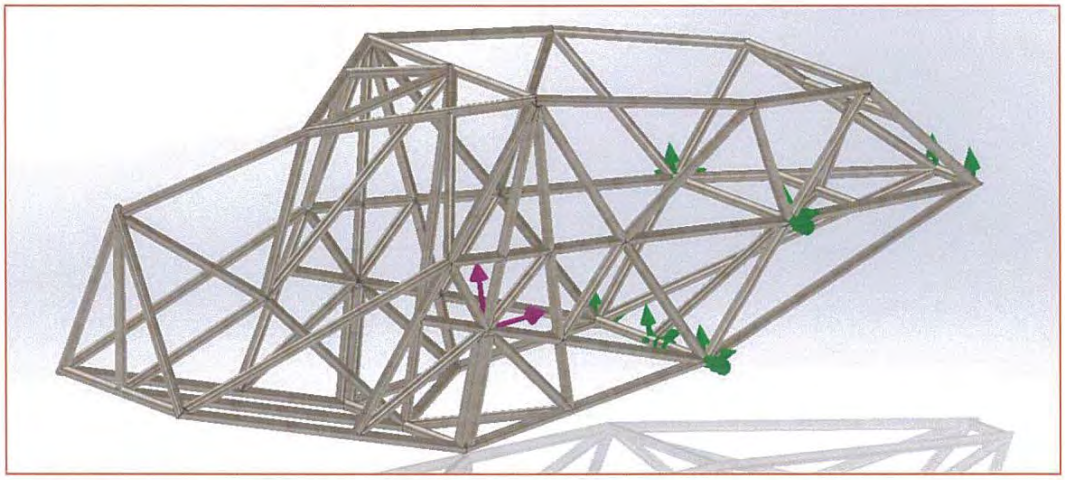

Figure 4-13: Impact loading simulation showing vertical and horizontal loads on front wheel, with fixed and restricted movement points at the rear wheel and seat attachment points respectively

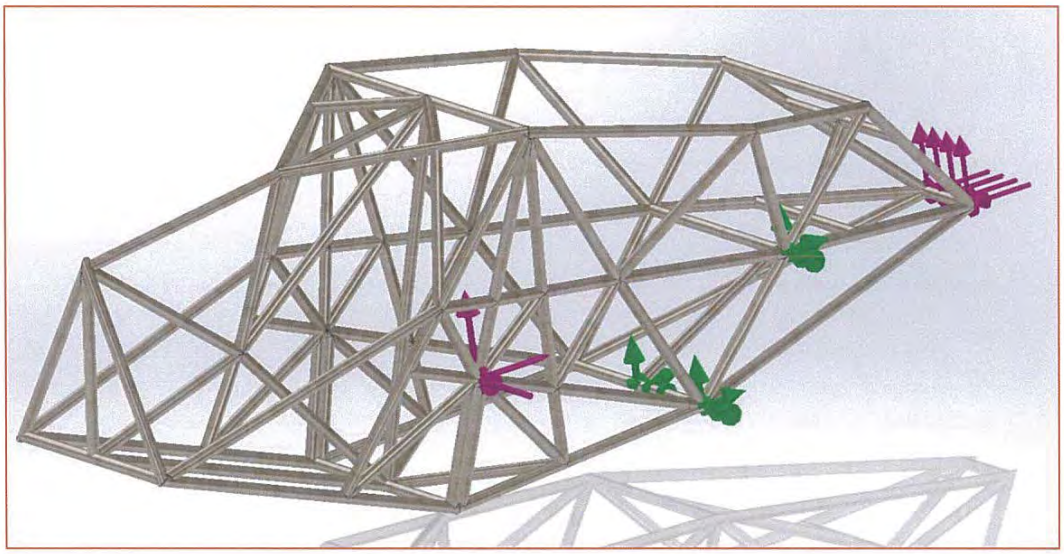

Figure 4-14: Cornering loading simulation showing vertical and horizontal loads and moments acting on front and rear wheel mounting points. Fixed areas shown represent the reaction force of the rider on the seat attachment points.

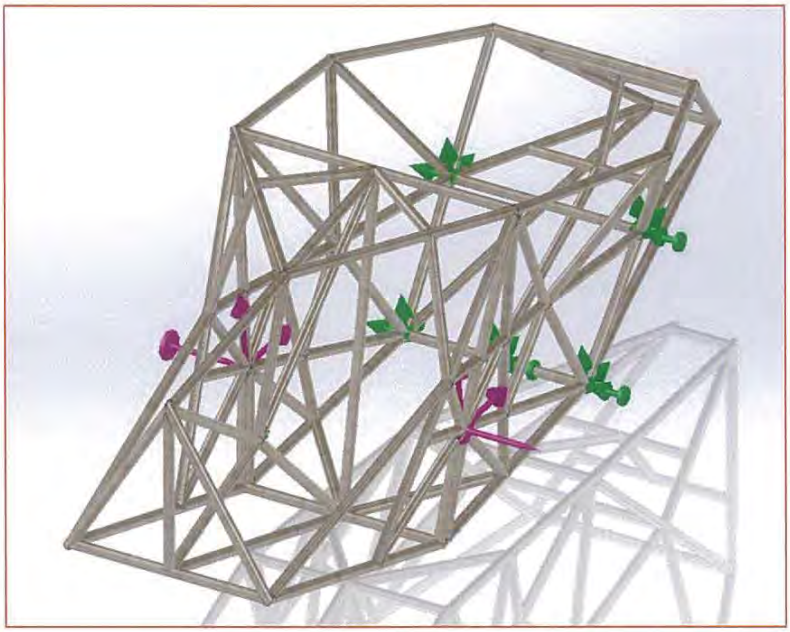

Figure 4-15: Braking loading simulation showing vertical, horizontal and moment application to front wheel axle mounts and fixed geometry at seat attachment area.

Each time the simulations were run on the model the results were assessed based on the lowest Factor of Safety (FOS) that was present in the frame. When one or more of the simulated loadings presented an area of frame where the FOS was lower than two (a value lower than one denoted failure in that area), that area of the frame was then modified via the addition of further frame members or the rearrangement of members to provide better structural support. Running the same simulation and inspecting the performance of that area then provided direct information regarding the effect that this change had on the integrity of the frame. Appendix **E** details final stage examples of this development process including the frame design, simulation results showing highlighted areas of low FOS, and accompanying frame design changes and subsequent simulation results with improved stress distribution.

4.5 SIMULATION RESULTS

After a number of iterations of the previously described design-test-modify-retest cycle had been performed, the simulated results presented satisfactory FOS, stress distribution and deflection values. Given that the frame would be under extreme loading conditions during the simulated events, in some places the FOS value was allowed to drop below two in mid sections of frame members and below one (although not significantly) in the direct vicinity of the joints.

The following sections present a summary of the results from each simulation along with a description of any notably high stress points in the frame and an explanation for why these were deemed tolerable for the design.

4.5.1 IMPACT WITH IRREGULARITY

Overall results from the simulated impact of the frame with a road surface irregularity produced low stresses in the frame members. Figure 4-16 shows the stress distribution in the frame as a function of the FOS value. Highest stresses occurred next to the fixed joint which was one of the seat mount points.

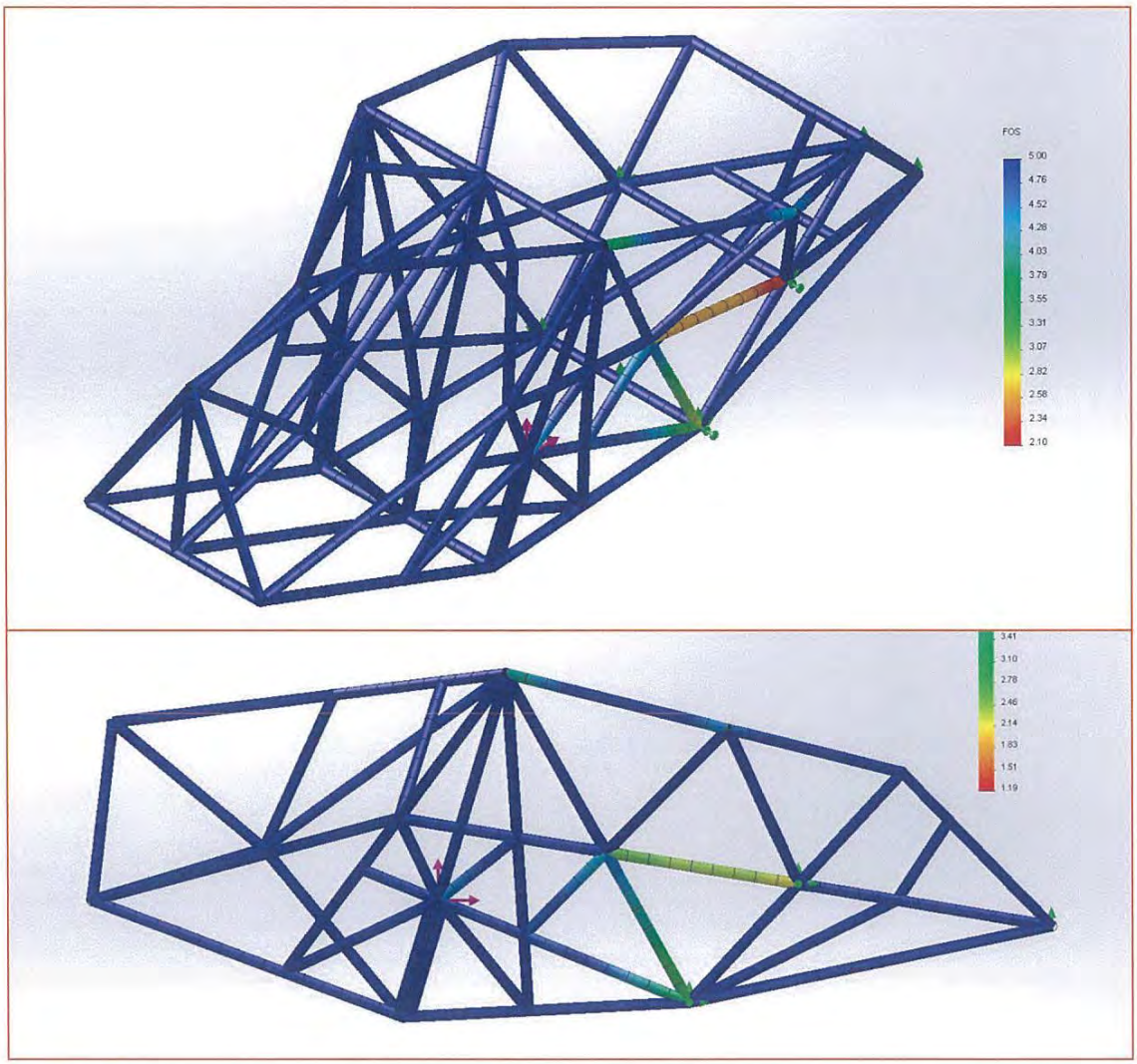

Figure 4-16: Impact loading simulation on final frame design. Highest stress concentrations/lowest FOS values highlighted

The lowest FOS value present in the frame under this simulation was 2.1. This is a satisfactory value for the result given the extreme nature of the scenario. The fact that this stress occurs in the vicinity of a joint as can be seen in Figure 4-16 that is rigidly fixed means that this stress would be likely to have better distribution in a more realistic version of the loading where the seat was included and the entire frame was allowed to flex in a more responsive manner. The addition of the wrapped fibre and resin joints that are proposed (examples described in Appendix F) will also improve the rigidity of the structure in this high stress area.

4.5.2 CORNERING LOADING

Results from the simulated loading of the frame under maximum capability cornering conditions produced high stresses in the frame in the region surrounding the mount for the outside front wheel axle. During the frame development, this joint was reinforced with a large number of frame members to distribute the load as much as possible. However as shown in Figure 4-17 the lowest FOS value in this region was still less than 1 (0.82, highlighted in red)

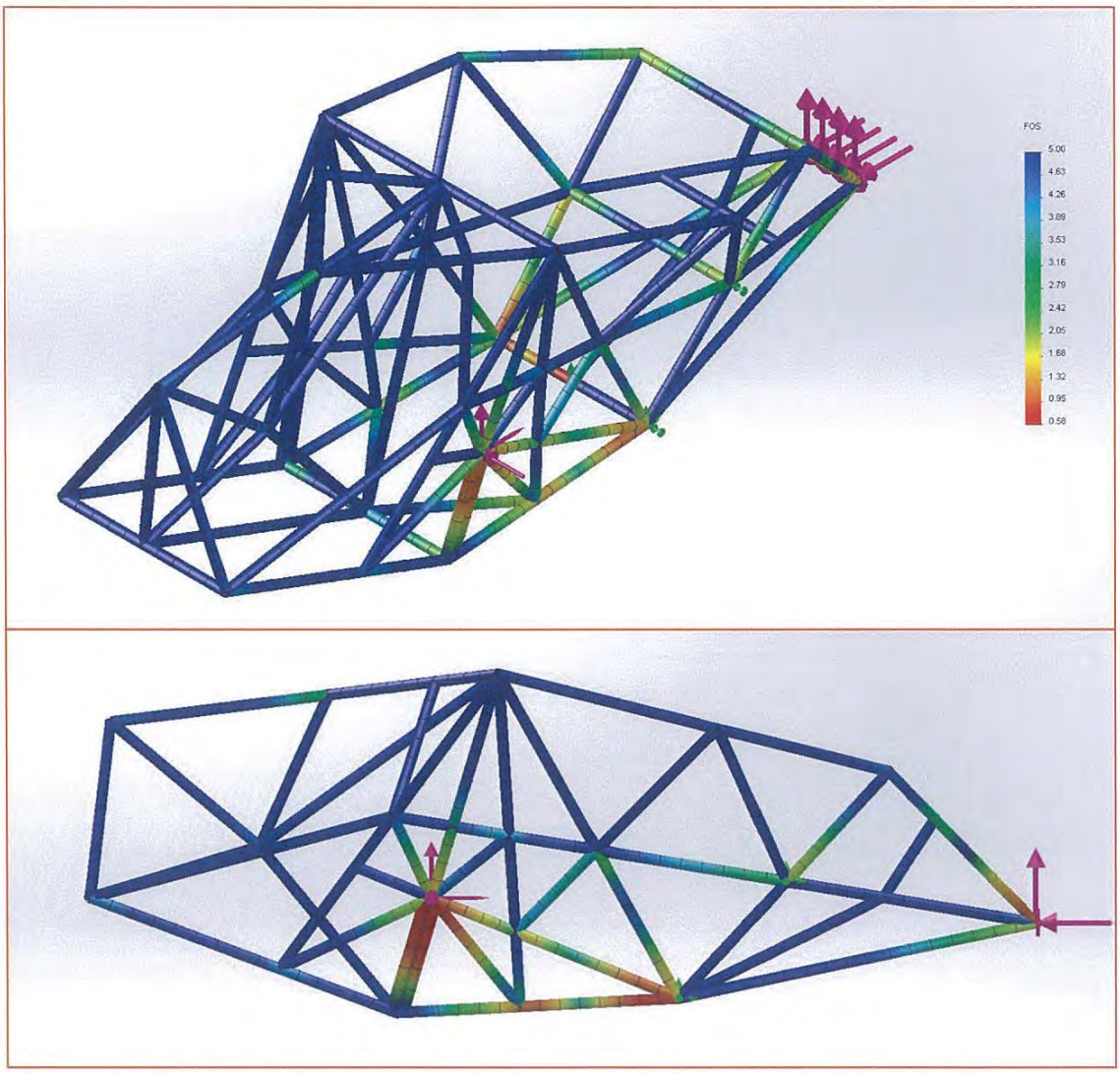

Figure 4-17: Cornering loading simulation on final frame design. Highest stress concentrations/lowest FOS values highlighted

Given that this high stresses are in the direct vicinity of the axle mounting joint, it can be suggested that the addition of the jointing materials during construction will have a significant enough impact on the performance of this area to reduce this stress by distributing it through other areas of the frame, in particular through that additional members which converge at that joint. The other main area of stress in this loading scenario is next to the seat mounting point, where the rigid fixtures were located during the simulation. In a more realistic scenario

the loads which are applied to the frame through the seat would be better distributed through the seat and this stress concentration would be reduced.

This simulation provided the highest stress concentrations and the lowest factor of safety out of the three that are described in this section. In order to investigate the highest loading

4.5.3 BRAKING

The brake induced deceleration scenario produced moderate stresses in the frame at the front wheel axle mount points. Due to the large number of frame members in the vicinity of this joint the application of the bending moment was distributed throughout this area of the frame. The lowest FOS value in this area was 1.9, and this was located in close vicinity to the front wheel axle mount joints.

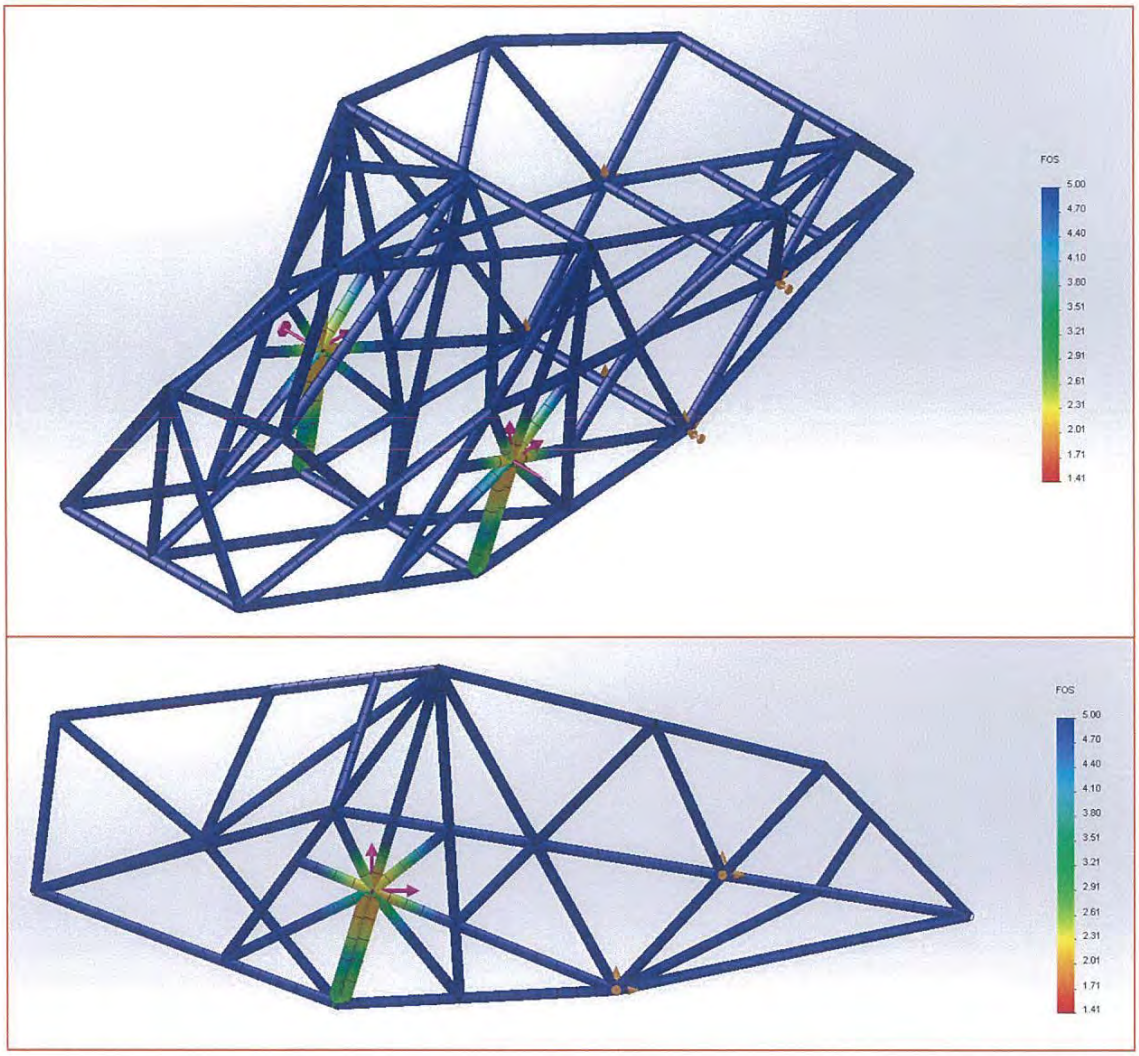

Figure 4-18: Brake deceleration loading simulation on final frame design. Highest stress concentrations/lowest FOS values highlighted

5 FRAME SECTION PROTOTYPING

In order to ensure that the results from the simulated scenarios were sufficiently accurate, it was necessary to construct a prototype of the bamboo frame and apply similar loading conditions to it in order to gauge the variation between the Solidworks modelled frame and an actual constructed version which incorporated the strength of the joints and the variability of the bamboo into one unit. Due to time and resource constraints it was decided not to produce a model of the entire frame; instead the area of highest loading was focused on. The most critically stressed frame members were modelled separately in another Solidworks part file. Previously simulated loading scenarios were then repeated on the new model to verify that the section of frame could be successfully isolated and still perform in a manner similar to the complete frame. The frame section exhibited similar load distribution characteristics and the results from the simulation showed very similar results for the maximum stress magnitude and location. A full-scale prototype of the frame section was then constructed and tested under similar conditions.

5.1 MODELLED FRAME SECTION

The section that contained the members observed to have the highest stressed concentrations was in the region of the front wheel mount, with the highest stresses being observed during the cornering loading scenario. The section for the model was decided to include the directly affected members, and the surrounding area where those members were attached to the rest of the frame was included also. Figure 5-1 shows the modelled frame section highlighted in a view of the entire frame final design. With the model of the prototype section displayed in Figure 5-2.

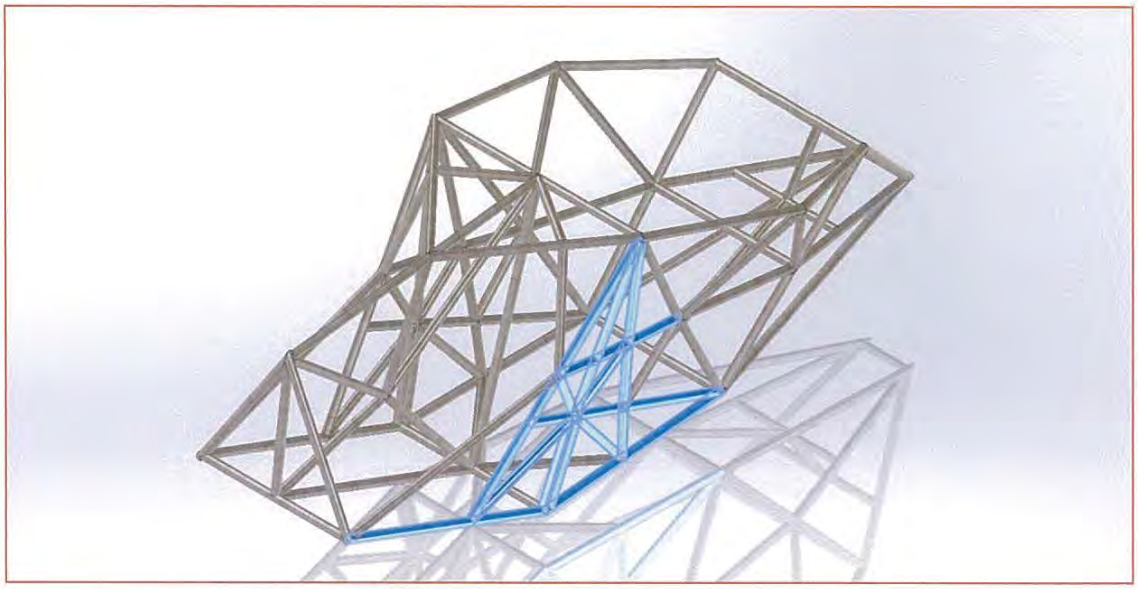

Figure 5-1: Complete frame with highlighted components to be modelled separately, constructed, and tested.

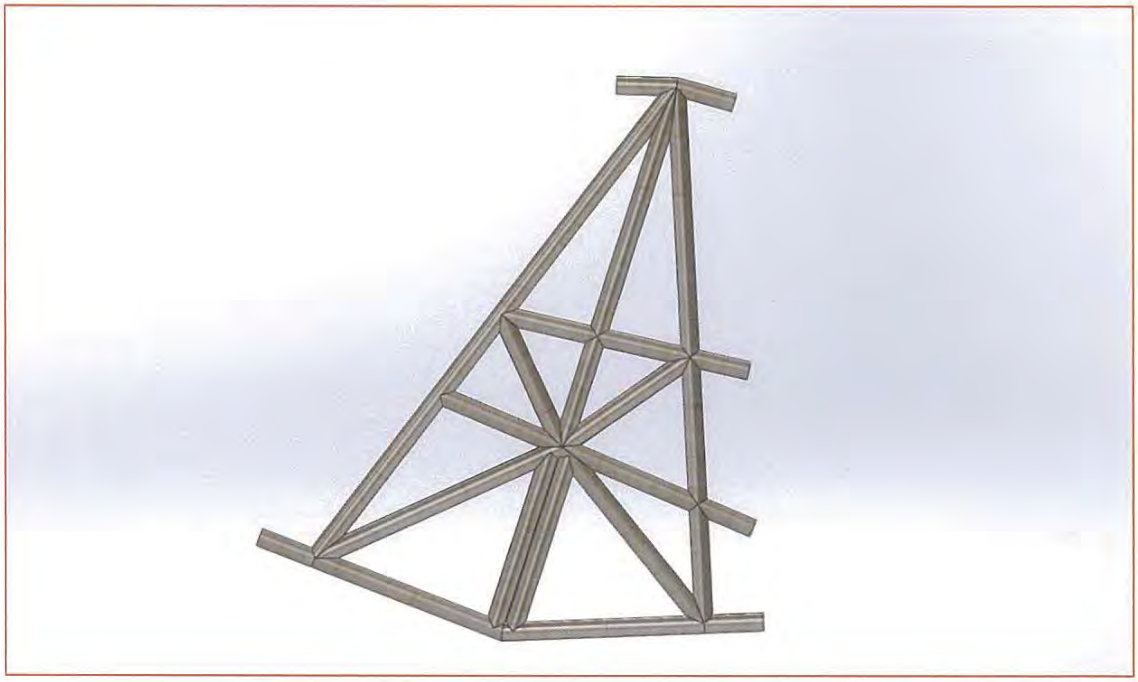

Figure 5-2: Prototype section modelled separately with truncated attachment points to emulate attachments to the rest of the frame

5.2 PROTOTYPE LOADING SIMULATION

Once the prototype frame section had been modelled, the simulation for the corner loading scenario (established as highest stress scenario) was repeated with the same input conditions as were applied to the full frame. In order to emulate the attachment points of this section to the rest of the frame in the complete design, each of the joints that the frame had been truncated to were designated as rigid fixtures. The results of this simulation are shown in Figure 5-3, they display a very similar stress distribution to that which was shown in the complete frame simulation. The two vertical members below the axle attachment point have the highest stress concentration next to the joint which the axle mounts to. As discussed in Section 4.5.2 this high stress area still has a FOS value of less than 1 (minimum of 0.74 at the point described) but as with the complete frame this was predicted to be influenced heavily by the construction of the joints between the members that will significantly increase the rigidity of this area.

Figure 5-4 shows a comparison between the deformation of the complete frame and the frame section. Both results are similar, the deformation has been exaggerated by the simulation but shows the same pattern.

Overall the prototype frame section presents what appears to be a representative isolated version of the performance of the entire frame, with the maximum stress scenario being in a similar range to the values in the entire frame, even though the surrounding supports have been removed.

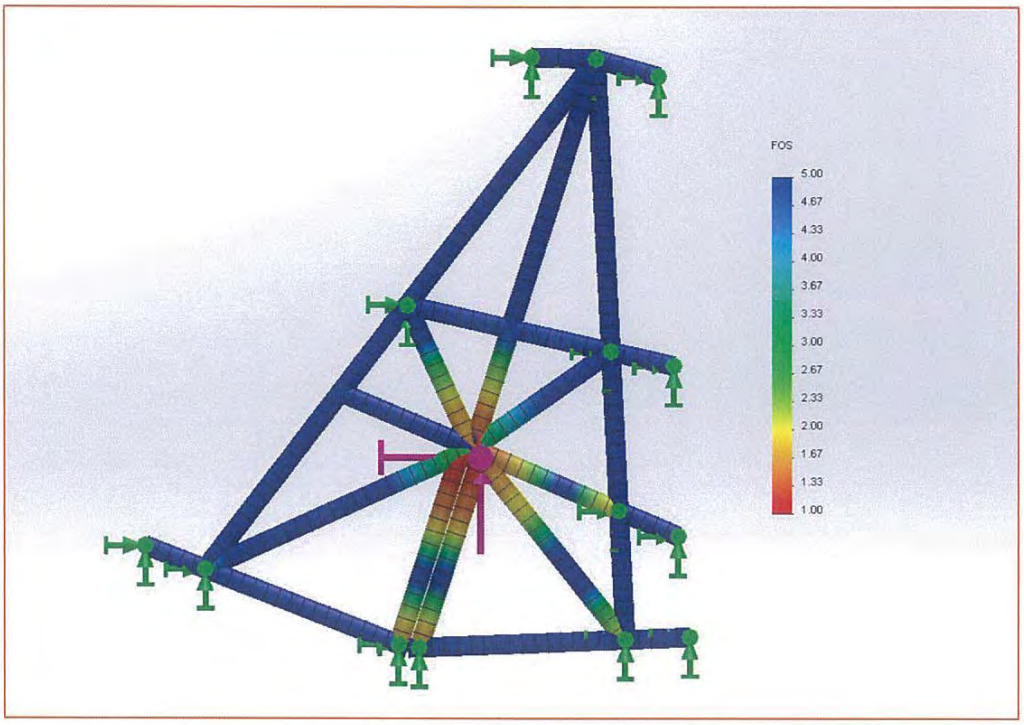

Figure 5-3: Stress distribution in prototype frame section showing areas of highest stress concentration

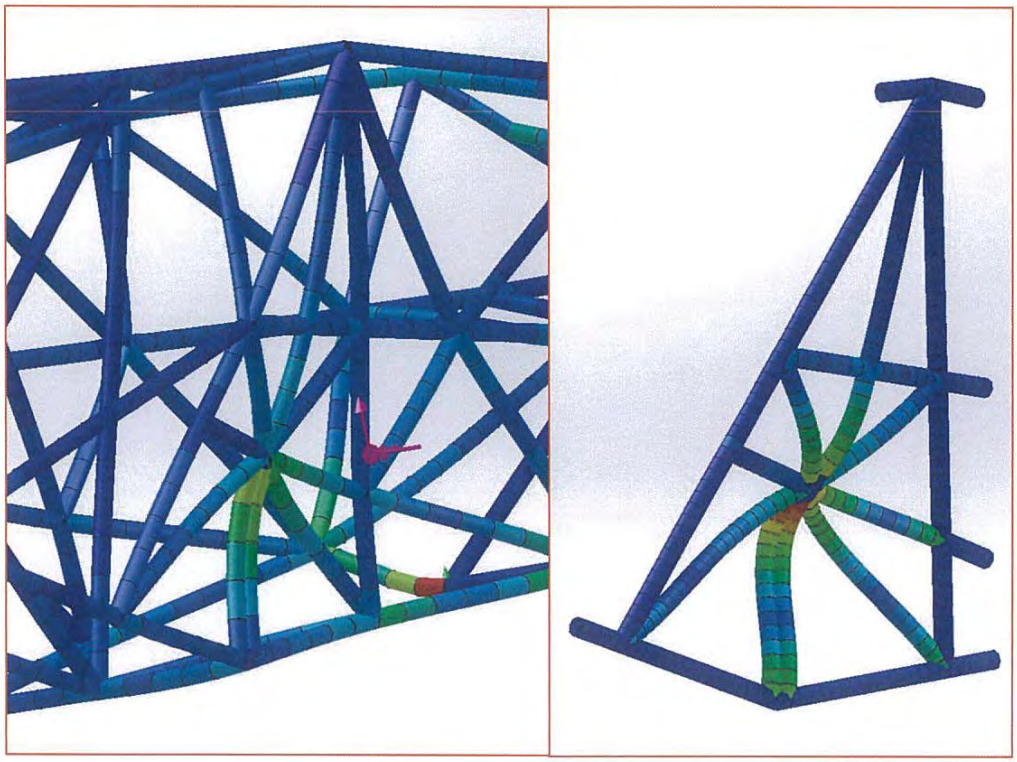

Figure 5-4: Comparison between loading induced deformation in full frame (left) and frame section (right)

5.3 PROTOTYPE CONSTRUCTION

Construction of the prototype frame section was performed with the *Himalayacalamus* specimens, and utilised an experimental joint construction technique which was based on researched examples of composite fibre wrapping techniques for bamboo bike frame joints. The frame was mounted to a rectangle of $20mm$ thick plywood using $150mm \times 12.5mm$ coach-bolts with washers welded to the shanks. The bolts heads were moulded into the joints and also ran through holes drilled in the frame members. The load application to the frame was provided through a round steel tube which was mounted to the central joint of the frame and extended to the point where the load contact between the wheel and the ground would occur in the loading scenario. Appendix F provides a sequential series of images and descriptions detailing the steps taken during construction, and the considerations made at each step. Figure 5-5 shows the final prototype on its support frame with all of the joints wrapped and the loading arm attached.

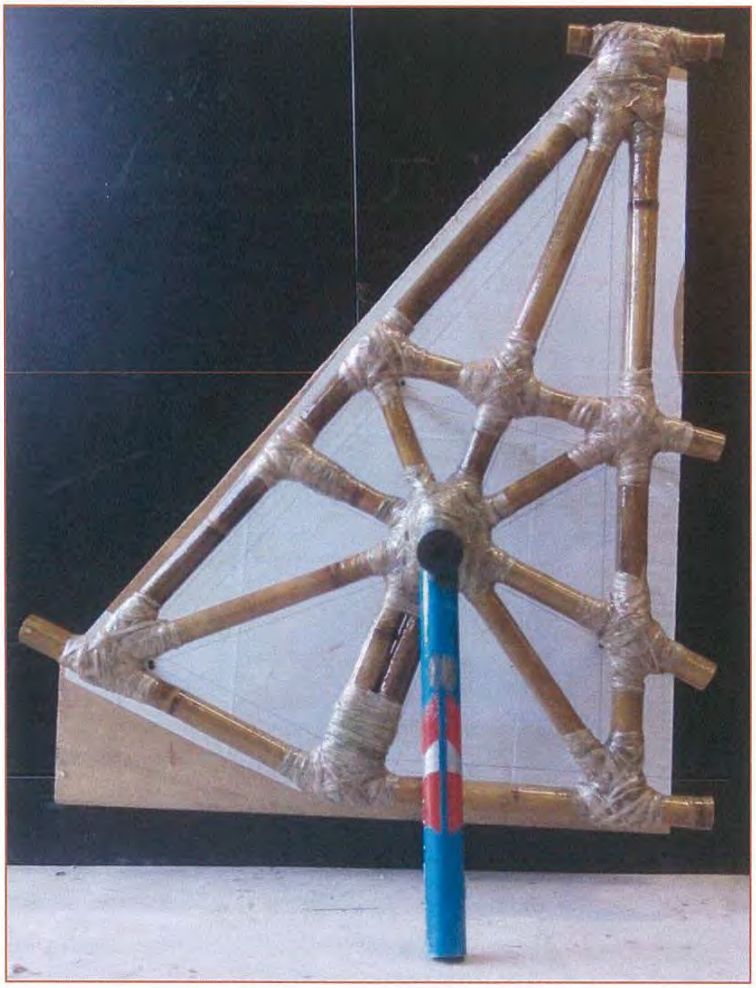

Figure 5-5: Final prototype frame with wrapped joints and load attachment point mounted

5.4 PROTOTYPE TESTING

Testing of the prototype was the validating step which provided the required results to compare the designed stress tolerance with the actual capabilities of the materials and construction techniques used. Originally the prototype was to be tested using the Dennison machine, however once construction was complete it was realised that the testing machine was too small to allow the positioning of the prototype in the compression area of the apparatus. A less precise technique was applied for the method of loading, and the process and outcomes are detailed in this section.

5.4.1 AIM

To load the prototype frame until failure and observe the failure mode and location on the frame for comparison against the Solidworks modelled simulation results. Loading conditions were designed to emulate the simulation that induced the highest stress concentrations in the Solidworks model, which was the cornering loading scenario.

5.4.2 APPARATUS

With the prototype mounted on the plywood board and the loading arm mounted to the front wheel axle mounting point, load could be applied directly into the frame. Because the Dennison machine did not provide enough space to perform this test it was decided to manually apply loads using weights in the 'heavy weights' room at the Unipol Gymnasium. Utilising gravity meant that the frame needed to be mounted so that the applied load would act in the desired direction. To ensure this, a free standing support structure was fabricated from timber which held the frame in an inverted position and on the required angle to apply the load in the same resultant direction as occurred in the cornering loading scenario.

Using values from the cornering scenario, the required angle was calculated to be 57° from horizontal (shown in Figure 5-6). With the prototype mounted to the support structure, the entire assembly was taken to the gym. Figure 5-7 shows the set up that was used to apply the gravitational load using the gym weights.

Figure 5-6: Loading application facilitated by support structure

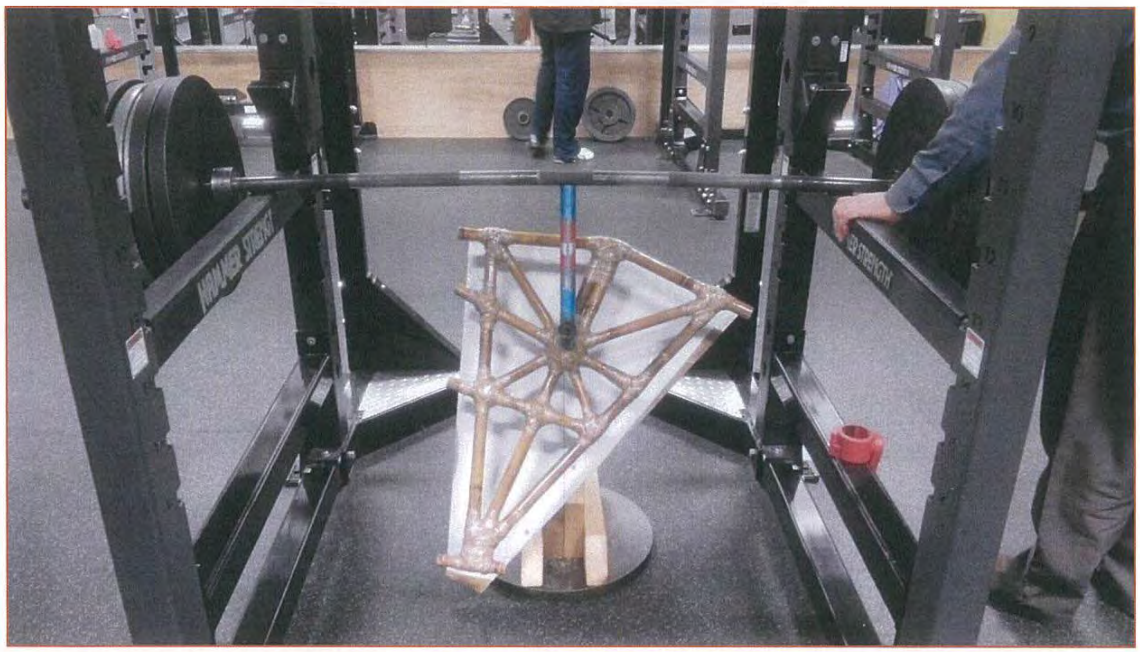

Figure 5-7: Loading of apparatus with weights to simulate applied loads during cornering simulation

5.4.3 PROCEDURE AND RESULTS

Weight was applied to the loading arm gradually in $40kg$ increments, by sliding a $20kg$ weight onto each end of the weight bar. The total mass of weights was increased until failure was observed in the structure. After the addition of $260kg$ of total mass (including $20kg$ weight bar and $6 \times 20kg$ weights on each end, the mass of the two individuals was also applied to the bar. Approximately three-quarters of their mass was supported on the ends of the weight bar before the prototype structure failed.

Failure in the structure occurred in the steel tube loading arm, this bent inwards towards the frame until the weight bar was resting on the support structure of the gym equipment (see Figure 5-7).

5.4.4 CALCULATIONS

Estimating the total mass that the structure was subjected to as the two individuals who applied their weight were indefinite about how much of their mass was being supported at the time of failure. The stated three-quarters is an estimate which has been used to calculate the loading value as shown in Equation 10

$$F_{test,total} = g \times (m_{weights} + m_{people}) \tag{10}$$

Where the mass of weights ($m_{weights}$) including the weights bar was $260kg$, the applied mass of the two individuals (m_{people}) was $0.75 \times 85 \times 2 = 127.5kg$ and gravity (g) is taken to be $9.81ms^{-2}$

Therefore the total force supported by the prototype under testing was:

$$F_{test,total} = 3.801kN$$

5.4.5 FACTOR OF SAFETY

Given that the prototype frame did not fail under the imposed conditions (failure at the support arm suggests that the front wheel is likely to have buckled under the loading before damage to the frame occurred) it is possible to state a minimum Factor of Safety value for the prototype when the observed and calculated loading capabilities are compared to the magnitude of the resultant load in the cornering scenario which acted on the same joint in the frame in the same direction (calculated in Equation 11).

$$F_{resultant,cornering} = \sqrt{F_x^2 + F_y^2} \tag{11}$$

Using data from Section 3.3.2, $F_{resultant,cornering} = 858N$

The FOS under this scenario can then be found using Equation 12:

$$FOS = \frac{F_{test,total}}{F_{resultant,cornering}} \quad (12)$$

Therefore the minimum value associated with the bamboo sections of the prototype frame is $FOS = 4.43$. This is much higher than the <1 value that the simulation results suggested.

5.5 PROTOTYPE PERFORMANCE ANALYSIS

The variation in performance between the Solidworks modelled and loaded prototype and the actual constructed and tested version is substantially different to produce a large variance in load tolerance and stress distribution. There are a number of reasons why this variation is likely to have occurred, some of which are explainable using the knowledge gained from this report. The following points outline the key variations between the Solidworks prototype model and the constructed prototype that have been identified.

- **Specimen properties variation** – During the investigation and testing of the *Himalayacalamus* mechanical properties for this project, a large variation in stress tolerance was discovered in the specimens tested. In order to maximise the FOS values and reduce the risk of unexpected failure, the lowest observed stress tolerance values from each experiment were treated as the minimum to be used during the design stage. The specimens used in the prototype construction could have had properties which easily exceeded this assumed minimum, meaning that their ability to tolerate loads and distribute stresses could have been much more substantial than the Solidworks model suggested. Other properties used in the Solidworks simulation were sourced from researched values that related different bamboo species; these could have provided a source of variation in the calculated force and stress distribution.
- **Culm dimensional variation** – The modelled prototype weldment used fixed cross sectional bamboo dimensions so that Solidworks could calculate the stress distribution in the frame. Culms used in the prototype construction were selected at random from the remaining population and not measured prior to use. Their diameter, wall thickness, and fibre density dimensions could easily have been different to those that were used by the Solidworks model. This would have contributed to their ability to tolerate loads and distribute stresses in the constructed prototype.
- **Joint construction** – The utilisation of a composite resin and flax fibre joining method that was unfamiliar and had little available technical data to inform the construction process with provided a large potential source of variation. Since little was known about the required size and shape of joints it was difficult to guarantee that they would provide load tolerance and stress distribution to the frame members. To counter this unknown entity the size of the joints was increased until they were bulky and very rigid. The main consequence of increasing the bulk of the joints was that they

were then likely to have a significant impact on the effective length of the frame members. In some of the shorter members the joint wrapping covered more than half of the total length of the member. This reduction in the 'free' length of the frame members would have reduced the amount of deflection that the frame sustained under loading and also increased the ability of the frame to distribute stresses over more of the frame members when loaded.

6 PROJECT DISCUSSION

This project has provided its author with valuable insight into the development and utilisation of new materials, and the complexities associated with this process. Overall this project has produced successful results in terms of the original aims. According to the gathered data and modelled designs it is possible to construct a functional velomobile using a bamboo spaceframe structure to provide the load and stress distribution required for expected use. Results for the estimated constructed mass of the frame suggest that the design would be comparable to commercially available models, while having a substantially lower materials cost due to the use of cheaper and less resource-intensive materials.

6.1 BAMBOO TREATMENT AND TESTING

The treatment and testing of bamboo specimens that was performed for this project played an integral part in determining the outcomes of the design process which the project set out to achieve. Results from the testing formed the technical basis for assessment and development of the successful frame design. These property testing results were obtained using the recommended techniques and fell within the appropriate expected ranges for full culm bamboo according to relevant research on similar tests of different species.

The tests and results described provided insight into the difference between the different stress tolerances for different loading orientations within the material, but more importantly the tests demonstrated the significance of the range of property values which could be present in any of the specimens. No clear visual clues were discovered which could be used to differentiate between the stronger and weaker specimens, and the range of results obtained from each of the tests was significant. The subsequent use of minimum tolerance values for design calculations was demonstrated by the prototype test have contributed to a substantial increase of the overall factor of safety of the material.

In order to provide a clearer outline of the material it would have also been beneficial to have included the obtainment of stress-strain relationship data from the tests performed, however this did not occur due to resource restrictions. Researched data used in place of this for elasticity and shear modulus values and Poisson's ratio is assumed to be sufficiently accurate to have produced reasonable results during the simulations.

6.2 FINAL DESIGN ASSESSMENT

The design and prototyping process demonstrates that it is possible to construct a velomobile frame from bamboo that would have the required strength and stiffness capabilities.

6.2.1 FRAME MASS

To conclude the initial assessment of the frame design success the calculation of likely total weight of the frame, and total weight of the built and fitted-out velomobile including the

required parts can be performed. The target mass for the fitted out velomobile was set at $25kg$ during the development work in this project, this mass is comprised of the individual mass of frame members, joints, wheels, drivetrain and steering components combined. Additional mass for seating and other components and fairing structure has also been included in this estimate.

Frame mass can be calculated by using an average mass per unit length for the *Himalayacalamus* culms of $0.25kg/m$ as was measured in the specimens gathered after the completion of heat treatment. The Solidworks model was comprised of individual frame members with a combined length of $35m$

Joint mass has been estimated based on the prototype construction results. For the 10 joints that were constructed $0.75kg$ of resin and $0.25kg$ of fibre was consumed. These quantities would vary depending on the size of the joint, however as the prototyped frame section contained some of the largest and most complex joints that would be present on the complete frame $0.1kg/joint$ can be treated as a reasonable estimate. The total number of joints in the frame was 49.

Values for mass of proprietary components are based on standard available high-end product weights. Additional fittings and components such as seat and fairing mass have been estimated based on the use of moderately light materials and standard construction techniques.

Table 6-1: Mass calculation of constructed velomobile using standard components

Component	Quantity	Mass per unit (kg)	Total Mass (kg)
Bamboo in frame	$35m$	$0.25/m$	8.75
Composite resin/fibre joints	49	$0.1/joint$	4.9
406mm wheel/tyre combo	3	1.2	3.6
Drive train group-set	1	3	3
Steering componentry	1	2	2
Seat	1	1	1
Fairing and additional components/fastenings	1	5	5
Total built mass			$\mathbf{28.25kg}$

Table 6-1 shows that the overall mass of the velomobile when constructed is likely to be higher than the initial estimate of $25kg$. A total mass of $28.25kg$ is still well within the range

of the mass of available velomobile models, which is between $20 - 30kg$ depending on the fitted components and materials used.

6.2.2 ACCURACY OF MODELS

The results from the simulated loading scenarios and the actual testing of the prototype frame showed that the models had a tendency to understate the strength and stress tolerance properties of the components being tested. This tendency towards lower factor of safety values has only been verified by one model under imprecise final testing conditions. However it can be suggested that due to the majority of input assumptions about material properties being made using the 'worst case' situations and values, that this understatement of safety is likely to be an accurate. Because of limitations with the models in terms of their ability to recreate the loading scenario and frame construction conditions, it is difficult to guarantee that the results for actual factor of safety under the loading conditions are correct. Based on results from the prototype testing it can be confidently suggested that the limitations of the Solidworks models and simulations only serve to generate a design which is safer than is suggested by the simulation results.

6.2.3 OPTIMISATION

The design process that was utilised for this project paid little attention to the optimisation of the frame in terms of minimising the overall mass while maintaining the load and stress distribution that would be required during use of the frame. During the development frame members were simply added and rearranged until the factor of safety was sufficiently high to deem the design successful. In order to improve the total frame mass and also reduce the complexity of the design to a point where construction could be justified, a further process of development is required to remove the unrequired members and to rearrange the frame so that the minimum number of frame members and joints are present. This would improve the resource use of the frame and also the manufacturing time required for construction. A further research area that could be investigated is the design and fabrication of the joints. Optimisation of this process based on actual material properties of the joint constituents would be likely to allow for reductions in materials use in the joints – leading to reductions in joint mass – and also to reductions in construction time of joints.

Further design optimisation could be performed using different types of bamboo. This project looked only at the largest diameter specimens of bamboo that are available locally, other species which grow in warmer regions could be obtained and assessed for use in a design which utilises a smaller number of large diameter frame members to achieve the same performance characteristics without the large number of joints that is required for this design.

6.3 CONCLUDING REMARKS

This project has provided a successful outcome which validates the goals of the proposed project by demonstrating that a velomobile space frame could be constructed from locally

sourced bamboo and would be able to provide the required performance which is expected of available commercial models. Conservative weight estimates for the frame and components required to make the velomobile rideable place it in the upper range of acceptable weight considering the limited features (i.e. no heavy suspension etc.) that it would possess. Without doubt this weight could be reduced by careful optimisation of the design features, to the point where it would be able to compete with available lightweight models.

Adapted mechanical testing methods used were verified by comparison with researched results to ensure that the ranges obtained were reasonable. Values obtained for a range of different stress tolerances in the material showed that the *Himalayacalamus hookerianus* species provided less structural integrity per unit area than some of the other more popular bamboo species used in construction elsewhere. However even with these properties the space frame was still able to be designed and prototyped with successful test results.

Models of the designed space frame and prototyped frame section demonstrated a tendency towards a lower factor of safety than was actually present in the prototyped version, meaning that there is good scope for producing a very safe structure which can perform as required.

7 APPENDICES

A. APPENDIX: LITERATURE REVIEW

Current Technologies in Human Powered Vehicle Frame and Fairing Design: A Critical Literature Review.

TOD COXHEAD 05007247

21/03/2014

This critical review investigates existing literature related to the topic of lightweight human-powered vehicle construction and design, with the purpose of investigating new possible construction methods for frame and fairing design. Technical topics covered include frame materials, frame design techniques, and aerodynamic fairing structure creation. Literature was sourced from a variety of locations and includes thesis papers, engineering reports, books, magazine and newspaper articles, blog posts and various types of other web-based content. All content discussed and referenced is relevant to the topic and this review demonstrates an accurate portrayal of the knowledge base that is publically available relating to the topic.

While the literature shows that commercial HPV manufacturers are generally focusing on using increasingly technical materials, other evidence suggests that potential exists to develop materials and technology such as bamboo frames and stretched skin fairings to create HPV designs that perform in a manner comparable to their commercial counterparts, whilst having a more desirable smaller environmental footprint.

Human Powered Vehicles: An Introduction

Human powered vehicles (HPV) are experiencing an increase in popularity due in part to a heightened public interest in the health, economic and environmental benefits that they provide to the user (Bauman, et al., 2008). Many different types of HPV's exist, and each is generally designed for a specific purpose. This review will focus on the frame construction and materials for the commuting and road transport sector of HPV technology, specifically the velomobile and where appropriate, the common bicycle. Peter Cox describes the velomobile as being: "...the ultimate level of innovation in human-powered vehicles...which encloses the seated positioned rider within an integral body shell, providing weatherproofing and luggage-carrying capacity" (Cox, 2010)(p. 129).

Bicycle Construction

The most common bicycle frame construction method is to use metal tubes (usually aluminium or steel) that are welded or brazed to form a diamond shape. Craig Calfee is a reputed bicycle frame manufacturer who contradicts this trend in a paper that analyses the range of materials available to bicycle builders today by saying "the future of cycling is moving away from metals ... Composite monocoque construction methods are becoming accepted

[by consumers] as the 'future of bicycles'" (Calfee, Technical White Paper, 2014). This summary is corroborated in an opinion piece by another bicycle manufacturer David Fancourt, who describes carbon fibre frames as the lightest and strongest available option for conventional bicycle frame shapes (Fancourt, 2013). This is further confirmed by the bulk of the high end frames available from top manufacturers (Specialized, 2014), (Trek, 2014) all being constructed using carbon fibre reinforced plastics.

As an alternative to composite construction, Calfee discusses lugged bamboo bicycle frame construction in another report and notes that "Bamboo is the smoothest riding frame material on the market" (Calfee Design, 2014). Journalist Matthew Sparkes agrees in his article for the Guardian (Sparkes, 2009). In another article Calfee cites the infinite size range of bamboo frame pieces as making it the ideal material to use for customizing frame performance characteristics (Calfee, Building Bamboo Bikes, 2014). Greg Jorgenson suggests that bamboo bicycles are also ideal for developing countries and small scale construction applications due to the availability of the materials and the level of simplicity associated with the construction process. (Jorgenson, 2010). Andrea Riedl notes in a web article that "if there were a prize for the bike with the lowest carbon footprint ... bamboo bikes would win it hands down" (Reidl, 2010). Literature produced by these authors all suggests that use of bamboo as a bicycle frame construction material produces strong, lightweight and economically viable structures.

Velomobile Construction

The most common commercial velomobile construction type is an integrated monocoque fairing (generally composite reinforced plastic), examples are high end production models such as the Trisled 'Avatar' (Kevlar reinforced composite) (Trisled Australia, 2013) and the Velomobile.NL 'Quest' (carbon reinforced composite) (Velomobile.NL, 2014). This construction method creates a strong and lightweight structure that can be easily shaped into an efficient aerodynamic profile. Another technique used for creating an aerodynamic shaped velomobile is to attach a lightweight superficial fairing to an existing recumbent bicycle or tricycle sub-frame; examples of this are the Steintrikes 'Leitra Avancee' (steel frame with reinforced plastic fairing) (Steintrikes, 2009), and the Mosquito 'Zero' (Wooden frame with isogrid structure fairing and stretched cover) (Mosquito Velomobiles, 2012). Comparisons between products of these two construction methods shows that lighter structures can be produced by utilising the skin on frame approach, however this is often at the cost of durability and mass-manufacturing capabilities.

Space Frame Design and Construction

Designing and constructing a space frame for an HPV involves a number of factors, materials are one key component. Alexander Vittouris and Mark Richardson investigated growing a frame using bamboo shoots that were shaped around formers while still juvenile. They had moderate success with developing curve shaped frame members and constructed a working

prototype of their design. From this they concluded that "the 'Ajiro' concept establishes that space frame construction of HPVs presents an alternative to 'body on frame' [monocoque] techniques presently used by velomobiles." (Vittouris & Richardson, 2011)(p. 14). Rich Nelson et al. have researched and built a bamboo velomobile for racing as part of a university project, and documented the process. They performed physical bamboo testing, as well as finite element analysis on their CAD modelled bamboo frame (Nelson, 2010). Their research showed that a strong bamboo space frame was feasible, and that it could be created to meet the load requirements of cycle racing without failure. They manufactured a composite glass fibre reinforced plastic fairing to create the aerodynamic shape, but this provided little if any of the structural integrity to the vehicle, and contributed a significant amount to overall the weight.

Lightweight Skin Structures

Using a thin lightweight skin to create an impervious aerodynamic surface-shape is a technique that has been utilised by both the aircraft construction industry and the marine vessel construction industry for some time. During the Second World War, Sir Barnes Wallis implemented stretched skin technology in aircraft that he designed, using a geodesic wooden frame to provide the shape and structural integrity of the aircraft (Kerley, 2007). Fabric covered wood framed aircraft are still common today, with some of the lightest aircraft being produced in this manner (Heintz, 2009) Christine de Merchant describes the geodesic design technique as having been developed by Inuit people originally for kayak manufacture (de Merchant, 2014) however this technique is still utilised by makers of kayaks and lightweight boats such as Geodesic Airolite and other companies. Kudzu Craft design and manufacture a similar kayak product, which has a stretched skin structure shaped over a wooden frame; however their frames are orthogonal in shape (Kudzu Craft, 2014). Although stretched skin construction has not been used extensively in HPV manufacture yet, Mosquito Velomobiles have produced a working prototype of a wood 'isogrid' (geodesic) framed velomobile with a stretched plastic skin, achieving a very low kerb weight (under 20kg) (Mosquito Velomobiles, 2012). Lightning Bikes also manufacture a stretched skin recumbent bicycle which uses the bicycles' functional space frame to support the skin covering (Lightning Cycle Dynamics, 2014). Other examples can be found of lightweight skin structures in velomobile construction, however these are almost always made by the owners; and no commercial examples are available – the supporting frame for the skin is created and mounted to an existing tricycle or bicycle frame, and foam or corflute plastic panelling is then added to create the skin. One example of this is the 'Facet V1 Velomobile' (Jeff-o, 2010).

Discussion

This literature review includes and references information, facts and opinions from a wide range of sources including thesis papers, engineering reports, magazine and newspaper articles, blog posts and various types of additional web-based content. Comprehensive online content searches were performed using strings of key words to obtain details of relevant literature, the majority of which was then sourced directly online. Numerous searches returned few results that were of any relevance or that were backed up by any significant data (particularly commercial product details). This lack of evidence and data could be caused by two possible scenarios: either literature is not available because the knowledge has not yet been discovered, or, literature is not available because the field of expertise is poorly documented and/or too commercially sensitive to be released. Both of these potential scenarios therefore provide confirmation that more well-documented evidence based research is needed in the field of HPV development, particularly where non-commercial or open source project applications are concerned. For the most part, commercial HPV construction appears to be focused on high performance, high value materials and technology for developments in frame and fairing design on velomobiles. Literature in this review displays convincing evidence that developing technologies in the bicycle industry such as bamboo frame construction could be suitable for use in the design of a light weight low cost velomobile. Kerb weights and aerodynamic performance could be optimised by employing a light stretched skin fairing structure, and possibly incorporating geodesic framing techniques to form efficient fairing shapes.

B. APPENDIX: HEAT TREATMENT

BA. PROCESS DEVELOPMENT

The following heat treatment process used on the bamboo stock was developed based on research and reading from various sources where similar processes have been described. The most commonly found application of this process is in rod making for fly fishing. Schott (2006) published results which outlined the application of this process and guidelines for its optimisation. Key features to avoid were 1) significant visual discolouration of specimens (browning etc.) and 2) exposure to temperatures in excess of 200°C (often the two features are linked) (Schott, 2006). Although this process was designed to reduce the moisture content, it is important to note that there was always going to be some moisture present in the specimens as dry bamboo has a tendency to balance its moisture content with the humidity present in the surrounding environment. There was no end goal for the moisture content level, except to remove excess water from the growing process, and encourage faster drying of the specimens.

BB. TREATMENT APPARATUS

To perform the heat treatment process, an apparatus in the ceramics department of the Otago Polytechnic was utilised. The set-up is shown in Figure 7-1 on the following page; it consisted of a thermostatically controlled electric kiln with an additional thermocouple probe mounted at the top front face. A steel basket framework seated on a ceramic plate was used to support the bamboo and maintain its upright position in the kiln.

BC. SPECIMEN PREPARATION

All bamboo sections to be heat treated were cut to similar lengths, this was performed by hand using a hacksaw with the bamboo supported in a v-block. The maximum length that could be placed vertically into the kiln was $800mm$, sections were cut to $750mm$ and the ends were cleaned with sandpaper. Due to heat expansion of the air inside the culms during heating, it was necessary to puncture the nodes to avoid cracking and explosion of the sections. This was performed using a length of $1.5mm$ spring steel wire which was sharpened on one end and inserted through the nodes inside the sections.

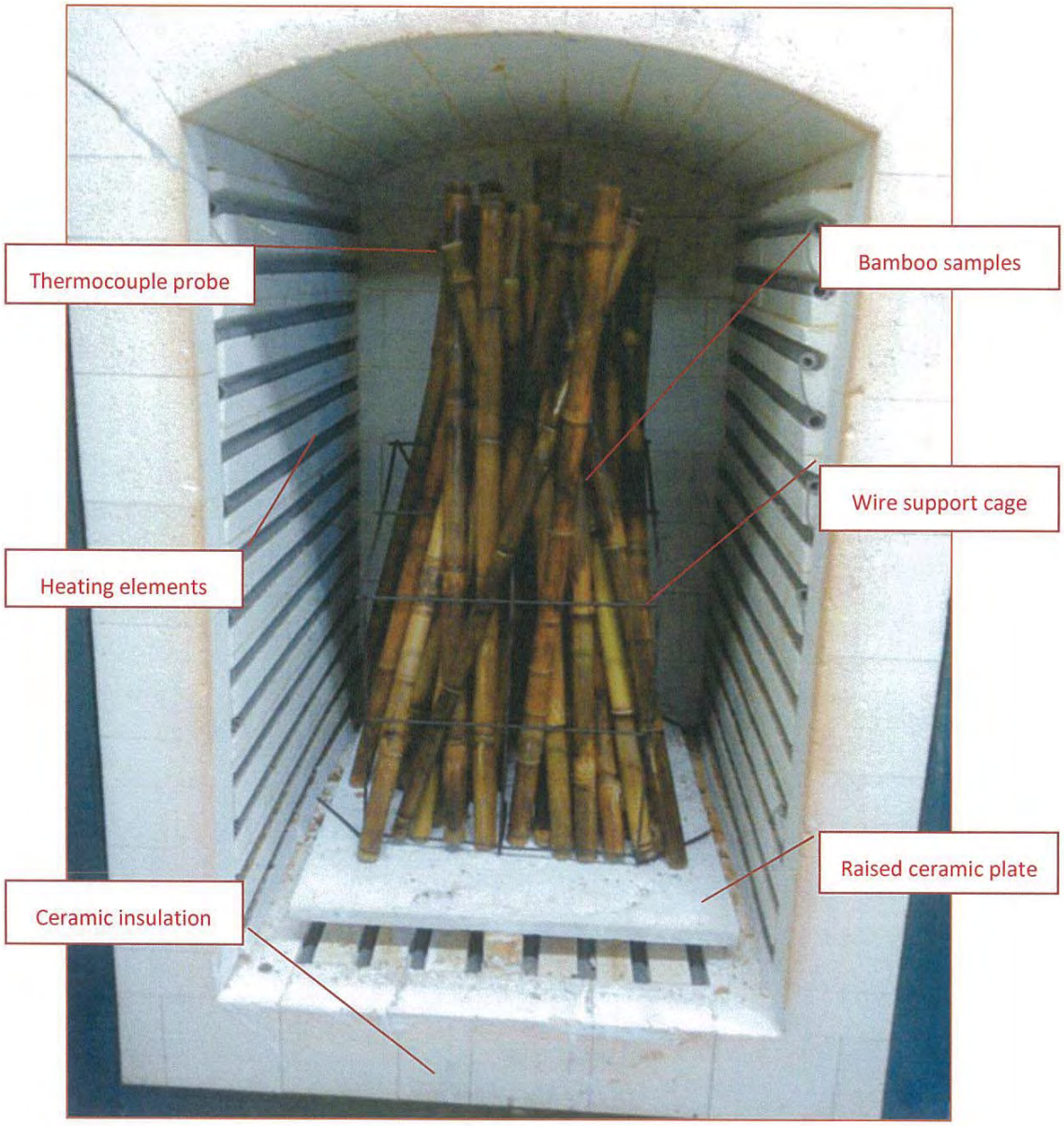

Figure 7-1: Main batch of samples in position in kiln with labelled apparatus features

BD. TRIAL TREATMENT PROCEDURE

In order to ascertain the best possible time period for heat treatment, a test run was carried out using the described apparatus and a small selection of four specimens. Specimens for this test were selected to obtain the maximum variety in wall thickness, initial surface colour, and mass so that the effect of prolonged heating on these variables could be observed independently. The following steps were performed with the trial specimens:

i. Weighed, measured and marked specimens
ii. Specimens placed upright in kiln with temp fluctuating between 150°C and 190°C
iii. After 10 minutes elapsed time, specimens were removed from kiln and a $25mm$ section was cut from top end of each specimen using a hacksaw. The removed section was marked with time and orientation (noting the cut edge), these were air cooled.
iv. Remaining sections of specimens were inverted and replaced to kiln.
v. At 10 minute intervals after this, specimens were removed and rearranged, with repeated removal and cataloguing of $25mm$ sections from each specimen as in iii.
vi. When visible browning could be seen on cut face of removed sections (smoothed with fine grade sandpaper to identify), the heat treatment process was stopped and specimens removed from kiln.

BE. TRIAL TREATMENT RESULTS

Figure 7-2 shows the rate at which the mass of the specimens reduced during heating; if this heating process had been continued then the gradient of these plotted lines it could be expected to reduce to almost horizontal at which point the moisture content would not be changing any more. This was not necessary as it was known that once removed from the kiln the samples would regain any moisture that was required to place them in equilibrium with their surrounding environment.

Rather than mapping moisture content it was decided that the colour of the specimens would be the guide for the extent of heating necessary. After 50 minutes of heating, samples from specimens began to show visible browning in the polished wall cross section. This colour change is an undesirable effect which reduces the integrity of the specimen by degrading the fibre structure (Schott, 2006)(p.9); it was concluded that two constant heating periods of 20 minutes each would be sufficient to treat the majority of the specimens without incurring significant discolouration and loss of structural integrity

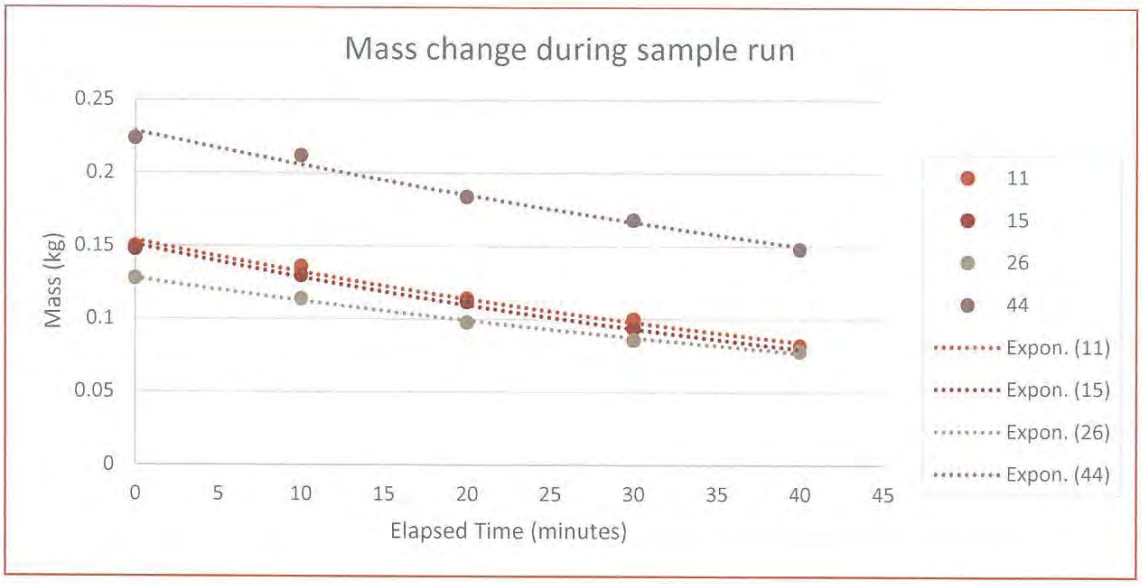

Figure 7-2: Plotted mass change during trial heat treatment

BF. APPLIED PROCEDURE

Having established the ideal time for heat treatment of specimens, the following procedure was utilised to treat the remaining specimens:

i. Weighed, measured and marked specimens
ii. Specimens placed vertically in kiln at temperature $150°C - 190°C$
iii. After 20 minutes elapsed time, specimens were removed from kiln, inverted, and returned to the kiln.
iv. After a further 20 minutes specimens were removed from the kiln and fillet stacked to air cool.
v. Once cooled, specimens were measured, colour categorized and weighed

BG. RESULTS

To identify any trends between visual characteristics and mechanical properties of specimens, a spreadsheet was used. Moisture loss (determined by mass), dimensional changes and colour changes were all compared before and after heating as part of this process. As no un-heat treated control specimens were tested (heat treatment was assumed to be valid based on the available information) it is not possible to assess the change in properties as a result of this applied process.

C. APPENDIX: BAMBOO TESTING

CA. STATIC BENDING

CA1 APPARATUS AND PROCEDURE

This experiment has been performed based on ISO 22157-2 guidelines, which provided the appropriate designs for the four point specimen support apparatus as shown in Figure 7-3 This structure incorporated pivoting formed wooden supports for the culms and was designed to avoid crushing of the culm wall during application of load to the specimen. The design that was used for this experiment was modified slightly from the recommended version in order to accommodate the shorter specimen length and to utilise cheaply available materials, this is shown in Figure 7-4.

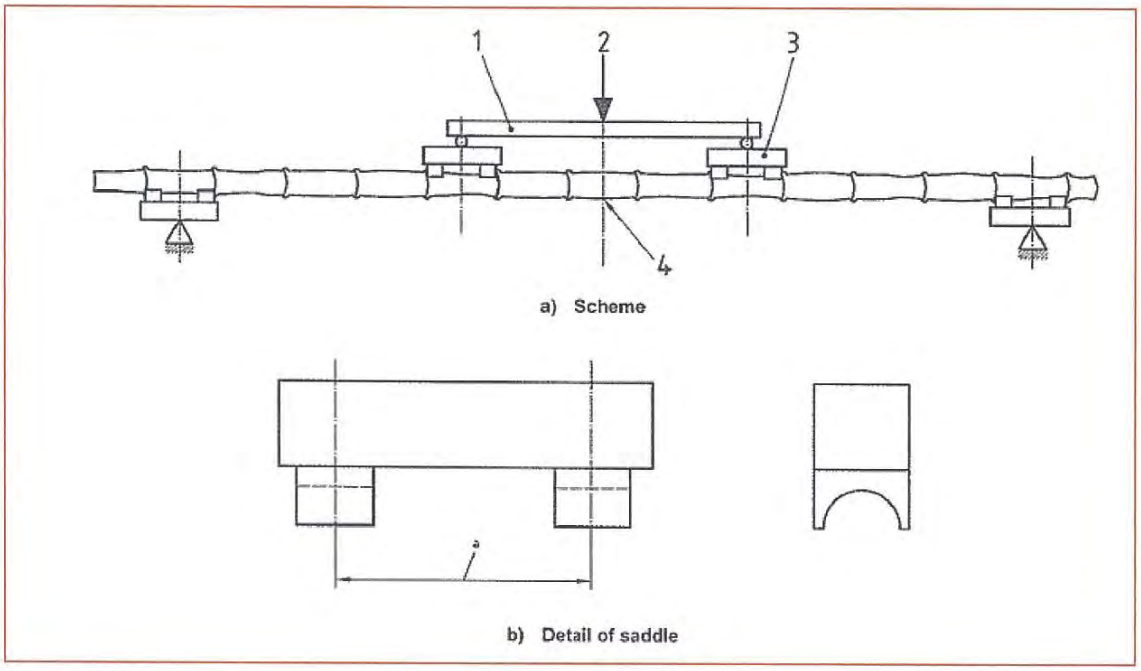

Figure 7-3: ISO 22157-1 recommended apparatus for four point static bending tests

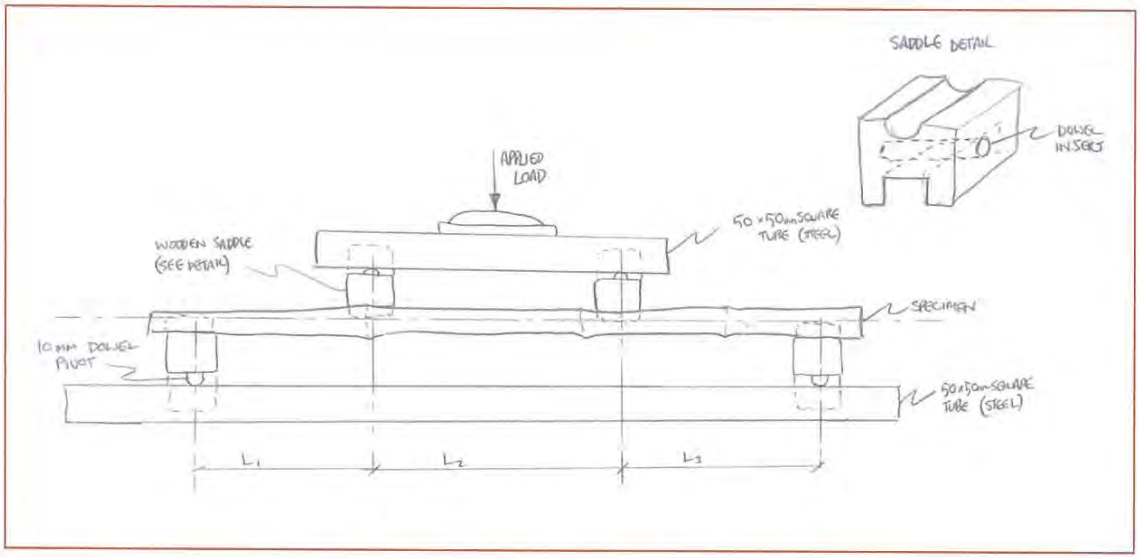

Figure 7-4: Diagram of constructed apparatus showing constructed wooden saddles in place and free span measurements L1 L2 and L3

In order to seat the apparatus directly beneath the crosshead of the Dennison machine it was necessary to place rollers underneath the lower square beam, an approximate $10N$ load was applied by the machine to hold the specimen and support apparatus in place. Lower supports were located as close to the ends of the specimens as possible, centred on the closest nodes that were present. Upper supports were centred on nodes that were within the correct area where possible, with the aim of locating them such that the spacing between each of the four supports was approximately equal. Where a node could not be located in the correct area the support acted directly onto the internode area of the specimen.

Once the specimen was arranged in the supports and the $10N$ holding load was applied, measurements of the spacing between each of the supports were taken and recorded along with the already measured average diameter and average wall thickness of the specimen. The digital gauge being used to measure deflection was zeroed at this point. Loading was applied to the specimen at an approximate rate of $0.5mm/s$ as per the instructions in ISO 22157-2, with a brief pause at each $100N$ interval to record the accumulated deflection. Failure point was recorded as a marked decrease in the applied load even as the crosshead continued to move, for most specimens this point was also audible (cracking sounds) and/or visible (through fracture formation in the specimen and non-uniform deformation.) This process was repeated with all ten specimens.

CAII RESULTS AND CALCULATIONS

Values displayed in Table 7-1 are those that have been used in the following calculations for the stress at failure in each specimen (assuming that the failure occurred as a result of the bending conditions). The free span measurement used for calculation is the maximum measured distance between any two support blocks in the setup for each specimen (refer Figure 7-4), as this is the point where the maximum bending moment is found.

Table 7-1: Bending test recorded values

Test Number	Specimen Number:	Diameter D (mm)	Wall thickness t (mm)	Max free span (mm)	Max Load at Failure P (N)
1	7	20.5	2	240	420
2	19	22.5	2	240	830
3	39	22	2	270	320
4	4	22	2.3	300	400
5	24	25	3	258	530
6	13	25.5	2.9	320	420
7	33	23	3	260	430
8	14	22	2.2	265	200
9	21	23	2.5	282	520
10	1	22	2.9	268	380

To calculate the bending moment M which caused failure in the culm, data from Table 7-1 can be substituted into Equation 14. To calculate bending stress, the second moment of area I_{xx} is found by treating the bamboo culms as a uniform diameter and wall thickness hollow tube and substituting values into Equation 15. Bending stress $\sigma_{bending}$ can then be found using Equation 16. Equation 17 shows the compiled complete equation for bending stress and this simplified to 18.

$$M = \frac{P \cdot L}{2} \tag{14}$$

$$I_{xx} = \frac{\pi(D^4 - (D - 2t)^4)}{64} \tag{15}$$

$$\sigma_{bending} = \frac{M \cdot D}{2 \cdot I_{xx}} \tag{16}$$

Therefore:

$$\sigma_{bending} = \frac{\left(\frac{PL}{2}\right) \cdot D}{2 \cdot \left(\frac{\pi(D^4 - (D - 2t)^4)}{64}\right)} \tag{17}$$

Which simplifies to:

$$\sigma_{bending} = \frac{16PLD}{\pi(D^4 - (D - 2t)^4)} \quad (18)$$

The following is a sample calculation demonstrating the use of Equation 18 to calculate the maximum bending stress present in specimen 7 during the first test. Table 7-2 shows the values calculated for all of the tested specimens, these were calculated using an Excel spreadsheet with the formulas entered into the cell coding.

$$\sigma_{bending} = \frac{16\times420\times240\times20.5}{\pi\times(20.5^4-(20.5-2\times2)^4)}$$

$$\sigma_{bending} = \frac{33062400}{321981.83}$$

$$\sigma_{bending} = 102.7MPa$$

Table 7-2: Calculated bending stress values

Test Number	Specimen Number	Second moment area I_{xx} (mm^4)	Bending moment M (N/mm)	Bending Stress $(MPa)/(N/mm^2)$
1	7	5031	50400	102.7
2	19	7763	99600	144.4
3	39	6346	43200	74.9
4	4	6999	60000	94.3
5	24	12778	68370	66.9
6	13	13362	67200	64.1
7	33	9637	55900	66.7
8	14	6789	26500	42.9
9	21	8584	73320	98.2
10	1	8118	50920	69.0

Table 7-3: Summary of critical values from bending stress experiment

Sample Size (n)	Min	Max	Range	Average	Standard Deviation
10	42.9Mpa	144.4Mpa	101.5Mpa	82.4MPa	**28.4Mpa**

CAIII DISCUSSION OF DATA VALIDITY

Results from this experiment show a substantial range of variation. A review of published data by Rottke (2002) (p. 10) suggests that the expected range could be anywhere from $74MPa - 276MPa$ - this is also a substantial range, and even though the species reviewed by Rottke

(*Guadua angustifolia*) is different from the *Himalayacalamus* that has been researched in this project, it is reasonable to expect that a broad range of answers might also be needed to accurately represent the samples used. Although the average bending stress (Table 7-3) falls within the range proposed by Rottke, half of the values calculated are below the proposed minimum. It is difficult to explain this discrepancy as there are a number of compounding factors which could easily have caused such variation. The following points outline some of the most prominent and likely reasons for this discrepancy, they are presented in a hypothetical/non-empirical format and any verification of their validity would require additional research and testing which is deemed outside of the scope of this project.

One substantial feature of this experiment which is likely to have had an impact on the resulting calculated bending stress values was shown by the types of failure mode which the specimens demonstrated at maximum load. Figures' 7-5a and 7-5b show two different failure types noted during the experiment, 7-5a demonstrates longitudinal splitting of the culm – similar to what one would expect to observe in a thin walled tube bending failure, and 7-5b appears to have failed as a result of the wooden saddle impacting the wall of the culm under large amounts of deflection and inducing a 'crush' failure.

Figure 7-5: Bending failure modes exhibited by specimens. Left (a) longitudinal splitting of culm. Right (b) Crushing of culm wall.

While this experiment was designed to initiate a bending failure in the specimen, one key feature of the apparatus design/experiment protocol was missed during planning. ISO 22157 discusses the minimum 'free length' of samples as needing to be more than $27 \times Diameter$ to avoid inducing 'transverse shear' failure in the specimen as it deflected under load. Initially, this author assumed that 'free length' referred to the total specimen length. It was not until later when calculation processes were being investigated that it was realised that 'free length' actually referred to the uninterrupted spacing between the saddles which were applying load to the specimen. Unfortunately this free length minimum could not have been achieved under the four point loading criteria as all of the samples had been cut to a length almost four times too short before this was realised.

Another feature of the apparatus design which contributed to the undesirable failure mode in the specimens was the shape of the wooden saddles and the design of the pivot points which they rested on. Support structure designs shown in ISO 22157 (see Figure 7-3) depict each saddle as being constructed from two thin shaped sections which are stuck together such that the load applied through them can act on a node. These saddles are then seated on a pivot which allows them to rotate through a large angle. The saddles constructed and used in these experiments (see Figure 7-4) were each cut from a single $100mm \times 50mm$ thick section of timber shaped to cradle the specimen, with a length of dowel inserted into the base so that when the saddles were positioned on the square tube they were able to pivot within a limited range to allow for radius curvature induced by deflection of the specimen under load. This radius of curvature was more extreme than expected, and in some cases the saddles were unable to pivot sufficiently to follow the shape of the specimen, and the load was then transferred through the edge of the saddle; The result of this is shown in Figure 7-6 where the failure has occurred at the impinging edge of the saddle (with load not being applied with even distribution or across a node).

Figure 7-6: Crush failure at edge of support possibly due to insufficient ability for support to rotate.

Based on these two sources of non-bending failure mode, it can be suggested that some of the specimens tested in the bending apparatus actually failed in shear, specifically transverse shear. While tests on transverse shear stress limits of the specimens were not performed for this project, it is possible that this would be lower than the bending stress limit, which would explain the failure in shear of some of the specimens before bending failure occurred, however some of the tested specimens did fail in what appears to be an example of static bending.

Since neither of these proposed causes of failure have been isolated or properly verified (would require more testing, for which resources and time are not available), the only appropriate assumption is that the minimum recorded specimen failures *could* have been caused by the bending scenario, even if this is unlikely. Use of any maximum bending stress values for design purposes should therefore implement the lowest calculated value of $42.9MPa$.

CB. SHEAR

CB1 APPARATUS AND PROCEDURE

In order to ensure that the failure of the specimen in was encouraged to occur in shear parallel to the fibres, an apparatus was designed in accordance with recommendations found in ISO 22157-2. This apparatus is shown in Figure 7-7, it comprised of two sets of opposing triangular steel $3mm$ thick plates which moved towards each other along a perpendicular rod-in-tube guide. Short sections of specimen were placed over the guide rod and the apparatus was slid together such that when load was applied using the testing machine, two quarters of the specimen were forced in an opposite direction to the adjacent two quarters causing the specimen to fail in shear parallel to the fibres in the specimen.

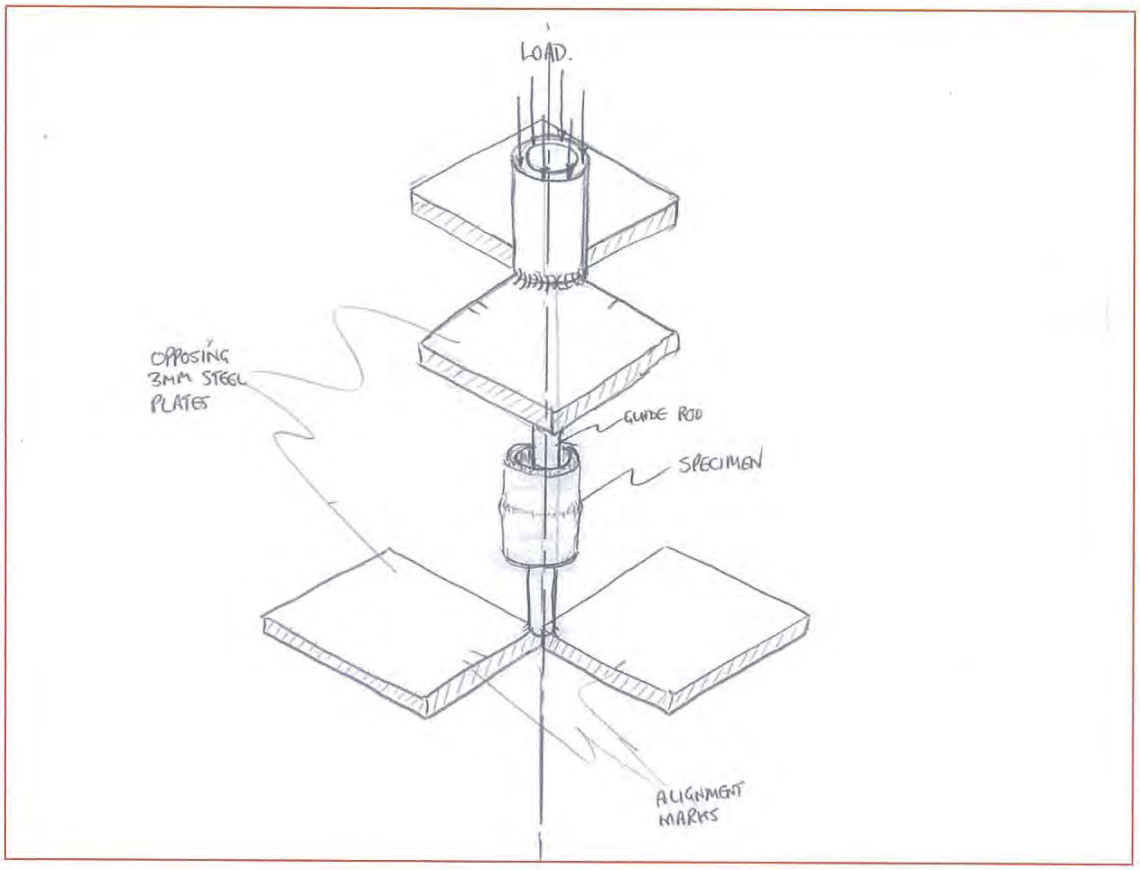

Figure 7-7: Shear apparatus showing separated view of upper and lower components and specimen located between shear plates

Specimens for this experiment were cut from the intact portions of specimens used in the static bending experiments using a band saw. According to recommendations in ISO 22157-2, specimens were cut to a length either equal to their diameter or $30mm$, whichever was longer. Once cut, the ends were sanded with fine grade paper to create a uniform flat surface which was perpendicular to the axis of the fibres. Specimens were then measured with length and average wall thickness being recorded for each. Approximately half of the specimens had a node located in the shear area.

Specimens were mounted in the apparatus so that they were centred relative to the plates described previously, the upper plates were slid down over the specimen and aligned using a set square to ensure that they lined up correctly and would not cause supported compression under loading.

A small initial load of $50N$ was applied to 'set' the apparatus in position. Increasing load was then applied to the specimens at a crosshead speed of approximately $0.05mm/s$ until the force reading started reducing, denoting failure in the specimen. At such a slow crosshead speed this dial was the only indicator of the failure occurring, audible cracking sounds and visible failure did not occur until the crosshead had moved a further one or two millimetres at which point four shear lines were clearly visible in the specimen as shown in Figure 7-8. Maximum supported load was recorded and the specimen was removed from the machine.

Figure 7-8: Shear lines visible in specimen after continued loading past failure point

CBII RESULTS AND CALCULATIONS

Recorded results from this experiment are displayed in Table 7-4 showing the dimensions of each specimen and the corresponding maximum supported load.

Table 7-4: Shear stress experiment recorded specimen values

Test Number	Specimen number	Length $L\ (mm)$	Wall thickness $t\ (mm)$	Node in specimen?	Max load at failure $P\ (N)$
1	7	35	2.8	N	1720
2	$13B$	29.8	3.6	N	2240
3	$24D$	37.3	3.2	N	3840
4	$33B$	31.8	2.6	N	2980
5	$24C$	39.1	2.5	N	3820
6	$1C$	28.8	2.4	N	2725
7	$13A$	28.7	3	Y	2740
8	$33A$	30.2	3.4	Y	3300
9	$24B$	31	4	Y	4140
10	$24A$	30	3.5	Y	3820
11	$1B$	30.4	3	Y	3640
12	$1A$	29.5	3	Y	3920

To calculate the shear stress $\tau_{parallel\ fibre}$ which caused failure in the specimen, the sum of all four cross sectional shear-areas $(\sum A)$ is needed. Calculation of this is shown in Equation 19, with the calculation of shear stress shown in Equation 20:

$$\sum A = 4 \cdot L \cdot t \tag{19}$$

$$\tau_{parallel\ fibre} = \frac{P}{\sum A} \tag{20}$$

Therefore $\tau_{parallel\ fibre}$ can be found using Equation 21:

$$\tau_{parallel\ fibre} = \frac{P}{4 \cdot L \cdot t} \tag{21}$$

The following is a sample process showing the calculation of the shear stress at failure of test 1, specimen 7. Calculated results for all of the specimens tested are shown in Table 7-5, these values were calculated using Excel.

$$\tau_{parallel\ fibre} = \frac{1720}{4 \times 35 \times 2.8}$$

$$\tau_{parallel\ fibre} = 4.4MPa$$

Table 7-5: Shear stress experiment calculated values

Specimen number	Shear Area $\sum A\,(mm^2)$	Shear Stress $\tau_{maximum}$ $(Mpa)/(N/mm^2)$	Node in specimen?
7	392.0	4.4	N
$13B$	429.1	5.2	N
$24D$	477.4	8.0	N
$33B$	330.7	9.0	N
$24C$	391.0	9.8	N
$1C$	276.5	9.9	N
$13A$	344.4	8.0	Y
$33A$	410.7	8.0	Y
$24B$	461.8	9.0	Y
$24A$	420.0	9.1	Y
$1B$	364.8	10.0	Y
$1A$	354.0	11.1	Y

Table 7-6: Summary of critical values from shear stress experiment

Sample Size (n)	Min	Max	Range	Average	Standard Deviation
12	$4.4MPa$	$11.1MPa$	$6.7MPa$	$8.45Mpa$	$1.94Mpa$

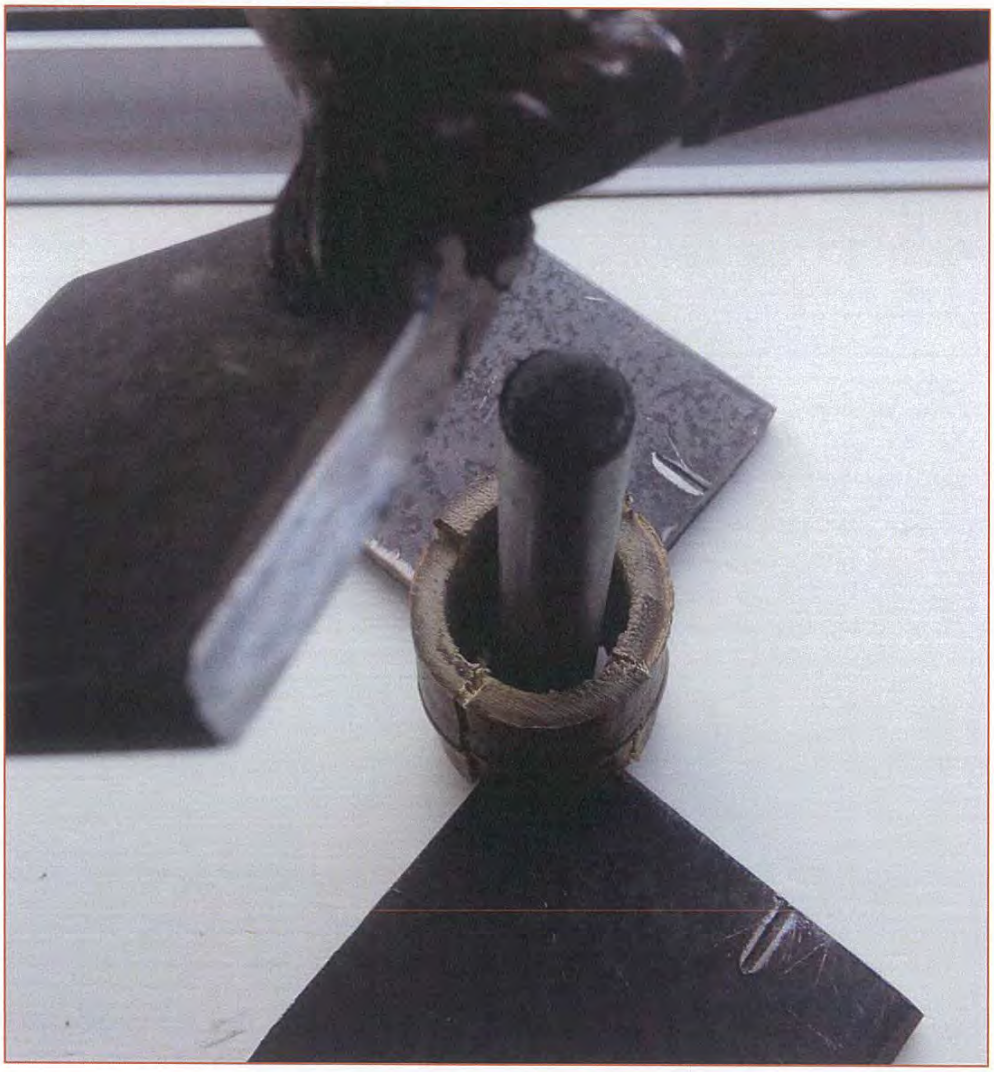

Figure 7-9: Shear failure points visible in specimen after removal of upper section of apparatus

Results from this experiment show considerable variation over a large range. None of the recorded results can be termed as outlying, and there appears to be no significant weakening as a result of the specimen having a node in it; however when compared to the reviewed published data from Rottke (2002) some of these values are lower than expected. Rottke's review suggests that based on available literature, the minimum 'thrust' (shear) value should be $9MPa$. This is higher than the calculated average of $8.45MPa$ (Table 7-6) and more than double the minimum calculated value of $4.4MPa$. The species reviewed by Rottke (G*uadua angustifolia*) is different from the *Himalayacalamus* that has been researched in this project, and it is reasonable to expect that a broad range of answers might be possible across species. As the specimens all appeared to fail in shear as planned, the only appropriate assumption is that the minimum recorded specimen failures have been caused by expected the shear forces. Use of any maximum parallel fibre shear stress values for design purposes should therefore implement the lowest calculated value of $4.4MPa$.

CC. TENSION

CCI APPARATUS AND PROCEDURE

For this experiment, the vertically aligned vice jaws on the Dennison testing machine were used to grip the samples while load was applied. In order to encourage the specimens to fail in pure tension it was necessary to shape them with a varying cross sectional area so that the vice jaws could achieve a solid grip on the ends of the specimen, while failure occurred in the unsupported section between the jaws. This setup is shown in Figure 7-10.

In accordance with recommendations found in ISO 22157-2, specimens were carved into approximate shape and size as per Figure 7-11 using a sharp knife. A total of ten specimens were tested, four with nodes and four without. Specimens with nodes were shaped to locate the node in the centre of the narrow section of the profile.

Figure 7-10: Specimen in position between vice-jaws of Dennison testing machine

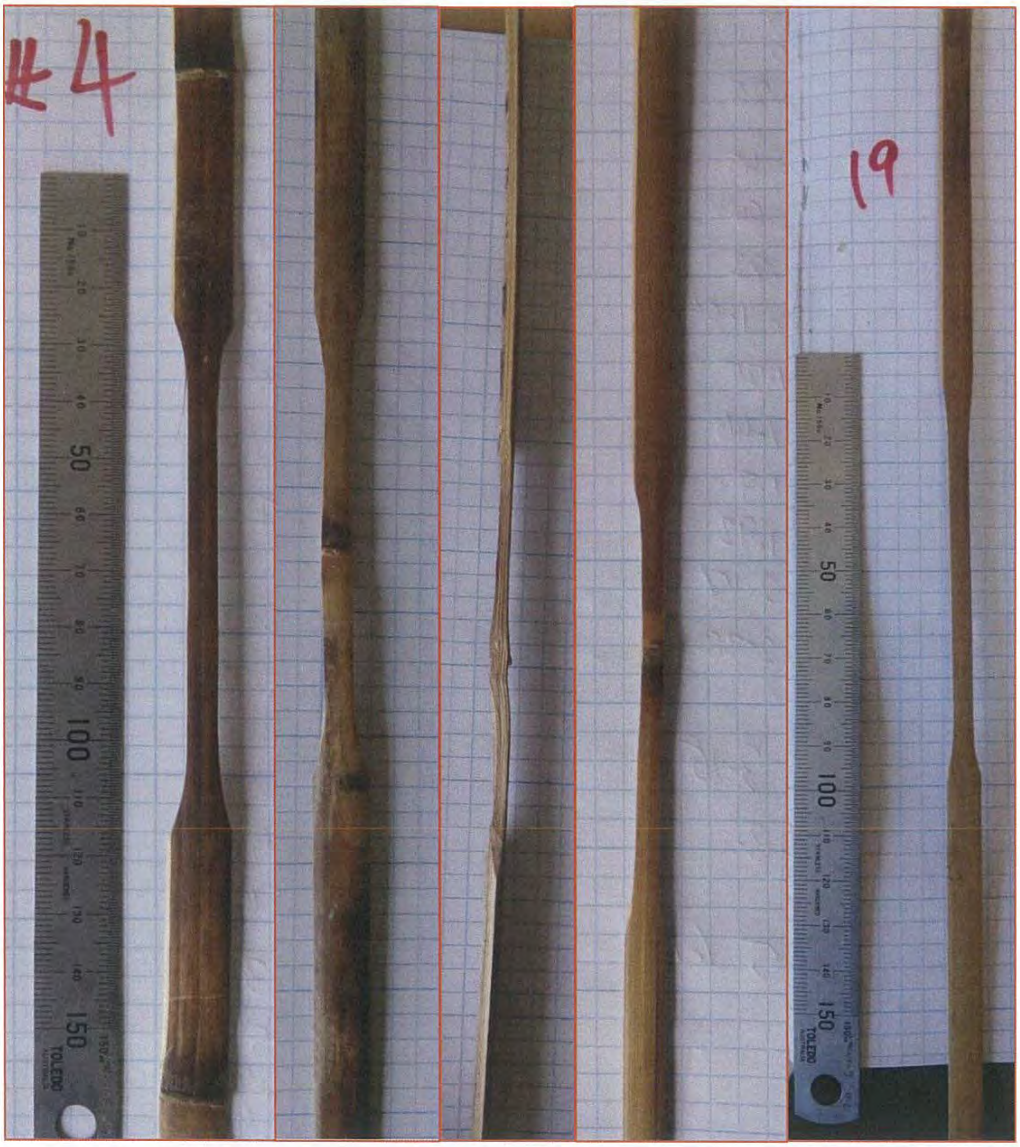

Figure 7-11: Selected specimens prior to tensile testing showing necked shape and larger ends for clamping

Once specimens had been prepared, measurements of the cross sectional area were taken. For the specimens with no node this was uniform along the length of the narrow section, for the sections with nodes these measurements were taken at the node itself.

With the vice jaws in the Dennison machine, one end of the specimen was orientated vertically in the upper jaws and clamped firmly in place. The crosshead was then lowered to locate the lower end of the specimen between the lower vice jaws, this was also clamped firmly to hold the specimen. Because the vice jaws tighten via a sliding wedge mechanism it

was necessary to carefully control the movement of the crosshead while tightening the lower set to take up any compressive force being applied to the specimen, this was performed while watching the machines loading gauge – when compressive forces were registered this rotated anticlockwise to below the zero mark, and the crosshead needed to be moved downwards to accommodate this.

Once the specimens were 'set' in place in the jaws (as evidenced by the loading gauge needle beginning to consistently rotate in the clockwise direction) a small load of $200N$ was applied and the machine was paused; the digital displacement gauge was zeroed at this point. Load was then applied to the specimens at a rate of approximately $0.1mm/s$, with a brief pause at each $100N$ increment to record the displacement and load values, continuing this until the needle on the loading gauge paused and began to recede, denoting that the specimen had failed. In most cases the failure point was clearly obvious as the specimen separated into two pieces and this caused a reduction of pressure on the lower vice jaws which then fell away, releasing the specimen loudly.

To capture the failure moment for later reference, a high frame-rate camera was directed at the specimen while loading was applied, as the specimens failed this was recorded at a rate of $400\ frames/s$.

CCII RESULTS AND CALCULATIONS

Recorded results for this experiment are displayed in Table 7-7.

Table 7-7: Tensile stress testing measured and recorded results

Test Number	Specimen Number:	Width $w\ (mm)$	Wall thickness $t\ (mm)$	Node in specimen?	Max Load at Failure (N)
1	$33A$	6.0	2.4	N	2670
3	$7A$	6.5	2.6	N	2950
5	$19A$	4.6	2.1	N	2450
10	$4A$	5.5	1.6	N	2420
2	13	5.2	6.6	Y	2490
4	$4B$	5.9	4.1	Y	2420
6	$19B$	3.9	3.8	Y	1600
7	$7B$	5.6	3.4	Y	1512
8	14	6.7	3.6	Y	1520
9	$33B$	6.0	4.0	Y	2300

To calculate the tensile stress $(\sigma_{tensile})$ present in the specimen causing failure, it is necessary to first calculate the cross sectional area of the specimen as shown in Equation 22. Following that Equation 23 is used to calculate the tensile stress, and Equation 24 shows the simplified version of this.

$$A = w \cdot t \tag{22}$$

$$\sigma_{tensile} = \frac{P}{A} \tag{23}$$

Therefore:

$$\sigma_{tensile} = \frac{P}{w \cdot t} \tag{24}$$

The following is a sample process showing the calculation of the bending stress at failure of test 1, specimen 33, calculated results for all of the specimens tested are shown in Table 7-8, these values were calculated using Excel.

$$\sigma_{tensile} = \frac{2670}{6.0 \times 2.4}$$

$$\sigma_{tensile} = 185.4MPa$$

Table 7-8: Tensile stress experiment calculated values

Test Number	Specimen Number:	Node in specimen?	Area $A\ (mm^2)$	Tensile Stress $\sigma_{tensile}$ $(Mpa)/(N/mm\text{^}2)$
1	$33A$	N	14.40	185.4
3	$7A$	N	16.90	174.6
5	$19A$	N	9.43	259.7
10	$4A$	N	8.80	275.0
2	13	Y	34.32	72.6
4	$4B$	Y	24.19	100.0
6	$19B$	Y	14.78	108.2
7	$7B$	Y	19.04	79.4
8	14	Y	24.12	63.0
9	$33B$	Y	23.70	97.0

Table 7-9: Summary of critical values for tensile test experiment

Node in specimen?	Sample Size (n)	Min	Max	Range	Average	Standard Deviation
No	4	$174.6MPa$	$275.0MPa$	$100.4MPa$	$223.7MPa$	$51.0MPa$
Yes	6	$63.0MPa$	$108.2MPa$	$45.2MPa$	$86.7MPa$	$17.7MPa$

CCIII DISCUSSION OF DATA VALIDITY

Results from this experiment show considerable variation, with the total range of $212MPa$ being 337% of the minimum value of $63MPa$. The results also show a substantial difference

between tensile stress capabilities across a nodal region (average $86.7MPa$) and across an intermodal region (average $223.7MPa$). Reviewed published data by Rottke (2002) does not comment on the variation between node and internode tensile properties however the range of values found in her review is $148 - 384MPa$, this appears to be a similar magnitude of overall difference (259%) to that found in the tensile experiments detailed in this chapter.

As can be seen in Table 7-8 and Figure 7-11, specimens which had a node present in the narrow area had a substantially larger cross sectional area at the point measured. In the full culm sections that specimens were prepared from for this experiment the node area actually spanned the entire width of the culm. In preparation of the specimens, some of this node area was removed with a sharp knife, but not all of it. The removal of material was limited to the softer inner node structure which was deemed to be incapable of supporting any tensile load, the hard fibrous portion of the node was retained in this process. Questions around the legitimacy of the quantity of material to be removed could be answered by testing standardised samples with and without nodes that had been pre-shaped to a fixed cross sectional area and could then be more accurately compared. As the results from this experiment show in many of the specimens tested, similar measurements of applied load at failure were taken ($\pm < 17\%$ of average value) regardless of the presence of a node in the specimen failure area.

On observing the tensile testing of these specimens, particularly via the slow-motion footage and also when inspecting the fractured specimens, it becomes apparent that some of the specimens with no node in the narrow section have in fact failed in parallel shear, where the teeth of the vice have failed to grip the specimen firmly enough and the wider support pieces have split to the width of the narrow section. This is shown in Figure 7-12 with two internode specimens compared after testing. All of the specimens which had a node present in the narrow area have failed at that node in tension, as shown by examples in Figure 7-13.

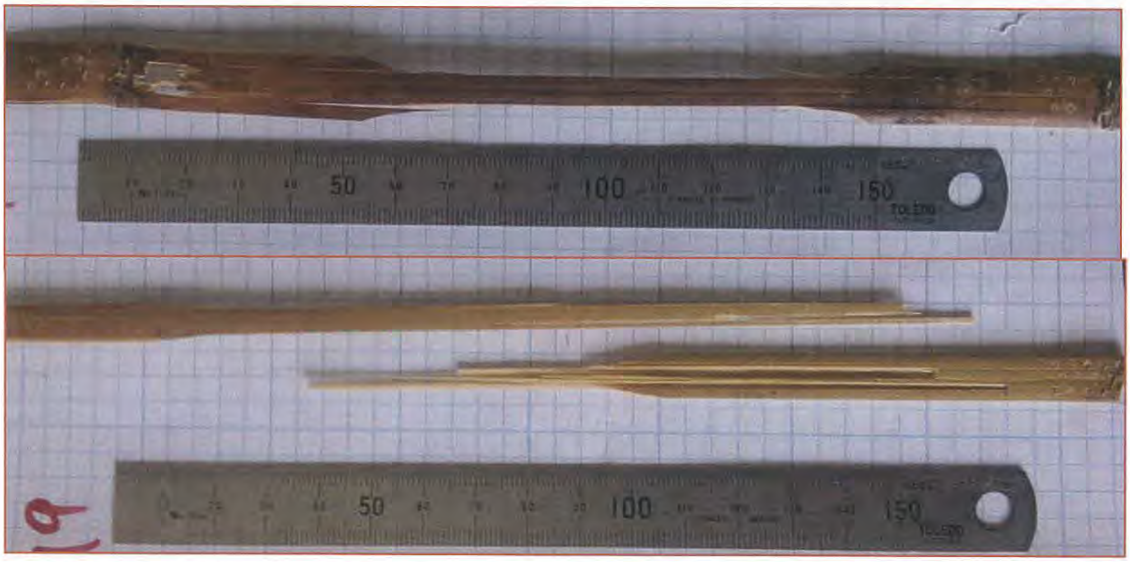

Figure 7-12: Shear failure (top) of tension tested specimen compared to tensile failure (bottom) note shear failure propagation at node

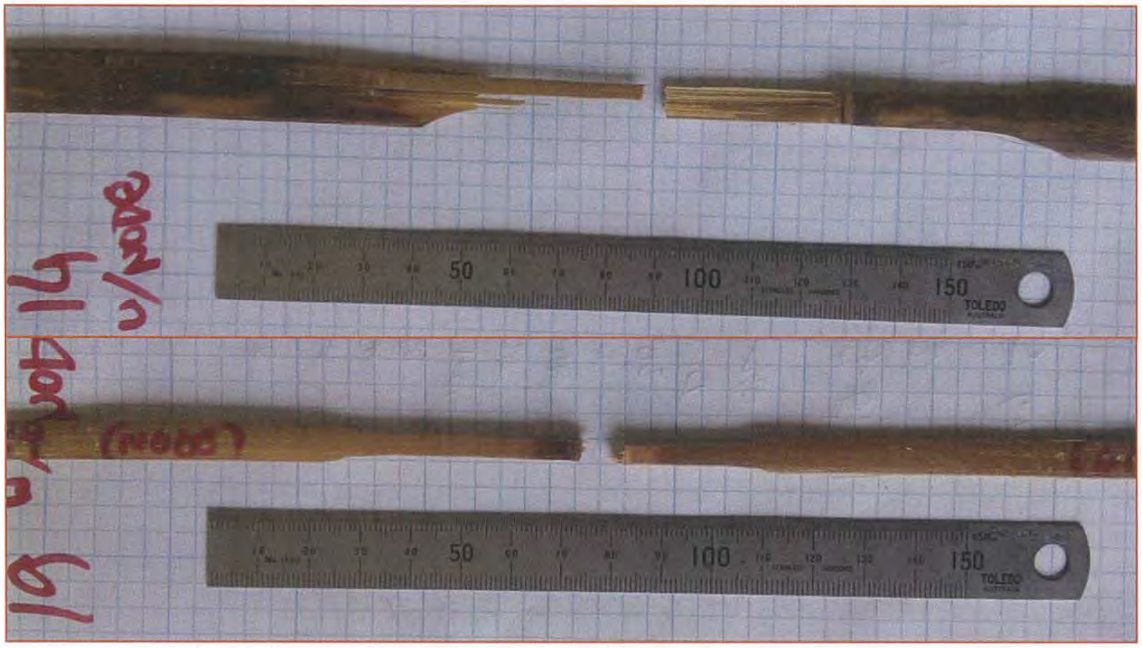

Figure 7-13: Failure at the node in specimens which had a node present in the narrow section

Due to the variation in the data gathered, and the probable use of specimens in the design and prototyping process for this project which have at least one node present in their length, the selection of useful data for determining the maximum tolerable tensile stress should be based on the minimum stress value found in these experiments of $63.0MPa$ to allow for any incongruities not substantiated by the testing process.

CD. COMPRESSION

CDI APPARATUS AND PROCEDURE

Testing specimens for compression failure involved cutting short sections from whole culm bamboo and subjecting them to compressive load through downwards movement of the crosshead of the Dennison universal testing machine.

Specimens for this experiment were cut from the intact portions of specimens used in the static bending experiments using a band-saw. In accordance with ISO 22157-2 recommendations, specimens were cut to a length approximately equal to or longer than their diameter. Once cut, the ends were sanded with fine grade sandpaper to create a uniform flat surface which was perpendicular to the axis of the fibres. Specimens were then measured with length, diameter and wall thickness being recorded for each. Approximately half of the specimens had a node located in the middle of their length.

To apply the compression loading, specimens were placed one at a time on a large steel cylinder which was located directly below the hemispherical bearing on the moving crosshead. The crosshead was lowered down onto the specimen and paused briefly at approximately $200N$ to allow the specimen to be 'seated' firmly in the apparatus. Load was

then applied at a crosshead speed of $0.01mm/s$ until the needle on the loading dial receded, denoting failure in the specimen. At such a slow crosshead speed this dial was the only indicator of the failure occurring, audible cracking sounds and visible failure did not occur. Maximum supported load was recorded and the specimen was removed from the machine.

CDII RESULTS AND CALCULATIONS

Recorded results from this experiment are displayed in Table 7-10 showing the dimensions of each specimen and the corresponding maximum supported load.

Table 7-10: Compression experiment recorded data

Test number	Sample Number	Diameter $D\ (mm)$	Wall thickness $t\ (mm)$	Max Load at failure $P\ (N)$
1	$33B$	21.5	2.3	8700
2	$33C$	22.1	3	7700
3	$33D$	20.75	2.6	9310
4	13	22.5	3	6900
5	1	21.5	2.2	6400
6	$7A$	22.1	2.7	7150
7	$7B$	22.1	2.5	7100
8	$7C$	22.3	2.7	7350
9	$24A$	24	3.2	11000
10	$24B$	24.6	2.5	9800
11	$24C$	24.7	2.75	8990

To calculate the compressive stress ($\sigma_{compressive}$) present in the specimen at failure it is necessary to calculate the cross sectional area A upon which the stress is acting. This can be found using Equation 25. The compressive stress calculation is shown in Equation 26 and the simplified version of this is shown in Equation 27.

$$A = \frac{\pi \cdot (D^2 - (D - 2t)^2)}{4} \tag{25}$$

$$\sigma_{compressive} = \frac{P}{A} \tag{26}$$

Therefore:

$$\sigma_{compressive} = \frac{4P}{\pi \cdot (D^2 - (D - 2t)^2)} \tag{27}$$

The following is a sample process showing the calculation of the compressive stress at failure of test 1 specimen 33B, calculated results for all of the specimens tested are shown in Table 7-11, these values were calculated using Excel.

$$\sigma_{compressive} = \frac{4\times8700}{\pi\times(21.5^2-(21.5-(2\times2.3))^2)}$$

$$\sigma_{compressive} = \frac{34800}{554.93}$$

$$\sigma_{compressive} = 62.7MPa$$

Table 7-11: Calculated stress results from compression tested specimens

Test number	Sample Number	Sectional Area $A\ (mm^2)$	Compressive Stress $\sigma_{compressive}\ (MPa)/(N/mm^2)$
1	$33B$	138.7	62.7
2	$33C$	159.3	48.3
3	$33D$	148.3	62.8
4	13	183.8	37.5
5	1	133.4	48.0
6	$7A$	164.6	43.5
7	$7B$	153.9	46.1
8	$7C$	166.3	44.2
9	$24A$	209.1	52.6
10	$24B$	173.6	56.5
11	$24C$	189.6	47.4

Table 7-12: Summary of critical values for compression test experiment

Sample Size (n)	Min	Max	Range	Average	Standard Deviation
11	$37.5MPa$	$62.8MPa$	$25.3MPa$	$50.0Mpa$	$8.0Mpa$

CDIII DISCUSSION OF DATA VALIDITY

Considering some of the other variation discovered between specimens during previous experiments, this experiment yielded comparatively consistent results. The range gathered has a minimum value similar to that suggested in data reviewed by Rottke (2002) where the minimum compressive stress for *Guadua angustifolia* was suggested to be $39MPa$.

One notable consideration regarding compression stress experiments is noted in ISO 22157-1 and also mentioned by Janssen (2000) and Arce-Villalobos (1993), this consideration relates to the behaviour of a cylinder when subjected to axial stress – because of the relationship between stress and strain in the material, as the material is compressed during loading it will deform in both axial and radial directions. Axial strain deformation is caused by the movement of the crosshead as it bears down on the specimen, however radial strain (change in diameter determined by Poisson's ratio) is restricted by friction between the end surfaces of the specimen and the faces of the apparatus which are in direct contact when the load is applied. This restriction of deformation under stress due to friction causes the specimen to maintain its structural integrity and shape at the ends under higher loads than would be possible if there was less or no friction present. Janssen (2000) suggests a solution for this which involves constructing a complex apparatus which allows the specimen to deform radially as the load is increased, in a manner more representative of a realistic compression scenario in a full culm specimen. This apparatus was deemed to be too complex for the scope of this project, however the result of not using it is that the stress data shown in Table 7-12 is likely to be higher than the actual maximum compressive stress capabilities of the specimens when the specimen is in a real world scenario. No data could be found which compared the variation in ultimate compressive stress between experiments using no friction reducing apparatus and those which did attempt to reduce the friction using the apparatus suggested by Janssen (2000).

Figure 7-14: Compression loading of specimen showing restriction on radial strain at ends leading to 'barrel' shape developing.

No marked difference was noted between specimens with and without nodes, this was in keeping with notes on results from ISO 22157-2 and also suggested to be the case by Rottke (2001). To ensure that this data does not misrepresent the properties of any given specimen in a compressive stress loading situation, the lowest value of $37.5MPa$ shall be used during the design process and always in combination with a safety factor.

D. APPENDIX: LOADING SCENARIO CONSIDERATIONS

In simulating loading scenarios it is important to note that there are a lot of variables which will affect the outcomes of any calculations made. For the purposes of producing the 'worst case' scenario, these variables have been extrapolated to their reasonable limit to determine the maximum possible loading that could be present under the conditions posed. The following points address as many of those variables as can be seen to have a substantial impact on the scenario's which this section investigates. The assumptions stated here are limited to those which are applicable to all of the scenarios in this appendix, under each calculation set the relevant other notable points have been identified and stated.

- **Velocity** – Considering that this velomobile is not designed for high speeds, but instead for commuting and general urban use, a maximum speed that matches the New Zealand urban speed limit of $50km/h$ $(13.89ms^{-1})$ is reasonable. This speed is difficult to obtain using pedal power alone, so it would generally only become a possibility when descending. It is assumed that no braking would be engaged prior to impacts or during cornering.
- **Wheel size** – The majority of common velomobile designs utilize standard $405mm$ diameter front and rear rims in combination with pneumatic tyres of approximately $30mm$ height. This yields an overall wheel diameter of $465mm$.
- **Tyre pressure** – The level of pressure that tyres are maintained at governs the amount of distortion that they are capable of providing to dampen energy transfer from road surface irregularities and also the amount of friction that the tyre can provide. This absorption of energy provides a form of suspension which makes the ride more comfortable but trades comfort for overall rolling resistance of the wheel. For these calculations it will be assumed that the tyre pressure is as high as possible – meaning that the tyres absorb as little of the impact loading resulting from road surface irregularities as possible.
- **Vehicle mass** – as noted in Section 4.1, combined mass of rider and velomobile is taken to be $110kg$. For the purposes of these calculations the centre of mass is located behind the front wheels, at a distance of $1/3$ of the total wheelbase length. Centre of mass of rider and velomobile are both assumed to be located at this point, no regard has been given for height of centre of mass
- **Surface irregularity shape** – Irregularities in the road surface come in a range of shapes and profiles. The worst possible scenario would be a raise in the road level (e.g. up the curb or onto a recently resurfaced section) with a straight and square edged shape.
- **Surface irregularity size** – While it is theoretically possible to encounter massive irregularities in the road surface, there is a limit to what could reasonably be expected, and therefore there needs to be a limit to what size irregularity it is reasonable to expect the frame to be able to tolerate without sustaining damage. On a standard

bicycle, impact with even a small step in the road surface at high speed would almost definitely cause an accident where the rider loses control of the bike. Most riders would be very lucky to come away from this unscathed regardless of how the bicycle frame performed during impact. A value of $100mm$ has been used for these calculations as a likely worst case scenario. This size also corresponds with the largest step that the front end of the velomobile could clear in order for the wheels to reach the step before the frame bottoms-out, the frame lowest point is lower than $100mm$, but this low point is located behind the front wheels.

- **Impact conditions** – Assuming that the irregularity was large enough to contact both wheels, the highest impact loading scenario would occur if both wheels contacted the irregularity at the same time – meaning that the vehicle approached on a path perpendicular to the edge of the irregularity. This has the effect of halving the impact load across both wheels. The calculation process for one individual wheel impacting an irregularity at speed has been deemed too complex for this report.

E. APPENDIX: SIMULATION DESIGN DEVELOPMENT

Simulation of loading scenarios during the development of the frame design provided direct feedback for the design process. This appendix shows the results of a selection of early simulations of applied loading and the subsequent frame design changes made in order to produce a design more capable of effectively distributing the induced stresses and maintaining a higher Factor of Safety (FOS) value for the most stressed areas of the frame. In a number of the simulated scenarios the results needed careful assessment to provide accuracy. Requirements of the Solidworks simulation program included the need to specify at least one 'infinitely stiff and rigid' fixed point. It was inaccurate to model the application of reaction forces on the frame as rigid and fixed as this did not allow the joints to twist or rotate. This was particularly relevant for the riders' mass on the seat. The seat attachment points were modelled as rigid, but this often led to very high forces in the area around the mounts which would have in fact have been distributed through the seat instead. The use of the beam type simulation technique meant that only members which could be classed as beams could be part of the simulated fixed and loaded features list. The modelling of a rigid seat on which to apply the evenly distributed riders' mass was therefore not possible, neither was the addition of axle mounting points for the wheels and other fixtures that would be required for the actual design. The stress values in the region of the seat mounting points were often elevated due to the unidirectional rigidity of the fixings (this can be seen in Figures' 7-16 and 7-18) and in most cases it was ignored and the emphasis for frame improvement was placed on the areas where loads had been applied to the frame in a specified manner.

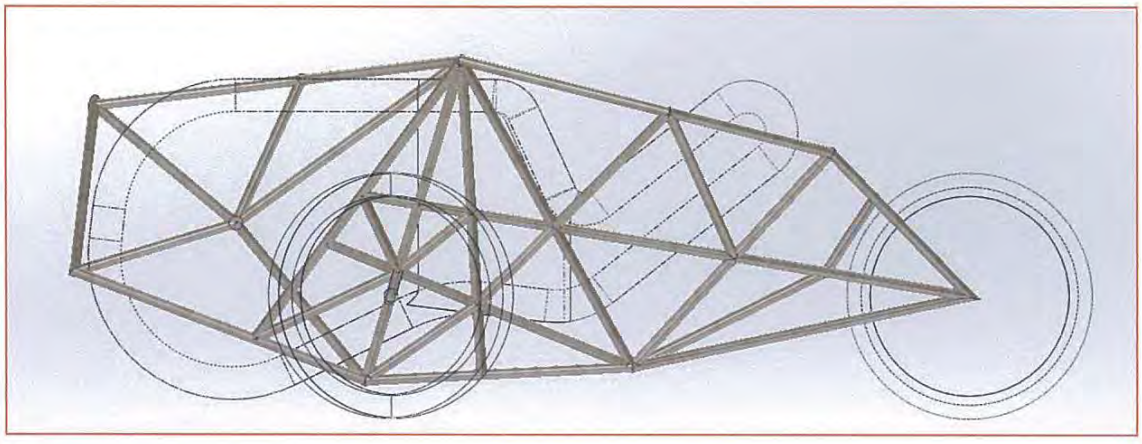

Figure 7-15: Earliest frame concept prior to first simulation showing dimensional clearance geometry

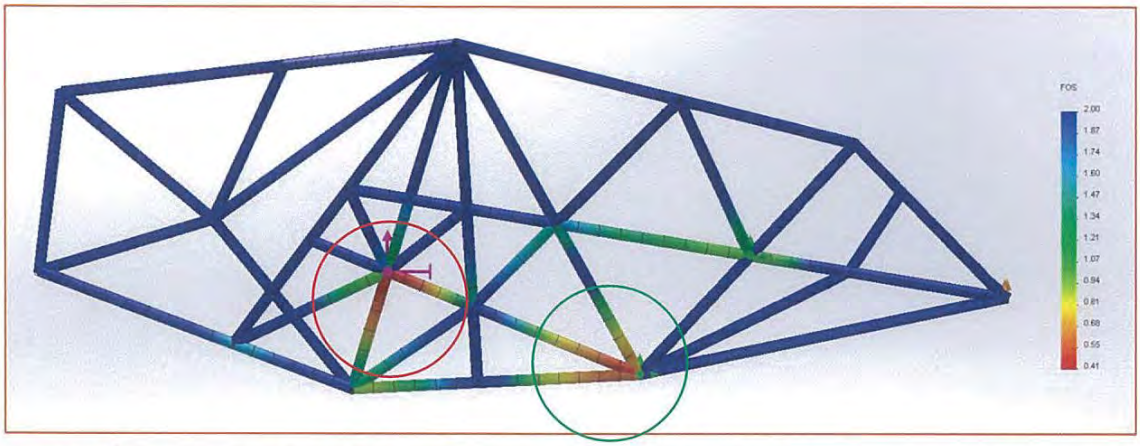

Figure 7-16: Highest stress simulation results for early frame concept. Loaded under simulated cornering scenario with circled areas where the FOS value is less than 1 (highlighted in red).

When the first simulations were performed it was immediately apparent that the highest stress concentrations in the frame were caused by the cornering loading scenario. The resulting moment due to the force acting at the radius of the wheel caused a significant inward twisting deformation to the frame; this induced a large amount of stress in the two frame members below the axle mount (shown circled in red in Figure 7-16). The stresses at these points had an FOS value of 0.42 at the edge of the joint. Note also in Figure 7-16 that the seat mount area displays a similarly low FOS as discussed earlier. The joint circled in green was rigidly fixed for the simulation which caused this high stress concentration to occur.

In order to reduce the concentration of induced stress around the axle, the frame was modified to have more members which met at the joint where the axle attachment point was located. These members were also supported by a rearrangement of the orientation of the members which were one joint distant from the axle attachment point. These changes are shown highlighted in Figure 7-17.

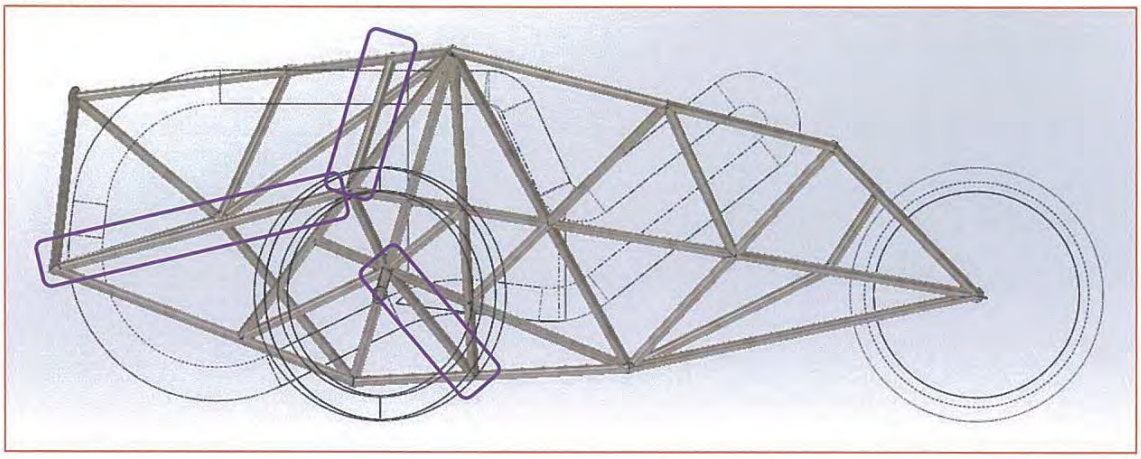

Figure 7-17: Modified frame after analysis of previous simulation results (Figure 7-16). Added/rearranged members highlighted in purple

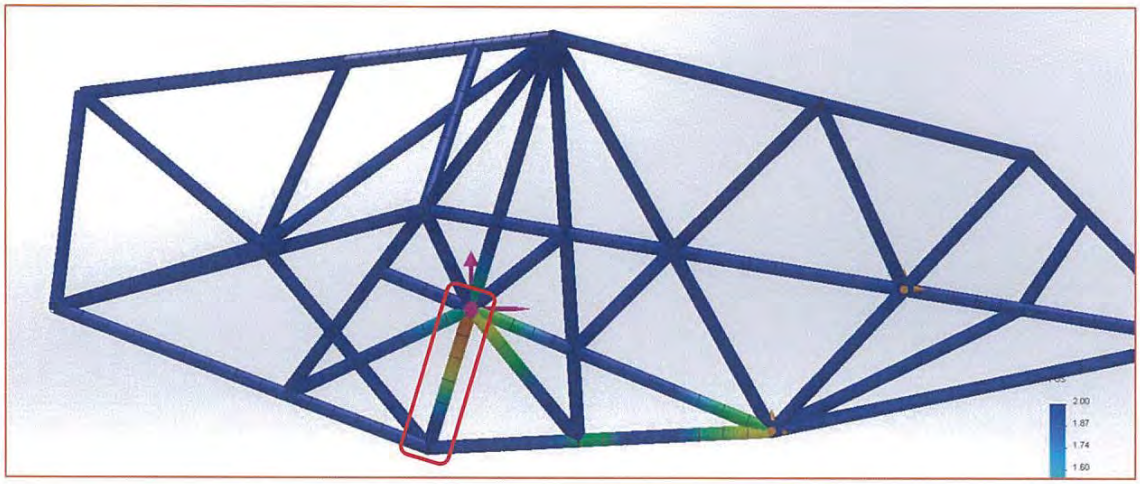

Figure 7-18: Simulation results from modified frame design, also loaded under simulated cornering scenario. FOS minimum still 0.42 but now only in one member (circled in red)

Analysis of the simulation results shown in Figure 7-18 shows that the changes to the orientation of the frame members under the highest stress proved to be beneficial to the stress distribution in the local region of that joint. Additional members are shown to be added in Figure 7-17, these members were not related to the stress in this loading scenario (as can be seen they had little effect on the results), instead they served to stiffen the front area to reduce the quantity of deflection that was present under this and the other simulated loading scenarios.

Further additions were made to the high stress region around the joint to which the load was being applied to in this cornering scenario, these changes are shown in Figure 7-19.

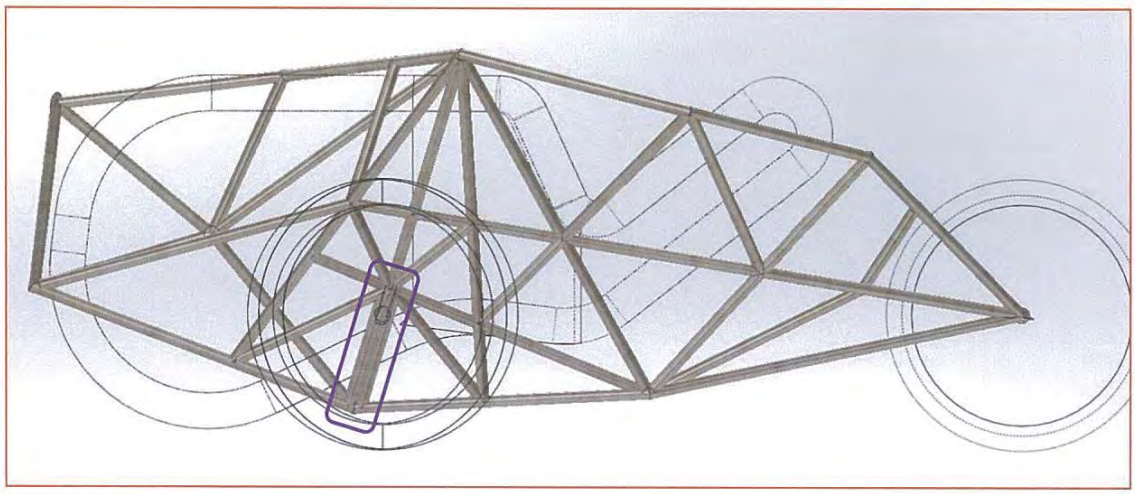

Figure 7-19: Modified frame after analysis of previous simulation results (see Figure 7-18). Modified region highlighted in purple.

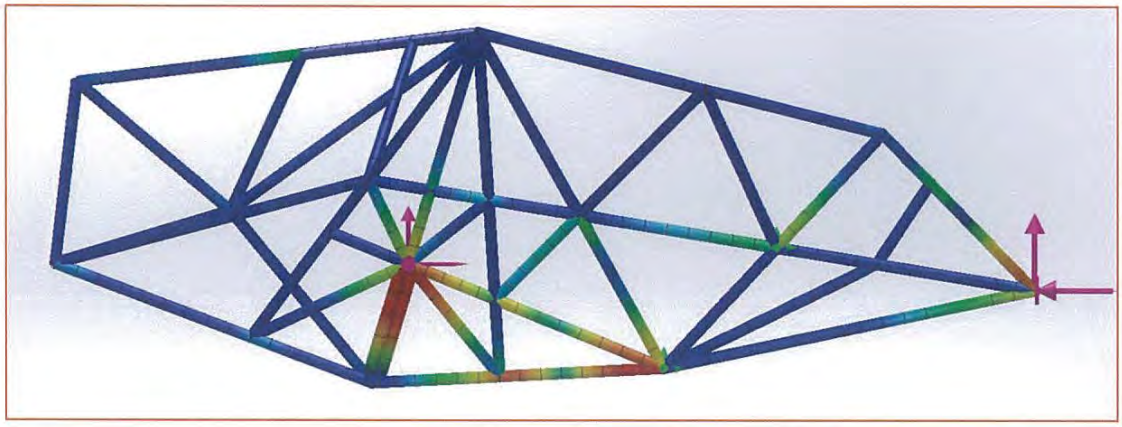

Figure 7-20: Repeated simulation following modifications shown in Figure 7-19, again loaded under simulated cornering scenario for highest stress concentration. FOS minimum of 0.89

After the addition of a parallel member to the highest stress concentration area and repeating the loading simulation the results showed a marked improvement in the maximum stress. Even though the FOS value was still less than 1 it was decided that this result was satisfactory because the simulation had not been able to consider the effect of the wrapped fibre joints on the stress distribution. In the case of such short frame members the joint structure will have a much more noticeable effect on the rigidity of the members, and will effectively shorten them even further. This hypothesis was proposed to explain the large and somewhat poorly distributed stresses shown in Figure 7-20 even after the addition of a 9^{th} frame member to that joint cluster.

F. APPENDIX: PROTOTYPE CONSTRUCTION

The construction of the prototype frame section was an experimental process in its own right, it was performed with little knowledge and no experience of the processes required to optimise the strength and durability of a bamboo frame with composite natural fibre and epoxy wrapped joints. During the construction a number of assumptions were made that were based on related knowledge of fibre reinforced plastics and on research of information available regarding the construction of bamboo bicycles. Most of this information was found in informal locations such as blog posts and through images of existing constructed frames. Where the information is of particular interest the source has been cited, however a number of the features of the construction method were developed based on assumed best practise. This appendix provides a summary of the steps taken during the construction, a series of figures showing what occurred at each step, and a description of the relative considerations made along the way.

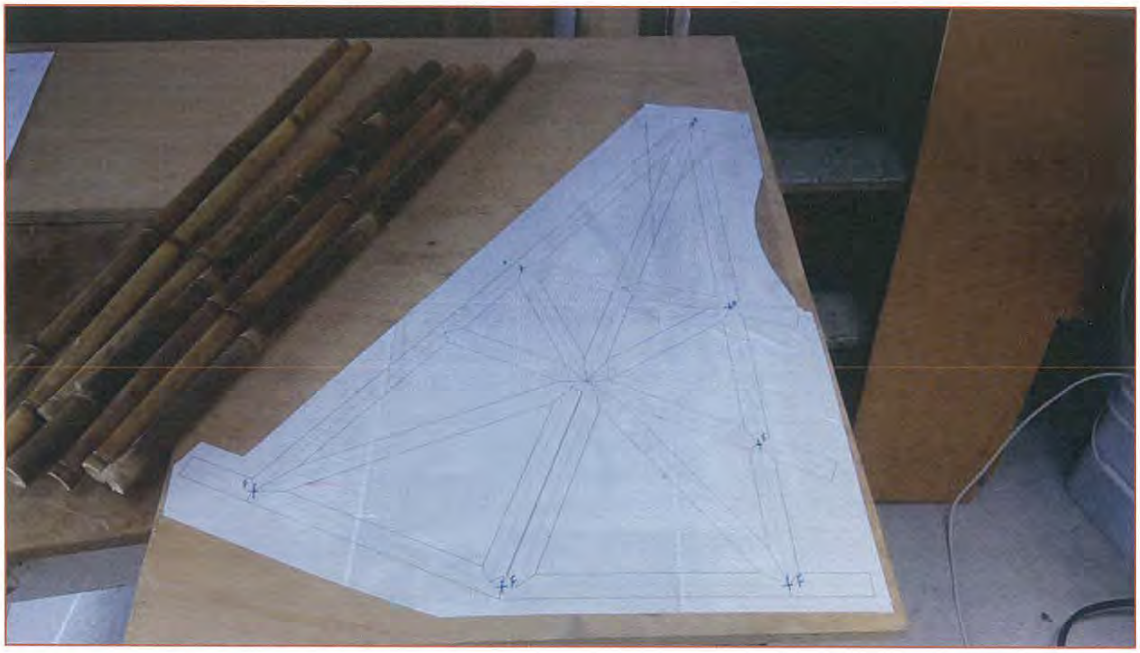

Figure 7-21: Frame design printed and laid out on the backing board.

In order to determine the layout of the members of the frame, a full scale image of the model was printed and glued down to the backing board. The backing board used was a section of $20mm$ plywood being used to maintain a rigid support for the frame during loading. This board provided the base for rigid fixtures mounted on the frame to be bolted directly to in order to emulate the rigid fixtures that were applied during the Solidworks simulation outlined in Section 4.4.3.

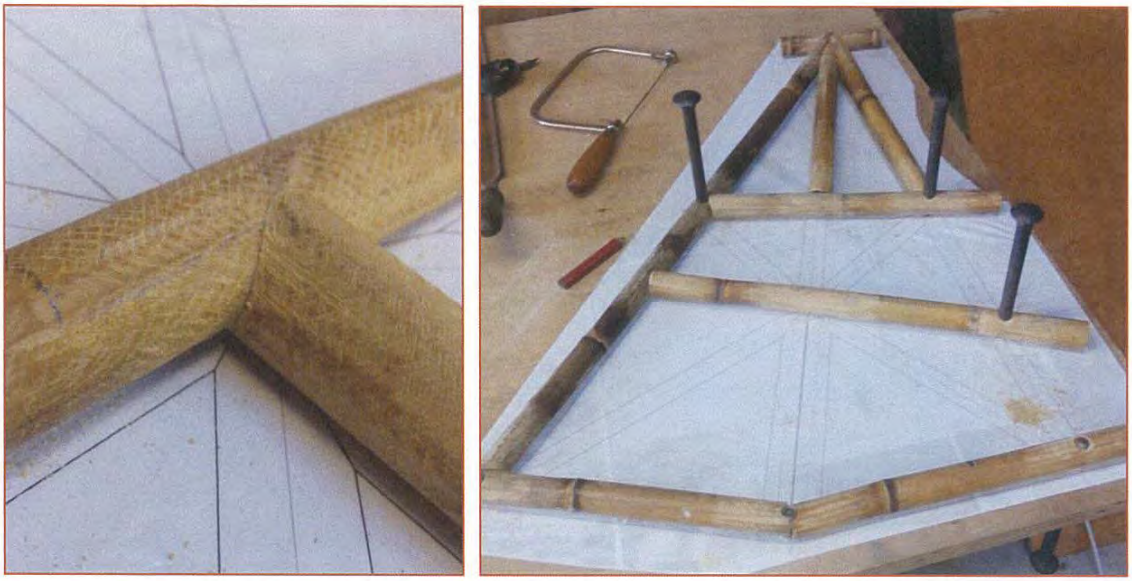

Figure 7-22: Frame members cut to size, mitred and pinned to the base with the coach bolts, note roughened surfaces at joints.

The frame members were cut to size based on the printed plan, as each was cut they were laid out on the plan and holes were drilled in members and the base where the bolts would later be located. Members were then pinned flat to the base in the appropriate position using the interference fit of the bolts to hold them in position. As each member was cut the ends were also carefully mitred by hand using a coping saw and a file to ensure that a close fit was obtained at the joints. Joint surfaces areas were also roughened to improve adhesion

Figure 7-23: Complete frame pinned flat in place, joints tacked together with additive-thickened epoxy resin.

Once all of the members were cut and shaped to fit together the frame was assembled and tack-glued together using 'Entropy Resin Super Sap CLR' two part epoxy resin with an additive called 'Q-cell' mixed in to obtain a high build consistency and better filling properties. This resin was selected because of its high plant based content and low toxicity and volatile organic compound release during use (Entropy Resins, 2014). The frame was held during glueing by the bolts that passed through the joints, and additional clamps where necessary. It is worth noting that this actual frame section on the entire modelled frame is not completely flat as it has been constructed here, however because the deviation from horizontal was less than $10mm$ on the designed frame this was negated to allow for ease of construction.

Figure 7-24: Flax fibres used in joint construction. Left: combed loose fibres; right: twisted into loose yarns of approximately 5mm diameter prior to wrapping.

For this project the fibres used in the joint construction process were sourced from an historic flax mill in Templeton which processes the leaves of New Zealand flax (*Phormium spp.*). The selection of flax fibres over other options such as glass, carbon or hemp fibers was based primarily on notes made by commercial frame builder Craig Calfee (2014) on the benefits of using materials that have a similar Coefficient of Thermal Expansion (CTE) to that of the bamboo. Carbon and glass fibres both have a much lower CTE than plant based materials such as flax or hemp fibres, this causes a tendency for the bamboo frame members and the constructed joint to expand at different rates during temperature changes, leading to a loss of integrity in the joint contact surfaces (Calfee, Building Bamboo Bikes, 2014). Availability of the flax fibre was the other key factor in the decision, being locally produced it was simple to procure in large quantities. Fibres were received in large loose combed bundles and were seperated into groups of approximately 15-20 fibres and twisted loosely to form yarns which could then be wrapped around the frame joint area.

Figure 7-25: Layering joints with impregnated fibre-resin matrix. Frame shown in final position lifted off backing board by fixings.

After the tacked joints had set the excess resin was removed and they were ready for wrapping with the fibre and resin matrix. The frame was lifted from the backing board and held in place by the coach bolts that were to become part of the joints later. These bolts had a square washer welded to their shank that located on the top side of the backing board, and a washer and nut beneath to fix them in place. Joints were built up in layers of resin impregnated fibre yarn that was wrapped in varying directions primarily based on the approximated direction of primary loads in the joint. The fibre was also placed to evenly cover the joint areas and distributed to avoid large pockets in the joint of either resin or air.

Figure 7-26 Joint wrapping process. Left: Wrapped resin impregnated fibres. Right: Perforated electrical tape used to remove excess resin and compress fibre matrix.

When the layering was complete and what appeared to be a sufficient quantity of fibres had been wrapped onto the joint the entire joint was then wrapped in PVC electrical tape which had been perforated with small holes. This was pulled as tight as possible while wrapping to squeeze as much excess resin from the joint and compress the fibres tightly together. Joints were then left to set before removing the tape.

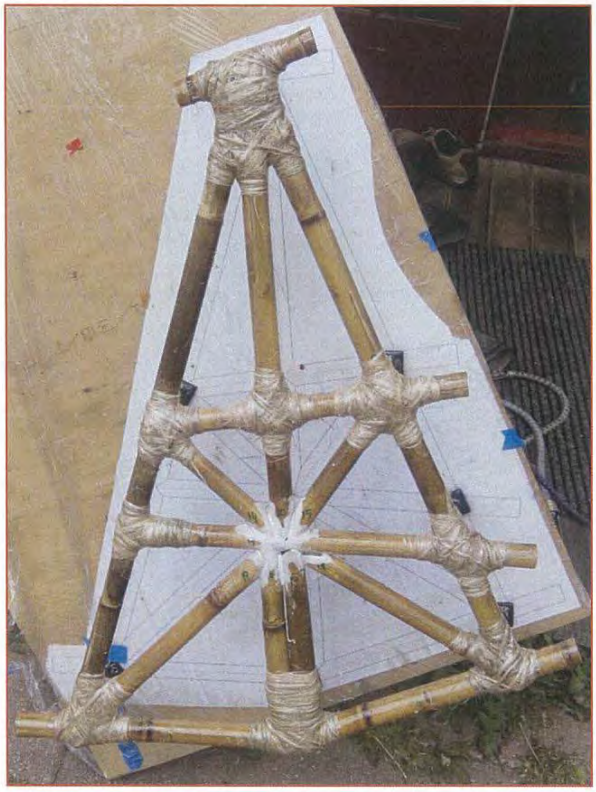

Figure 7-27: Prototype frame with 9 of the 10 joints wrapped and set.

Figure 7-28: Load application point held in position prior to joint wrapping. Note end-piece welded on at 90 degree angle to increase joint rigidity.

The final joint in the frame was the connection of the arm which through which the force of the prototype testing would be applied to the frame. This arm was fabricated such that its dimensions emulated the wheel that would be mounted at this point in the actual design. The arm was fabricated from steel tube of an old bike frame with additional perpendicular member welded to the end of the arm to increase the contact strength of the joint. The addition of this perpendicular member also served to better replicate what would be mounted at this point in the actual design – a steering kingpin mounting fitting of a similar alignment and shape. The layout of this arm is shown in Figure 7-29 with an overlaid circle showing the aligned position of the $0.465m$ diameter front wheel contact patch with the ground.

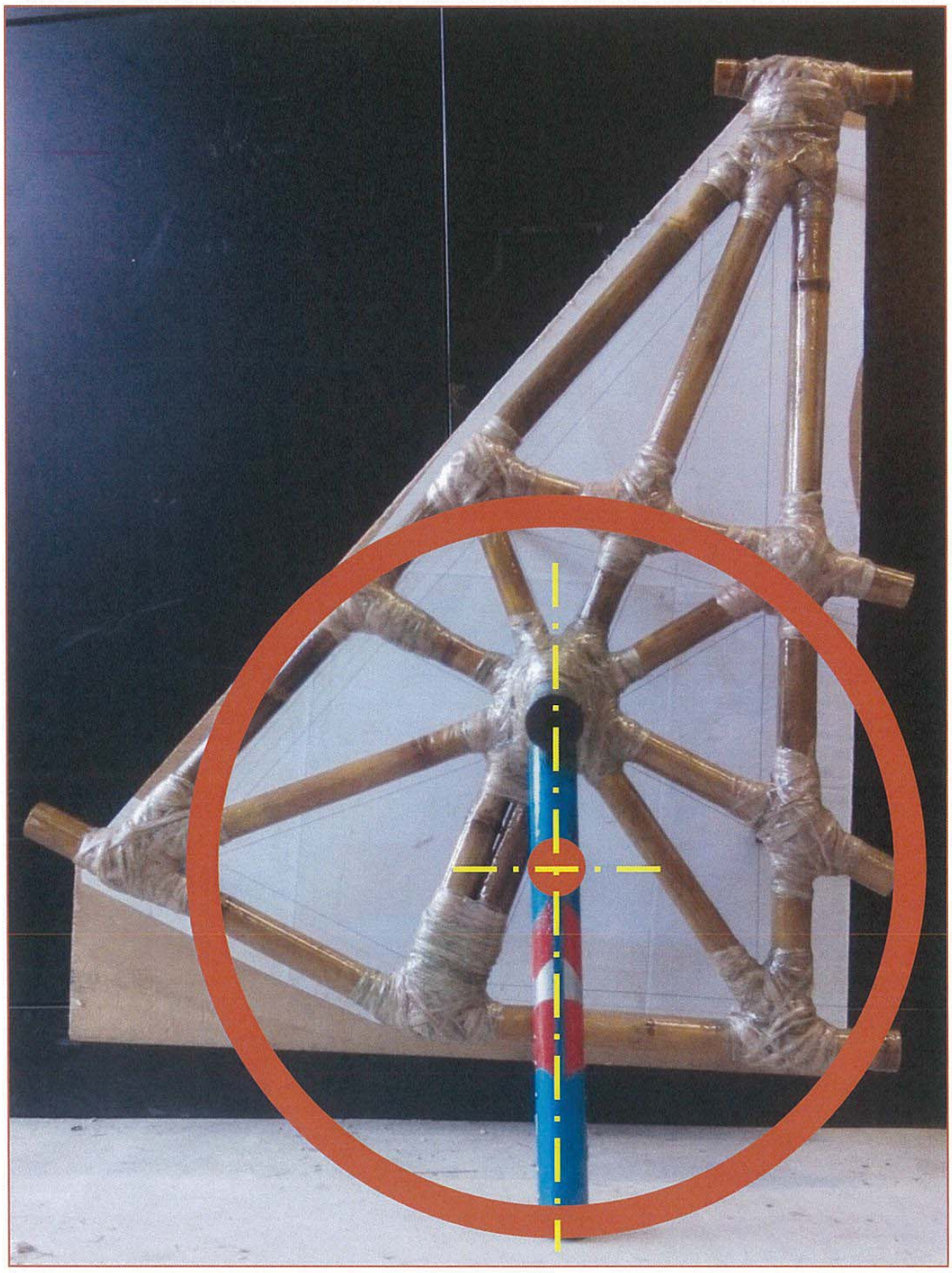

Figure 7-29: Overlay of front wheel position on loading member of frame section showing alignment of wheel contact patch with ground

8 REFERENCES

Arce-Villalobos, O. A. (1993). *Fundamentals of The Design of Bamboo Strucutures.* Eindhoven: Eindhoven University of Technology. Retrieved 09 16, 2014, from http://alexandria.tue.nl/extra3/proefschrift/PRF9B/9303473.pdf

Bamboo Bike Supplies. (2013, 11 23). *Composite Lug Wrapping with Hemp Fibres*. Retrieved from Bamboo Bike Supplies: http://bamboobikesupplies.com/pages/hemp-composite-wrapping

Bauman, A., Rissel, C., Garrard, J., Ker, I., Speidel, R., & Fishman, E. (2008). Cycling: getting Australia moving – barriers, facilitators and interventions to get more Australians physically active through cycling. *Australiasian Transport Research Forum* (pp. 594 - 596). Gold Coast: ATRF.

Calfee Design. (2014). *Is Calfee Bamboo for You?* Retrieved 03 20, 2014, from Calfee Design: http://calfeedesign.com/is-bamboo-for-you/

Calfee, C. (2014). *Building Bamboo Bikes.* Retrieved 03 20, 2014, from Bamboosero: http://www.bamboosero.com/technical/building-bamboo-bikes/

Calfee, C. (2014). *Technical White Paper.* Retrieved 03 19, 2014, from Calfee Design: http://calfeedesign.com/tech-papers/technical-white-paper/

Cox, P. (2010). *Moving People; Sustainable Transport Development.* New York: Palgrave Macmillan.

de Merchant, C. (2014). *Skin on frame boatbuilding method*. Retrieved 03 20, 2014, from Skin On Frame Boatbuilding: http://www.christinedemerchant.com/boat-styles-skin-on-frame.html

Entropy Resins. (2014, 11 10). *Technical Data Sheet.* Retrieved from Entropy Resins: https://entropyresins.com/wp-content/uploads/2014/03/TDS-CLR-System.pdf

Fancourt, D. (2013, 07 15). *Why Buy A Carbon Fibre Bike?* Retrieved 03 19, 2014, from Cycle Torque: http://cycletorque.wordpress.com/2013/07/15/why-carbon-fibre/

Go-One. (2014, 05 05). *Go-One Evo-R*. Retrieved from Go-one Velomobiles: http://www.go-one.de/html/cms/?slides=go-one-evo-r

Heintz, C. (2009). *Wood, Aluminium, Steel and Composites*. Retrieved 03 20, 2014, from Experimental Aircraft: http://exp-aircraft.com/library/heintz/material.html

HeroBike. (2014, 11 13). *Semester Bicycle*. Retrieved from Hero Bike: http://www.herobike.org/products/the-semester-bamboo-bike

Hill, C. A. (2006). *Wood Modification: Chemical, Thermal and Other Processes.* Chichester, England: John Wiley & Sons.

Jansen, J. J. (2000). *Designing and Building with Bamboo.* Technical University of Eindhoven. Eindhoven: International Network for Bamboo and Rattan.

Jeff-o. (2010). *Facet V1 Velomobile*. Retrieved 03 20, 2014, from Instructables: http://www.instructables.com/id/Facet-V1-Velomobile/

Jorgenson, G. (2010, 09 02). *Bangkok*. Retrieved 03 20, 2014, from CNN Travel: http://travel.cnn.com/bangkok/play/smooth-rides-bangkoks-first-bamboo-bike-owner-859118

Kerley, D. (2007, 06). Barnes Wallis. *Airvibes*, pp. 7-8.

Kudzu Craft. (2014). *Skin Boats*. Retrieved 03 20, 2014, from Kudzu Craft: http://www.kudzucraft.com/

Lightning Cycle Dynamics. (2014). *Introduction to recumbent bicycles*. Retrieved 03 20, 2014, from Lightning Cycle Dynamics: http://www.lightningbikes.com/introduction.html

Milan Velomobile. (2014, 05 05). *Milan SL*. Retrieved from Milan Velomobile: http://www.milan-velomobil.de/milansl.htm

Mosquito Velomobiles. (2012). *Mosquito Zero*. Retrieved 03 20, 2014, from Mosquito Velomobiles: http://www.mosquito-velomobiles.com/mosquito_zero.htm

Nelson, R. (2010, 05 16). *Single Rider Human Powered Vehicle: Bamboo Recumbent Bike w/ Full Aerodynamic Fairing*. Retrieved 03 20, 2014, from Silverfish Longboarding: http://www.silverfishlongboarding.com/forum/longboard-board-building-q-discussions/139563-single-rider-human-powered-vehicle-bamboo-recumbent-bike-w-full-aerodynamic-fairing.html

Reidl, A. (2010, 01 08). *Bamboo Bikes: The Ultimate Eco-Friendly Ride*. Retrieved 03 20, 2014, from Speigel.de : http://www.spiegel.de/international/zeitgeist/bamboo-bikes-the-ultimate-eco-friendly-ride-a-670689.html

Rottke, D. I. (2001, 01 01). *Bamboo as a Building Material.* Retrieved 09 16, 2014, from Institute for Structural Design, Aachen University: http://bambus.rwth-aachen.de/eng/fr_referate.html

Rottke, D. I. (2002, 01 01). *Mechanical Properties of Bamboo.* Retrieved from Institute for Structural Design, Aachen University: http://bambus.rwth-aachen.de/eng/fr_referate.html

Schott, W. (2006, 11 01). *Bamboo in the Laboratory.* Retrieved from Power Fibers: http://www.powerfibers.com/BAMBOO_IN_THE_LABORATORY.pdf

Schwalbe. (2014, 06 05). *Tire Dimensions*. Retrieved from Schwalbe.com: http://www.schwalbe.com/en/reifenmasse.html

Sparkes, M. (2009, 07 22). *Green Living Blog*. Retrieved 03 20, 2014, from The Guardian: http://www.theguardian.com/environment/2009/jun/22/bamboo-bike?commentpage=1

Specialized. (2014). *Specialized*. Retrieved 03 20, 2014, from Road Bikes: http://www.specialized.com/us/en/bikes/road

Steintrikes. (2009). *Leitra Avancee*. Retrieved 03 18, 2014, from Steintrikes: http://www.steintrikes.com/trike/leitra.php

Trek. (2014). *Trek Models*. Retrieved 03 20, 2014, from Trek Bicycles: http://www.trekbikes.com/au/en/bikes/road/models/

Trisled Australia. (2013). *Avatar*. Retrieved 03 18, 2014, from Trisled: http://www.trisled.com.au/avatar.asp

Velomobile.NL. (2014). *Quest*. Retrieved 03 18, 2014, from Velomobile.NL: http://en.velomobiel.nl/quest/carbon.php

Vittouris, A., & Richardson, M. (2011). Designing Vehicles for Natural Production: Growing a Velomobile from Bamboo. *Australasian Transport Research Forum 2011 Proceedings* (pp. 1 - 21). Adelaide: Planning and Transport Research Centre WA.